Norwegian University of Life Sciences
Faculty of Science and Technology (REALTEK)
Department of Physics

Philosophiae Doctor (PhD)
Thesis 2022:59

Experimental and theoretical evaluation of thermodynamic properties of low melting chlorides suitable for liquefaction of biomass

Eksperimentell og teoretisk evaluering av termodynamiske egenskaper til lavtsmeltende klorider egnede for flytendegjøring av biomasse

Sepideh Niazi

Experimental and theoretical evaluation of thermodynamic properties of low melting chlorides suitable for liquefaction of biomass

Eksperimentell og teoretisk evaluering av termodynamiske egenskaper til lavtsmeltende klorider egnede for flytendegjøring av biomasse

Philosophiae Doctor (PhD) Thesis

Sepideh Niazi

Norwegian University of Life Sciences
Faculty of Science and Technology (REALTEK)
Department of Physics

Ås 2022

Thesis number 2022:59
ISSN 1894-6402
ISBN 978-82-575-2008-3

Supervisors and Evaluation Committee

Supervisors:

Associate Professor Heidi S. Nygård (Main supervisor)
Faculty of Science and Technology (REALTEK)
Norwegian University of Life Sciences (NMBU)
P. O. Box 5003 REALTEK-NMBU, NO-1432, Ås, Norway

Professor Espen Olsen (Co-supervisor)
Faculty of Science and Technology (REALTEK)
Norwegian University of Life Sciences (NMBU)
P. O. Box 5003 REALTEK-NMBU, NO-1432, Ås, Norway

Evaluation Committee:

Professor George Chen
Department of Chemical and Environmental Engineering
Faculty of Engineering, University of Nottingham
University Park, Nottingham NG7 2RD, UK

PhD Ana Maria Martinez
SINTEF Industry, Metal Production and Processing
P.O. Box 4760 Torgarden, NO-7465 Trondheim, Norway

Professor Jorge Mario Marchetti
Faculty of Science and Technology (REALTEK)
Norwegian University of Life Sciences (NMBU)
P.O. Box 5003 REALTEK-NMBU, NO-1432 Ås, Norway

Acknowledgements

This project would not have been possible without the support of many people. First, I would like to express my deepest appreciation to my main supervisor, Associate Professor Heidi S. Nygård, for her professional guidance, enthusiastic encouragement, and support. I am very thankful for your willingness to open your door widely for scientific discussion and your constructive feedback. You have been an inspirational and amazing supervisor. I sincerely thank you for your constant interest in following intensive research activities closely, and for your comments to guide me in the correct direction. I am also deeply indebted to my co-supervisor, Professor Espen Olsen, for his valuable suggestions, advice, and useful critiques. You motivated me to study and learn more and more by asking challenging questions. I will always appreciate your skills, knowledge, and willingness to seek solutions. Our weekly meeting with both of you played an important role in my project progress and in smoothing my research route. Without your guidance, support, and reinforcement, this endeavor would not have been possible, nor could it have become such a fruitful thesis.

This research work was financed by an H2020 project named "ABC-Salt". I would sincerely thank Professor H.J. (Erik) Heeres, the project manager, and all work package leaders for your help, advice, and encouragement during my research work. I would express my gratitude to all people involved in ABC-Salt for having wonderful collaboration, discussion, general meetings, and social events together.

The modeling part of my work was done during my virtual internship at GTT-Technologies in Germany. I am especially thankful for the patience and guidance I received from Dr. Moritz to Baben, who was my responsible supervisor, and for the daily supervision of Dr. Bruno Reis during this internship. Thank you for your professional guidance and your help in understanding FactSage and Calphad. The collaboration was very useful, and the knowledge and expertise of modeling you shared are invaluable to my research at NMBU. Words cannot express my gratitude to all GTT staff, especially Professor Klaus Hack, who arranged my internship, Wajahat M. Khan and Joao Rezende for answering my technical questions, and Bahador Boroumand for your assistance in giving me access to the internal software during my internship.

I would also like to extend my thanks to my friends and colleagues at NMBU. Wonderful memories from our events, gathering and coffee breaks gave me the energy and motivated me for the next step in my work. Thanks for the scientific discussion and general advice throughout my PhD project. I would like to thank Agnieszka, Marija, Ingeborg and Amalie. I would never forget our amazing times together. I also want to thank Åshild who helped

me at the very beginning of my PhD and showed me the setup and equipment in the lab. I would like to appreciate Sahar, Sahameh and Fahimeh for every time we spent together and sharing your positiveness. Thanks to Sondre and Alexander for working together in the lab, sharing our feeling about our failed experiments and adventure in the lab!
I am particularly grateful for the assistance given by Arne Svendsen and Tom Ringstad for quick assistance in rebuilding the system when I had new ideas or accidentally broke some parts of the existing setup. The experimental part of this thesis had not been possible without your technical support. I would like to thank Marko Jakovljevic for helping me to fix the broken equipment connections and Fredrik Arnesen Stulen for assisting me to find the necessary tools for my experiments. I also want to appreciate Christian Solheim who helped me in XRD analysis.
I gratefully acknowledge the support and advice of the administrative and technical staff, particularly, Berit H. Lindstad, Mona, V. Kristiansen, Tone Rasmussen, Camilla Brun, Torgeir Pedersen, Signe Kroken and Andreas Svarstad Flø.
I would also like to thank all my loved ones in my home country particularly my husband's parents who have been behind me and encouraged me throughout my PhD study from a very long distance. My appreciation also goes to Ebrahim for sharing your experience in finishing your PhD, and encouragement throughout my PhD study.
Most importantly, my heartfelt and endless gratitude goes to my family. To my beloved parents, Saeed and Simin, and my dear brother, Sohrab, for their unconditional, unequivocal, and loving support throughout my entire life. To my loving husband, Behnam, I am forever thankful for the unconditional love, support, and encouragement throughout the entire process and every day. It is impossible to summarise in a few sentences just how much your support meant to me in this unique period. Thank you all for the strength you gave me. I love you all!

Ås, Sepideh Niazi
June 2022

Summary

For many decades, molten salts have been employed in various industries due to their thermodynamic and physical properties. Climate change and the importance of renewable energy to stave off the worsening effects of rising global temperatures have opened the door for molten salts to be employed in new technologies. Molten salts have attracted a lot of attention in the energy and renewable energy sectors due to their high heat capacity, low vapor pressure, low viscosity, stability at high temperatures, low cost, etc. Biofuel production from waste stream lignocellulosic, as a renewable energy source, can take advantage of molten salts. This study is part of an EU project named "ABC-Salt" that aims to produce sustainable liquid biofuels through hydro-pyrolysis from various lignocellulosic waste streams. Molten salts, due to their ability to dissolve organic (and inorganic) materials, can be employed in liquefying biomass as a feed stream for biofuel production. Liquefying biomass in molten salt can make the feed pumpable. Moreover, the rapid heating of biomass in molten salt can enhance product quality. The spent molten salt should be purified and reused in the cycle to make the process more economically and environmentally attractive.

The main aim of this study was to select and characterize molten salts suitable for ABC-Salt. This work consists of experimental studies and theoretical modeling. The crucial thermodynamic properties of the suitable molten salt are a relatively low melting point (~200°C), high thermal stability at the high-temperature hydro-pyrolysis unit (500°C), low hydrolysis level in contact with water in biomass, and good transport properties.

In the current study, two molten salt systems were investigated and compared. Four compositions of $ZnCl_2$:KCl:NaCl (Salt #1:60:20:20, Salt #2: 59.5:21.9:18.6, Salt #3: 52.9: 33.7: 13.4, and Salt #4: 44.3:41.9:13.8 mol%) and three compositions of KCl:CuCl (Salt #5: 32:68, Salt #6: 34:66, and Salt #7: 36:64 mol%) were selected for the experimental investigations. Melting points using the cooling curve method and thermal stability employing thermal gravimetry analysis (TGA) up to 500°C were examined for all seven compositions. The hydrolysis level of each composition was assessed by adding water vapor to the molten salt. Chlorides can react with water to generate highly corrosive hydrochloric acid (HCl). The formed HCl was measured by analyzing the outlet gas from the reactor at intervals of 50°C up to 500°C. The results show that KCl:CuCl with a melting point of around 146°C, very high thermal stability, and no HCl formation of up to 500°C is an interesting alternative for liquefying biomass. However, the appearance of the

stainless steel/nickel setup indicates that this molten salt is highly corrosive and can ruin the construction material.

Although the results for the binary system showed higher stability in terms of mass loss and hydrolysis, the thermodynamic properties of the ternary system still make it an interesting alternative to the ABC-Salt project. Among the salts from the ternary system, Salt #4 has been found to be the most promising alternative, with a melting point of 205°C and mass loss of 0.2% up to 500°C. No HCl formation was detected for Salt #4 up to 350°C and it slightly increased by increasing the temperature reaching 1300 ppm_v at 500°C. To inhibit HCl generation, the effect of metal oxide was investigated, which showed that adding zinc oxide (ZnO) to the salt can significantly decrease HCl formation by reaction between ZnO and HCl. Moreover, the modeling results show that increasing the pressure suppresses the HCl and $ZnCl_2$(g) formation meaning a lower amount of corrosive gas and a lower vapor pressure and mass loss in the high-pressure system.

After liquefying the biomass, the spent molten salt needs to be purified from the contaminants after it leaves the hydro-pyrolysis unit before being reused in the system. In this study, the electrolysis method was used to examine the molten salt purification, with a focus on Salt #4. Although molten salts can be contaminated with many components, theoretically, it is impossible to remove all of them with electrolysis. Therefore, a few impurities with electrode potential within the electrochemical window of the salt were selected for further investigation. To simulate the spent salt, impurities were added to the molten salt, and cyclic voltammetry and chronoamperometry were carried out in a few experiments. Cu, Fe(II), Fe(III), and Mn were introduced to the molten salt by adding CuCl, $FeCl_2$, $FeCl_3$, and MnO_2. The results showed that Cu and Fe(III) were fully extracted from the molten salt, whereas only partial removal of Fe(II) and Mn was achieved after a few hours.

Hydrolysis was one of the main focuses of this work due to the lack of theoretical and experimental data in the literature. In the present work, potassium chloride (KCl) was selected for further study because it is the salt used in both $ZnCl_2$:KCl:NaCl and KCl:CuCl systems and is also popular in many other salt mixtures. The liquid phase of a hydrolyzed KCl solution was modeled using the Calphad technique. The thermodynamic modeling of the liquid phase was carried out based on the subregular solution model using the Redlich–Kister polynomials in FactSage. The binary subsystems of H_2O–KCl, H_2O–HCl, H_2O–K_2O, and KCl–KOH were critically assessed. To the authors' knowledge, this is the first time that chlorides, oxides, and water are modeled as a single liquid phase. The thermodynamic parameters were optimized considering all experimental data available from the literature, and binary phase diagrams were generated.

Although binary KCl:CuCl was not selected as the best alternative for ABC-Salt, it is still a very interesting molten salt for many purposes. There is a phase diagram for this system in the literature based on the experimental data, but no thermodynamic parameters have been calculated for this system, and no database was found for the KCl:CuCl solution. Therefore, Calphad modeling of the binary KCl:CuCl molten salt was performed in this study, and the solution was modeled with a subregular solution model using Redlich–Kister polynomials. A phase diagram of the system was generated based on thermodynamic data and experimental results. The results show that the predicted eutectic point of the binary system was located at T = 145.9°C and 64.9 CuCl mol%. The calculated results are in excellent agreement with the values measured in the current work and in the literature.

Norsk sammendrag

I mange tiår har saltsmelter blitt brukt i ulike industrier på grunn av deres termodynamiske og fysiske egenskaper. Klimaendringer og viktigheten av fornybar energi for å avverge den verste effekten av global temperaturøkning har åpnet en dør for at saltsmelter kan brukes i nye teknologier. Saltsmelter har tiltrukket seg mye oppmerksomhet i energi- og fornybar energisektoren på grunn av deres høye varmekapasitet, lave damptrykk, lave viskositet, stabilitet ved høye temperaturer, lave kostnader, etc. Biodrivstoffproduksjon fra avfallsstrømmer basert på lignocellulose, som en fornybar energikilde, kan dra nytte av saltsmelter Denne studien er en del av et EU-prosjekt kalt "ABC-Salt" som har som mål å produsere bærekraftig flytende biodrivstoff gjennom hydropyrolyse fra ulike lignocelluloseholdige avfallsstrømmer. Saltsmelter kan, på grunn av deres evne til å løse opp organiske (og uorganiske) materialer, brukes til å gjøre biomasse flytende og videre bruke det som tilførselsstrøm for biodrivstoffproduksjon. En flytende blanding av biomasse og saltsmelter kan pumpes og lettere føres videre i prosessen. Dessuten kan rask oppvarming av biomasse i saltsmelter forbedre produktkvaliteten. Den brukte saltsmelten bør renses og gjenbrukes i syklusen for å gjøre prosessen mer økonomisk og miljømessig attraktiv.

Hovedmålet med denne studien er å velge og karakterisere saltsmelter egnede for ABC-salt. Arbeidet består av eksperimentelle forsøk og teoretisk modellering. De avgjørende termodynamiske egenskapene til det passende smeltede saltet er relativt lavt smeltepunkt (~200 °C), høy termisk stabilitet ved høytemperatur-hydropyrolyseenheten (500 °C), lavt hydrolysenivå i kontakt med vann i biomasse og god transport eiendommer.

I dette arbeidet ble hovedsakelig to saltsmeltesystemer undersøkt og sammenlignet. Fire sammensetninger av $ZnCl_2$:KCl:NaCl (Salt #1:60:20:20, Salt #2: 59,5:21,9:18,6, Salt #3: 52,9: 33,7: 13,4 og Salt #4: 44,3:41,9:13,8 mol%) og tre sammensetninger av KCl:CuCl (Salt #5: 32:68, Salt #6: 34:66 og Salt #7: 36:64 mol%) ble valgt for eksperimentelle undersøkelser. Smeltepunkter ved bruk av kjølekurvemetoden og termisk stabilitet ved bruk av termisk gravimetrianalyse (TGA) opp til 500 °C ble undersøkt for alle syv sammensetningene. Hydrolysenivået for hver sammensetning ble vurdert ved å tilsette vanndamp til saltsmelten. Klorider kan reagere med vann og generere svært etsende saltsyre (HCl). Den dannede HCl-gassen ble målt ved å analysere utløpsgassen fra reaktoren i intervaller på 50 °C opp til 500 °C. Resultatene viser at KCl:CuCl med et smeltepunkt på rundt 146 °C, svært høy termisk stabilitet og ingen HCl-dannelse opp til 500 °C er et interessant alternativ for å flytendegjøre biomasse. Utseendet til oppsettet av

rustfritt stål/nikkel indikerer imidlertid at denne saltsmelten er svært etsende og kan ødelegge konstruksjonsmaterialet.

Selv om resultatene for det binære systemet viste høyere stabilitet når det gjelder massetap og hydrolyse, gjør de termodynamiske egenskapene til det ternære systemet det fortsatt til et interessant alternativ for ABC-Salt-prosjektet. Blant saltene fra det ternære systemet har Salt #4 vist seg å være det mest lovende alternativet, med et smeltepunkt på 205 °C og massetap på 0,2 % opp til 500 °C. Ingen HCl-dannelse ble detektert for Salt #4 opp til 350 °C, men den økte til 1300 ppm_v da temperaturen ble økt til 500 °C. For å hemme HCl-dannelsen ble effekten av metalloksid undersøkt, som viste at tilsetning av sinkoksid (ZnO) til saltet kan redusere HCl-dannelsen betydelig grunnet reaksjon mellom ZnO og HCl. Dessuten viser modelleringsresultatene at økning av trykket undertrykker dannelsen av HCl og $ZnCl_2(g)$, noe som betyr en lavere mengde korrosiv gass og et lavere damptrykk og massetap i høytrykkssystemet.

Det brukte saltsmelten, etter å ha gjort biomassen flytende når det forlater hydropyrolyseenheten, må renses fra forurensningene før det brukes på nytt i systemet. I denne studien ble elektrolysemetoden brukt for å undersøke rensingen av saltsmelten, med fokus på Salt #4. Selv om saltsmelter kan være forurenset med mange komponenter, er det teoretisk umulig å fjerne alle med elektrolyse. Derfor ble noen få urenheter som har elektrodepotensialet innenfor det elektrokjemiske vinduet til saltet valgt for videre undersøkelser. For å simulere det brukte saltet ble det tilsatt urenheter til saltsmelten og syklisk voltammetri og krono-amperometri ble utført i noen eksperimenter. Cu, Fe(II), Fe(III) og Mn ble introdusert til saltsmelten ved å tilsette CuCl, $FeCl_2$, $FeCl_3$ og MnO_2. Resultatene viste at Cu og Fe(III) ble fullstendig ekstrahert fra det smeltede saltet mens fjerning av Fe(II) og Mn var delvis fullstendig etter noen timer.

Hydrolyse var ett av hovedfokusene i dette arbeidet på grunn av mangelen på teoretiske og eksperimentelle data i litteraturen. I dette arbeidet ble kaliumklorid (KCl) valgt for å studeres videre siden dette saltet inngår i begge de valgte saltsystemene og også er populært i mange andre saltblandinger. Væskefasen til en hydrolysert KCl-løsning er modellert med Calphad-teknikken. Den termodynamiske modelleringen av væskefasen utføres basert på den subregulære løsningsmodellen ved å bruke Redlich Kister-polynomene i FactSage. De binære undersystemene til H_2O-KCl, H_2O-HCl, H_2O-K_2O og KCl-KOH ble kritisk vurdert. Så vidt forfatteren vet, er dette første gang at klorider, oksider og vann modelleres som en enkelt flytende fase. De termodynamiske parameterne er optimalisert med tanke på alle eksperimentelle data tilgjengelig fra litteraturen og de binære fasediagrammene ble generert.

Selv om det binære KCl:CuCl ikke ble valgt som det beste alternativet for ABC-Salt, er det fortsatt en veldig interessant saltsmelte for mange formål. På den andre siden, til tross for at det finnes et fasediagram for dette systemet i litteraturen basert på eksperimentelle data, er det ikke beregnet noen termodynamiske parametere for dette systemet, og ingen database ble funnet for KCl:CuCl-løsningen. Derfor ble det utført Calphad-modellering av det binære KCl:CuCl-smeltede saltet i denne studien, og løsningen er modellert med en subregulær løsningsmodell ved bruk av Redlich-Kister-polynomene. Fasediagrammet til systemet er generert basert på termodynamiske data og eksperimentelle resultater. Resultatene viser at det forutsagte eutektiske punktet til det binære systemet er lokalisert ved T = 145,9 °C og 64,9 CuCl mol%. De beregnede resultatene er i god overensstemmelse med de målte verdiene i dette arbeidet og litteraturen.

List of papers

Paper I

Niazi, Sepideh; Olsen, Espen; Nygård, Heidi S. "Hydrolysis of eutectic compositions in the $ZnCl_2$: KCl: NaCl ternary system and effect of adding ZnO." Journal of Molecular Liquids 317 (2020): 114069. https://doi.org/10.1016/j.molliq.2020.114069.

Paper II

Niazi, Sepideh; Bonk, Alexander; Hanke, Andrea; to Baben, Moritz; Reis, Bruno; Olsen, Espen; Nygård, Heidi S. "Thermal stability, hydrolysis and thermodynamic properties of molten KCl-CuCl." Materialia 21 (2022): 101296.
https://doi.org/10.1016/j.mtla.2021.101296.

Paper III

Niazi, Sepideh; Olsen, Espen; Nygård, Heidi S. "Electrochemical removal of Cu, Fe and Mn from molten $ZnCl_2$:KCl:NaCl". Submitted to Journal of Separation and Purification Technology.

Paper IV

Niazi, Sepideh; Nygård, Heidi S.; Reis, Bruno; to Baben, Moritz. "Thermodynamic modeling of KCl-H_2O and its binary subsystems including H_2O-HCl, KOH-H_2O and KCl-KOH". Submitted to CALPHAD Journal.

Additional scientific contributions

Oral presentations

Niazi, Sepideh; Olsen, Espen; Nygård, Heidi S. "Thermal stability of molten $ZnCl_2$:KCl:NaCl in contact with water vapor". The Molten Salts and Ionic Liquids Discussion Group (MSILDG) Christmas meeting, December 14, 2020.

Niazi, Sepideh; Olsen, Espen; Nygård, Heidi S. "Hydrolysis of molten $ZnCl_2$:NaCl:KCl and effect of adding ZnO". The 10th Global Conference on Materials Science and Engineering (CMSE) 2021, August 2, 2021. **Winner of the best oral presentation.**

Niazi, Sepideh; Olsen, Espen; Nygård, Heidi S. "Thermal stability of molten KCl:CuCl in contact with water vapor". Molten salt 2021, December 2, 2021.

Poster presentation

Niazi, Sepideh; Olsen, Espen; Nygård, Heidi S. "Comparing properties of molten $ZnCl_2$: KCl: $NaCl$ and $CuCl$: KCl for the purpose of biomass liquefaction in bio-oil production". NorRen summer school 2021, August 8, 2021.

Niazi, Sepideh; Olsen, Espen; Nygård, Heidi S. "Electrochemical study of Cu from $ZnCl_2$:KCl: $NaCl$ molten salt". 28th EUCHEM Conference on Molten Salts and Ionic Liquids. Patras (Greece), June 7, 2022.

Abbreviations and definitions

CaL	Calcium looping technology
Calphad	Calculation of phase diagram
CCMS	Carbon capture in molten salt
CSP	Concentrated solar power
CV	Cyclic voltammetry
FactPS	Fact pure substances
FTIR	Fourier Transform Infrared spectroscopy
HHV	Higher heating value
HTF	Heat transfer fluid
MP	Melting point
MSR	Molten salt reactor
ND	Not detected
PCM	Phase change material
ppm_v	Part per million in volume
RK	Redlich-Kister
rpm	Round per minute
TES	Thermal energy storage
TGA	thermal gravity analysis
XRD	X-Ray Diffraction
d	Diameter
Cp	Specific heat capacity
E_η	Activation energy
H	Enthalpy
R	The universal gas constant
S	Entropy
T	Temperature
η	Viscosity
ρ	Density

Table of Contents

1 Introduction

1.1 General Introduction

Molten salts are engineering fluids with various applications (1). The term “molten salt” typically refers to “melts of inorganic compounds” composed of anions and cations (2). The main characteristics of this kind of fluid are a liquid state in an extensive range of temperatures, stability at high temperatures, the ability to dissolve many organic and inorganic compounds, high heat capacity per unit volume, low vapor pressure, low viscosity, and reasonable cost (3,4). Molten salt-based technologies can be traced back to the nineteenth century, when alkali metals were isolated from corresponding fused salts (1,5). Molten salt applications have been growing for two centuries in many industries.

More recently, molten salts have been employed in the energy sector to face urgent problems regarding energy consumption and environmental protection (6). Renewable energies, such as solar power, wind energy, nuclear energy, and biofuels, have recently attracted huge attention as solutions for an environmentally friendly transition from fossil fuels to renewable energy. Shifting to renewable energy can help reduce greenhouse gas emissions and limit future climate impacts. Moreover, it can ensure reliable, timely, and cost-efficient delivery of energy (7). The intermittent nature of some renewable sources, such as solar power and wind power, makes these renewable sources dependent on energy storage systems (8). Interest in employing molten salts in energy application and thermal energy storage is growing. Molten salts have excellent properties in energy storage, such as high heat capacity and high thermal stability, in addition to low vapor pressure and low cost (6). They found their place in different energy-generating industries (e.g., solar power, nuclear energy, batteries, and biofuels) and have been employed as a source for energy storage in various sectors and carbon capture techniques.

As a renewable energy source, biofuels are not an exception in taking advantage of molten salts. Although there are various processes for converting biomass to more valuable energy forms, pyrolysis/hydro-pyrolysis can use the benefits of molten salts to enhance biofuel production (9). Molten salts can be used to liquefy biomass and as an effective reactive medium. Moreover, they have a large heat capacity and are very stable at high temperatures. Molten salts can be used over a wide range of temperatures, from 120°C to over 1000°C. These properties make them good candidates for rapid heat supply in the thermal processing of biomass (10).

1.2 Study aim and objectives

This work is part of an H2020 project called ABC-Salt, "Advanced Biomass Catalytic Conversion to Middle Distillates in Molten Salts," with agreement number 764089. ABC-Salt aims to produce sustainable liquid biofuels (middle distillates) from various lignocellulosic waste streams for the transport industry, both on roads (biodiesel) and in the air (jet fuel). The project has three main steps: liquefaction, hydro-pyrolysis, and stabilization (hydrodeoxygenation) (Figure 1.1). The first two processes were carried out in a molten salt environment.

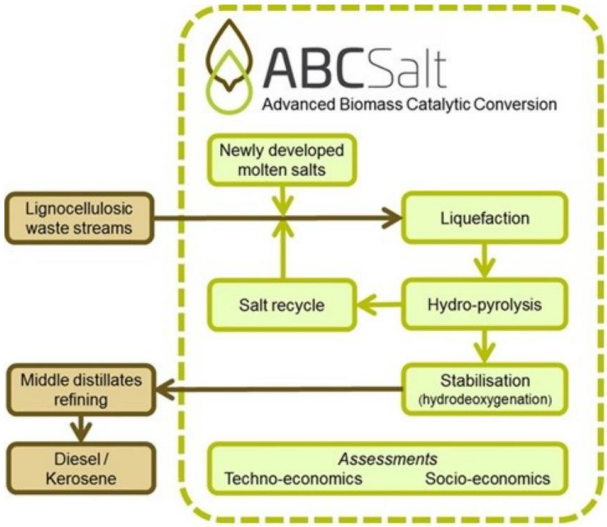

Figure 1.1. Schematic representation of the ABC-Salt project.

Molten salts were employed to simplify the process and optimize yield production. Feeding solid biomass to the reactor is one of the main issues in pyrolysis. The complexity of this increases for high-pressure reactors, such as those commonly used in hydro-pyrolysis. Problems such as plugging, clogging, leakages, and uneven flow can lead to low production rates and poor product quality. Liquifying biomass in molten salts before feeding it into a high-pressure pyrolysis reactor can resolve these problems. It can facilitate the pumping of biomass and thus give better control of the feeding system. Further, the good heat transfer characteristics of the molten salt can optimize the vapor yield and minimize char and gas formation, as the heating rate of biomass particles subject to pyrolysis is significant for the yield (11,12).

The current work aimed to find and characterize proper molten salt candidates for the ABC-Salt project. The suitable molten salt needs to liquefy the biomass under mild conditions

and have a melting point of around 200°C. This temperature should be low enough to avoid producing byproducts, such as ash or char, and sufficiently high to liquify biomass. The selected molten salt requires high thermal stability to prevent salt decomposition at high temperatures and to make salt recycling possible. It is also essential that the salts do not react chemically with the constituents of biomass particles' constituents and provide minimum corrosion to metal pipes and containers. Hydrolysis is a possible reaction due to the presence of water in the biomass. Water may react with the salts and form highly corrosive gases, such as HCl or HF, if chlorides or fluorides are used, respectively (13,14). Therefore, the minimum rate of hydrolysis is a considerable area of focus for this study. Further, the proper molten salt must have good transport properties, such as low viscosity and low vapor pressure.

The ternary molten salt $ZnCl_2$:KCl:NaCl was the first candidate for ABC-Salt. According to the literature, it has excellent transport properties and a low melting point (15,16). The thermodynamic properties (melting point, thermal stability, and hydrolysis) for four different compositions (Salt #1: 60:20:20, Salt #2: 59.5:21.9:18.6, Salt #3: 52.9:33.7:13.4, and Salt #4: 44.3:41.9:13.8 mol%) of the salt were studied in **Paper I**. The effect of adding metal oxide (ZnO) on hydrolysis HCl formation was also investigated in this study. Another interesting salt for ABC-Salt was KCl:CuCl, due to its very low melting point and low viscosity, but very few studies were found regarding the salt properties. **Paper II** mainly focused on the thermodynamic properties of this binary system by investigating and comparing the properties of three different compositions (Salt #5: 32:68, Salt #6: 34:66, and Salt #7: 36:64 mol%). Comparing the results from **Paper I** and **II** showed that Zn-based Salt #4 was the most promising alternative as a biomass liquefier, and this salt was therefore the main focus for further studies.

To limit salt consumption and disposal costs, recycling the spent molten salt as many times as possible in the ABC-Salt process is essential. This requires a purification step because biomass ashes and char may accumulate in the molten salt (which can negatively affect molten salt properties, including melting point, viscosity, etc.). Performing electrolysis experiments with an electrochemical analyzer (AUTOLAB) was considered for the possible removal of ash/minerals from Salt #4, and this was investigated in **Paper III**.

Apart from experimental studies, another aim of the study was to perform simulation and modeling in FactSage to create a database for unknown salt systems. Although $ZnCl_2$:KCl:NaCl was chosen as the best alternative for ABC-Salt, KCl:CuCl was still considered a very interesting molten salt system due to its promising thermodynamic properties. There is a phase diagram for this system in the literature based on experimental data (17), but no thermodynamic parameters have been calculated for this system, and no

database was found for the KCl:CuCl solution. Therefore, Calphad modeling of the binary KCl:CuCl molten salt was performed in this study, and FactSage was employed to assess the thermodynamic parameters and generate the phase diagram (**Paper II**). This optimization is a necessary first step for further studies to enable thermodynamic calculations of practical interest for biomass liquefaction or other applications, such as copper electrodeposition from salts or solvent metallurgy.

To the author's best knowledge, **Papers I and II** were the first experimental studies investigating the hydrolysis reactions for $ZnCl_2$:KCl:NaCl and KCl:CuCl molten salt systems. The presence of chloride, water, and hydrochloric acid in the hydrolysis process and the effect of metal oxide in the system provide a system in which no FactSage database was found. Since potassium chloride (KCl) existed in both molten salt systems in the current work and is a prevalent salt in different applications, KCl and its oxide were selected for further modeling. In **Paper IV,** the thermodynamic modeling of the liquid phase of a hydrolyzed KCl solution was carried out based on the subregular solution model using the Redlich–Kister (RK) polynomial in FactSage. The binary systems of H_2O–KCl, H_2O–HCl, H_2O–K_2O and KCl–KOH were critically assessed. The KOH associate was included in the liquid phase model to take into account short-range ordering. The thermodynamic parameters were optimized by considering all the experimental data available from the literature. The phase diagram and model parameters were derived from software-assisted optimization.

2 Literature Review

Molten salts have been used in many applications since the 19th century, and their technologies are still under development (5,18). The thermodynamic properties of these fluids make them very interesting as mediums for heat transfer, heat storage, coolant, solvent, etc. However, every single salt has specific thermodynamic properties, making it suitable for a particular application. Molten salt systems are usually employed as a mixture (not a singular salt) that could have different properties from single salts. Therefore, assessing the thermodynamic properties of different compositions of salt mixtures is essential.

This chapter starts by presenting the important properties of salts and molten salts (Chapter 2.1 and 2.2) that are necessary to consider in categorizing the salts presented in Chapter 2.3. The application of molten salt in energy sectors such as nuclear energy, solar power plants, batteries, and carbon capture is presented in Chapter 2.3.1. Chapter 2.3.2 and its subchapters cover information about the application of molten salt in biofuel and hydro-pyrolysis more specifically, since the aim of the current study is directly linked to them.

2.1 Salt and molten salt

Salt, in chemistry, is a substance produced by the reaction of an acid with a base. This process is called a neutralization reaction (19). For example, sodium chloride can be produced through the neutralization reaction between HCl and sodium hydroxide (NaOH), as shown in Eq. 1:

$$NaOH + HCl \rightarrow NaCl + H_2O \quad (1)$$

A salt consists of the negative ion (anion) of an acid and the positive ion (cation) of a base (20). Salts can also be generated through a reaction between halogens and alkali metals, called a combination reaction. The component ions in a salt compound can be either inorganic (e.g., Cl^-) or organic (C-H bound, such as acetate, $CH_3CO_2^-$). The main differences between organic and inorganic are listed in Table 2.1 (21,22).

Table 2.1. The main difference between organic and inorganic compounds.

Organic salts	**Inorganic salts**
Based on carbon	Not based on carbon
Mainly covalent bonding	Mainly ionic bonding
Low boiling point, and melting point	High boiling point and melting point
Soluble in nonpolar solvents	Soluble in polar solvents (water)
Nonconductors	Conduct in solution and molten
Limited thermal stability	High thermal stability

The different properties of these salts are mainly due to their chemical bonds. Ionic and covalent bonds are two main types of chemical bonding. In an ionic bond, one atom donates an electron to another atom (see Figure 2.1). This means that one atom has a positive charge, while the other has a negative charge. This phenomenon makes the ionic bond polar, which stabilizes both atoms (23). Atoms contributing to ionic bonding have large difference electronegativity values from each other (typically >1.7) (24). Electronegativity is an index of the tendency of an atom to attract electrons toward itself and increases from left to right across the periodic table (25). Therefore, ionic bonds usually occur between metals and non-metals. NaCl, as an inorganic salt, has an ionic bond in which Na (with an electronegativity of 0.9) donates its electron (to become Na^+) and Cl (with an electronegativity of 3) gains the electron (to become Cl^-).

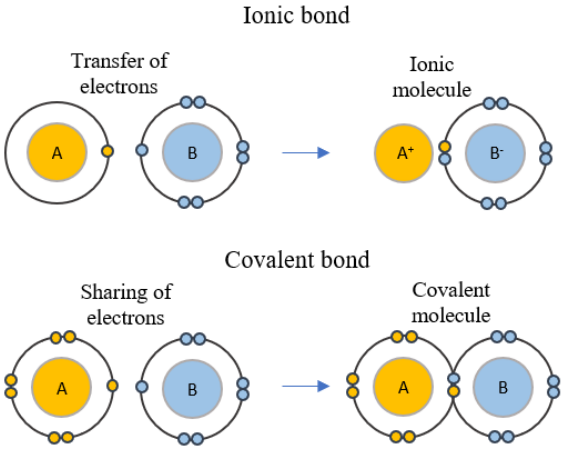

Figure 2.1. Ionic vs covalent bond.

In covalent bonding, electrons are shared equally between atoms. The electrical charge in a covalent bond is evenly distributed between the atoms, so the bond is nonpolar. A covalent bond between atoms with slightly different electronegativity values results in a polar bond. However, the polarity in a polar covalent bond is less than in an ionic bond (23). Although most inorganic salts have ionic bonding, some cases have covalent bonding, such as $ZnCl_2$ (16). Zinc (Zn) with an electronegativity of 1.6 makes the electronegativity difference 1.4 with Cl, which is out of the ionic bonding group. The low melting point of this salt can strengthen covalent bonding (24).

Although organic salts have various applications in life and industry, they are beyond the scope of this study due to their limited thermal stability, low boiling point, and low conductivity.

Inorganic salts play a vital role in normalizing the functions of the human and animal bodies. A wide variety of inorganic salts are used in various applications, such as healthcare, agriculture, and construction (26). However, molten salt is another aspect of salt employment in industry. Molten salt is a salt which melts and becomes a liquid at elevated temperatures. Molten salts have significant technological importance due to their thermochemical properties (27). They are employed in various industries according to their thermochemical properties and prices. Salts have different costs, mostly related to their abounds in nature and production expenses. Generally, some salts (such as metal chlorides) have a relatively low price compared to others (e.g., nitrates and nitrites) because of their abundant natural reserves of them (28).

2.2 Thermochemical properties of molten salt

Melting point

Melting/ freezing point (MP) is one of the most important properties of salt since it marks the minimum temperature for salt utilization in the liquid state. Generally, salts have high melting points, but a mixture of different compositions makes their properties tunable. For example, when a cubic ionic chloride such as sodium chloride (NaCl) (table salt) and KCl with high melting points (>750°C) is mixed with tetrahedral covalent chloride such as Zinc Chloride ($ZnCl_2$) with a lower melting point (290°C) in a particular proportion, a eutectic mixture is formed with a substantially lower melting point around 205°C (28,29). Moreover, the high boiling point of the molten salts provides a wide range of operating temperatures in high-temperature utilizations.

Thermal conductivity

The thermal conductivity of molten salts is a critical property for the efficient design of heat storage technologies. This property is related to heat transfer behavior. Higher values are preferred to achieve higher heat exchange efficiency (30). However, thermal conductivity is a complicated property to measure, since convection and radiation reduce the energy transferred by conduction. Therefore, minimal experimental data is available for molten salts' thermal conductivity, and many methods have been used to estimate thermal conductivity based on simple physical properties, such as melting point, density, and heat capacity (31,32). The mixture of salts generally has less thermal conductivity than the proportional mean of the constituent salts. This is expected due to a general increase in the disorder of the short-range quasi-crystalline lattice of the molten salts with the addition of another salt (33).

Heat capacity

The high specific heat capacity (Cp) of molten salts is a well-known property that makes them the most widely used thermal energy storage (TES) material for high-temperature applications. This property controls the capacity of the temperature rise that can be transferred or stored (30). The Dulong–Petit equation (Eq. 2) is the most common method for estimating the heat capacity for molten salt mixtures (34). For the mixture of alkali and alkaline earth halides, the equation is (35):

$$C_p = n\frac{\sum(x_i N_i)}{\sum(x_i M_i)} \tag{2}$$

where Cp is the heat capacity (cal/g K) of the molten salt mixture, N_i is the number of atoms in each component, M_i is the molecular weight (g/mol) of each component, and x_i is the molar fraction of i^{th} component. n is the heat capacity factor (cal/mol K) which denotes a contribution of n per mol of each atom in the salt mixture, and it is 8 for alkali and alkaline halides. The Dulong–Petit equation is considered a very good approximate prediction of heat capacity in cases where no experimental data are available. However, this equation does not consider the temperature, which can cause inaccuracy for the heat capacities of halide salts, which are highly temperature dependent (34).

Viscosity

The viscosity (η) is an important property that strongly influences the pumping cost in the system. Low viscosity can decrease energy consumption in the process of pumping by reducing friction (36). The viscosity of the strong liquids is calculated using Eq. 3 (37):

$$\eta = A \exp\left(\frac{E_\eta}{RT}\right) \quad (3)$$

Here, A is a constant and E_η is the activation energy. R is the universal gas constant (J/K mol) and T is the molten salt temperature (K).

Molten salts usually have low viscosity at high temperatures. Although the viscosity is measurable by a high-temperature viscometer, there are several models to predict the viscosity of molten salt mixtures (34).

Density

The equation for the density of the molten salt mixture can be expressed as Eq. 4:

$$\rho_m = \frac{1}{\sum \frac{w_i}{\rho_i}} \quad (4)$$

where ρ_m denotes the density of eutectic salt, and w_i and ρ_i denote the mass fraction and density of individual molten salt, respectively (34). Salt density is not fixed, and it varies with salt composition (38).

Thermal stability

The high thermal stability of molten salts is required for many applications to avoid salt decomposition at high temperatures and to make salt recycling possible. Molten salt systems have very different thermal stability. Some mixtures (nitrites) decompose at a temperature above 400°C. The reason for thermal decomposition in the air is the oxidation reaction of nitrite to nitrate (39). The other groups (chlorides, fluorides) are stable at higher temperatures up to 700–800°C (35,40,41).

Vapor pressure

The vapor pressure of the molten salts and the stability of the construction materials in contact with the salt (piping/ containers) are two critical issues for molten salt applications at elevated temperatures (28). Molten salts usually have a neglectable vapor pressure that ensures stable working conditions at high temperatures. Generally, their vapor pressure increases slowly when the temperature increases, and there is a significant increase in vapor pressure at very high temperatures (28).

Solvent capability

Molten salts can act as solvents (for organic and inorganic materials), and some melts have catalytic properties. The high operating temperature of these liquids could cause changes

in the equilibrium of the reactions. Inorganic molten salts have been used in gas chromatography to separate volatile inorganic halides from organic substances (42). These fluids are an efficient solvent for cellulose in a wide range of degrees of polymerization (43). Nitrate mixture eutectics have been employed as a solvent on glass fiber paper (42).

Corrosivity

The high operating temperature of molten salts causes corrosion in metal in contact with the molten salt. This corrosion mode involves the dissolution of an alloying element (setup) at hot spots and the deposition of those elements in cooler spots. Corrosion is also strongly dependent on the temperature and flux velocity of salts (44). Atmospheric air plays a significant role in inducing corrosion in molten salt systems by providing oxygen to the system (28).

2.3 Molten salt categories and their applications

The properties of molten salts have long been of interest for a wide range of applications. Molten salts consist of a large class of fluids (chlorides, fluorides, nitrates, etc.), so they span an extensive range of properties. Salts from the same group usually have similar thermodynamic properties and are used for similar applications. Binary mixtures present a simple eutectic point in their phase diagram, while a decreased melting point is expected when more components are added (45). Table 2.2 shows some important properties of the most common salt mixtures in the different groups.

The 19th century is considered a period of molten salt technology efflorescence. At the beginning of the molten salt applications, they were used to extract metals and isolate alkali metals from their fused hydroxides. The laws of electrolysis using molten salts were discussed at that time. With advances in metallurgical industries in the 20th century, molten salts were widely used for metal preparation and purification. Separating a large amount of uranium using molten salts was an achievement that opened the way for a new approach (5).

Table 2.2. Thermochemical properties of the most common molten salt systems in various groups.

Group	Salt compositions	Melting point (°C)	Decomposition temperature (°C)	Heat capacity (kJ kg^{-1} K^{-1})	Reference
Nitrates-Nitrites	$NaNO_3$:KNO_3 (solar salt)	240	565	1.55 (500°C)	(46,47)
	KNO_3:$NaNO_3$:$NaNO_2$	142	450	1.56 (300°C)	(48,49)
	$NaNO_3$:KNO_3:$Ca(NO_3)_2$	130	450	-	(50,51)
	$LiNO_3$:$NaNO_3$:KNO_3	118	550	1.58	(52)
	$LiNO_3$:$NaNO_3$:KNO_3:$CaNO_3$	93	450	1.51	(53)
Carbonate	$LiCO_3$:$NaCO_3$:KCO_3	397	670	1.61	(54)
Chlorides	KCl:$MgCl_2$	430	>700	0.999 1.02 (500-800°C)	(34)
	$NaCl$:KCl:$MgCl_2$	383	>800		(28,34,55)
	$NaCl$:$MgCl_2$:$CaCl_2$	407	650	-	(56,57)
	$ZnCl_2$:KCl:$NaCl$	204	>800	0.81 (300-600°C)	(15,48,58)
	KCl:$MgCl_2$:$ZnCl$	356	>700	0.866	(59)
Fluorides	LiF:NaF:KF	454	>700	0.98+1.06e-3 T	(41)
	NaF:BF	385	>700	1.51	(60)
	KF:BF	460	>700	1.31	(61)
	KF:ZrF	420	>700	1	(60)

Molten salts have been used as coolants in nuclear and non-nuclear applications, such as fission power plants, fusion, or hybrid reactors, hydrogen production, long-distance heat transport, nuclear fuel reprocessing, chemical industry, oil refineries, and shale oil processing (60,62). In early studies, molten fluorides, such as alkali fluorides, were considered reactor coolants (60), with structural corrosion appearing to be the main issue (63). The high cost of fluorides and high melting points are other considerable problems.

In the 21st century, molten salts have attracted much attention in emerging energy applications, such as solar energy, battery technology, and biofuels. They have a high thermal capacity, making them suitable and safe for energy storage. Molten salts can also conduct heat and electricity due to their high conductivity (64). In the last decades, nitrate,

and nitrite mixtures have been studied as a heat storage medium in concentrating solar power plants. Because nitrites are not stable and oxidize at a temperature higher than 350°C, nitrates attracted more attention (45). Although nitrate salts are employed in many large-scale storage plants, worldwide nitrate salt mines and production are restricted (48). Moreover, there are limited applications to high temperatures, and they decompose at temperatures above 600°C (65).

Chloride salts are promising candidates in high temperatures as an abundant thermal storage medium with a lower cost than nitrates (48,66). However, whereas nitrate salts have been widely studied as heat storage media, chloride salts have received less attention. Nitrate salts have been proposed as sensible storage media, whereas chlorides have mainly been suggested as potential LHS media, and their potential as sensible heat storage has been neglected (6).

One of the earliest studies proposed chloride salts (e.g., NaCl) as a part of a mixture with nitrate salt mixtures (67). Pure chloride salts such as $FeCl_3$ (68) and binary, ternary, and quaternary chloride salts, mainly consisting of KCl, NaCl, CuCl, $MgCl_2$, and $ZnCl_2$, have been studied by many researchers (6). NaCl and KCl are abundant in nature and have a high boiling point. When they mix with low melting tetrahedral covalent chloride, they form an eutectic with a much lower melting point than NaCl or KCl (48). Although molten salts have been investigated in many applications, there is still a lot of interest and potential to study molten salts in new approaches, such as renewable energies, and to improve their functions in developed systems.

2.3.1 Molten salt application in energy sectors

The first use of molten salts in the energy industry was in 1950, when Oak National Laboratory (ORNL) employed molten salts in a nuclear-powered aircraft engine. Four years later, in 1954, ORNL shifted its molten salt focus to nuclear reactors. The high thermal stability of molten salts makes them an interesting fluid in nuclear reactors, since they would not decompose at high temperatures. In the late 20^{th} century, molten salt applications expanded to other renewable energy industries as well as a medium for post-combustion carbon capture, as depicted in Figure 2.2.

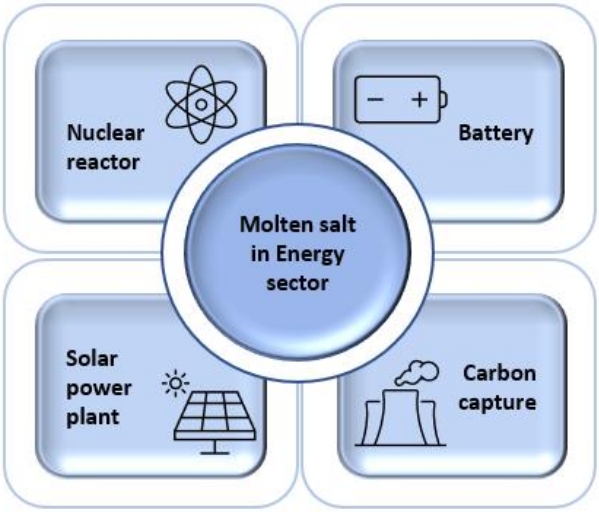

Figure 2.2. Various applications of molten salts in the energy market and industries.

Nuclear reactors

The first molten salt reactor (MSR) built by ORNL was completed in 1954. MSRs engage high-temperature liquid salts as coolants. Liquid fluoride or chloride salts are proposed as primary and secondary salts. According to a report from ORNL (69), the eutectic mixture of LiF:BeF_2 is suitable for MSRs due to its good thermodynamic and neutronic properties.

Solar power plant

The first solar power plant that used molten salts for energy storage was developed in 1993 by Sandia National Laboratories (64,70). Molten salts play the role of both heat storage medium and heat transfer fluid (HTF) in the plant (71). Currently, the molten salts and their eutectic mixtures used in concentrated solar power (CSP) plants are HITEC ternary salt mixture (53:7:40 mol% KNO_3:$NaNO_3$:$NaNO_2$) and binary salt mixture solar salt (60:40 mol% $NaNO_3$:KNO_3) (72). However, many researchers added another nitrate, such as $Ca(NO_3)_2$ and $LiNO_3$ to the solar salt to reach a lower melting point and avoid the risk of solidification (45).

Battery

Molten salt batteries are a category of high-energy density and high-power density batteries that employ molten salts as electrolytes. The first molten salt batteries originated during World War II. In the mid-1960s, rechargeable batteries were introduced, and later, lower temperature molten salt batteries were developed that use $NaAlCl_4$ with Na^+-beta-alumina ceramic electrolyte. These batteries are used as power backups in the telecommunication

industries, oil and gas, and railways. In 2010, sodium/metal halide batteries that used Na-$NiCl_2$ as an electrolyte were introduced.

Carbon capture

Carbon capture in molten salts (CCMS) is based on a similar principle as calcium looping technology (CaL), but the absorption of CO_2 is implemented by the active substances ($CaO/CaCO_3$) dissolved or partly dissolved in molten salts. Rapid gas–liquid reactions enable efficient absorption by dissolving metal oxide as an active substance in a liquid (molten salt). Using molten salts has the advantages of faster reaction kinetics, higher CO_2 sorption capacity, and avoiding solid attrition issues (73).

2.3.2 Molten salt application in biofuels

One of the energy sources that can profit from the advantage of molten salt to enhance production is biofuel. Pyrolysis/hydro-pyrolysis, as one of the most common processes for converting biomass to biofuel, can be more efficient by employing molten salt in the process (11,12). The current study focuses on the molten salt properties that could facilitate it use as a biomass liquefier in biofuel production through hydro-pyrolysis.

Biofuel is one of the primary replacements for fossil fuels to decarbonize the transport sector. According to the International Energy Agency's report, the world's demand for liquid fuels is continuously increasing, as shown in Figure 2.3. Biofuel demand was reduced in 2020, mainly due to mobility restrictions due to the COVID-19 pandemic (74). There is great interest in producing fuel from renewable resources, such as biomass, and several processes have been proposed to produce biofuel from lignocellulosic biomass (75). Pyrolysis and hydro-pyrolysis are among the most common and promising methods for converting low-value lignocellulosic biomass into valuable renewable liquid fuel (76).

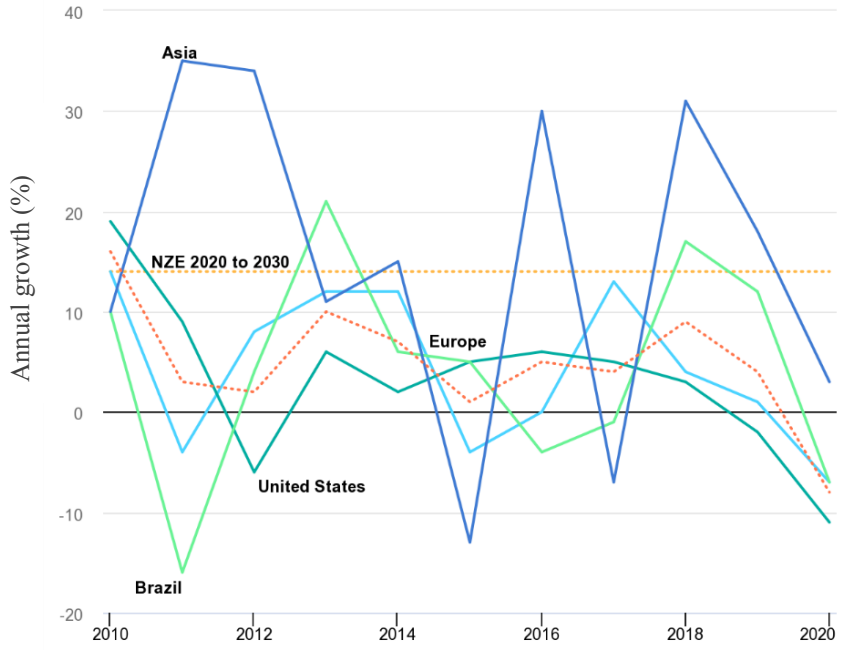

Figure 2.3. Annual biofuel demand growth, 2010-2020 vs. net zero scenario (74).

2.3.2.1 Pyrolysis and hydro-pyrolysis in general

Fast pyrolysis is one of the most promising methods for converting biomass into valuable products. It is the rapid thermal degradation of organic materials in the absence of oxygen at 500–600°C (77). Fast heating causes the decomposition of large biomass molecules into smaller ones. These molecules are released in the form of volatile compounds, which are rapidly cooled to room temperature and form liquid fuels. Although the biofuel production in this process can be up to 75 wt% of the original biomass (the rest is char and permanent gasses CO, CO_2 and CH_4) (78,79), the oxygen content in biofuel is roughly 35–40 wt%. The presence of oxygen not only leads to a higher heating value (HHV) compared to gasoline and diesel but also has high acidity (pH 2–3), which makes it corrosive to construction materials (80). Hydrotreating can be applied to overcome these challenges. This process involves re-evaporating the oil and reacting with H_2 at a very high pressure (100–170 bar) and 310–375°C (81). This process leads to biofuel production of 26–30 wt% of the original biomass. However, this process is expensive and slow (80).

Hydro-pyrolysis is the decomposition of the biomass in the presence of H_2 (82). In hydro-pyrolysis, the released H_2 radicals react with volatiles released from biomass. The oxygen can be removed in the presence of a catalyst and released in the form of water, CO and CO_2

and hydrocarbon is produced (75). One of the advantages of hydro-pyrolysis is that the required pressure for the process is much lower than the pressure needed for hydrotreating (30–50 bar compared to 100–170 bar for hydrotreating). Moreover, the process is exothermic, generating heat that can help sustain endothermal pyrolysis reactions in the reactor (83).

2.3.2.2 Molten salt applications in pyrolysis and hydro-pyrolysis

In the late 20th century, molten salts were employed to develop biomass pyrolysis in a few studies. The results showed that using molten salts could improve the yield production of, for example, phenolic compounds (84,85). This indicates that molten salts could have catalytic effects. Another possible advantage is that the heating rate of biomass particles in molten salts is higher than in an inert atmosphere (86) or in a fluidized sand bed (87). Some challenging technical issues remain unresolved regarding the pyrolysis reactor, such as feeding the solid biomass into the reaction unit. The complexity of this increases for high-pressure reactors, such as hydro-pyrolysis, includes problems such as plugging, clogging, leakages, and uneven flow, which lead to low production rates and poor product quality. Liquifying biomass before feeding it into the high-pressure pyrolysis reactor can resolve the aforementioned problems, which were examined through the ABC-Salt project. It can facilitate the pumping of biomass and thus give better control of the feeding system.

Molten salts are considered promising biomass liquefiers because they can maximize the liquid fraction in the fast pyrolysis process downstream. Other advantages of employing molten salts are the solubility of biomass in molten salts (88), the high thermal conductivity of the molten salts, and the possibility of using solar energy to heat and melt the salt. The molten salt is also a heat carrier and a possible catalyst in the following up hydro-pyrolysis step (84). Additionally, they have favorable transport properties, such as low viscosity, leading to the rapid enclosing of the biomass particles (5). Molten salts can be recycled after removing char and ash. The salt criteria for biomass liquefaction are, in many ways, similar to those for high-temperature phase change materials (PCM) for thermal energy storage. Favorable properties of a proper fluid include high heat capacity, high conductivity, low vapor pressure, high boiling point, low viscosity, and low cost (28,60).

3 Rationale behind case study properties

This chapter provides supplementary information, which is essential to explaining the case study. In Chapter 3.1, the theoretical background of $ZnCl_2$:KCl:NaCl and KCl:CuCl molten salt systems is discussed to explain the reason for selecting them for thermodynamic properties investigation in the current study. Chapter 3.2 mostly explains how the specific impurities were selected for study in the purification step. The last subchapter covers the theoretical background of the modeling technique employed in this study.

3.1 Choosing the proper molten salt for ABC-Salt

Among all the molten salt groups, chlorides have the most essential properties for biomass liquefaction, including low melting points and high thermal stability. Although many chlorides have been investigated in the literature for several applications, an eutectic mixture of $ZnCl_2$, KCl and NaCl is one of the most promising candidates for the present purpose, which is discussed in **Paper I**. This ternary mixture is non-toxic, non-flammable, has a melting point around 200°C, and is stable at even higher temperatures compared to other ternary mixtures (89). NaCl and KCl are available in large amounts. They have high heat capacities and low vapor pressures but too high melting points (>750°C) for this purpose. However, a cubic ionic chloride mixture such as NaCl or KCl with tetrahedral covalent chloride such as $ZnCl_2$ with a lower melting point in a particular proportion forms a eutectic mixture with a substantially lower melting point (28,29). All three single salts ($ZnCl_2$, KCl, and NaCl) and their mixtures have high stability even at high temperatures. Low vapor pressure (<1 atm) at high temperature (up to 800°C), low melting point (~200°C), high thermal conductivity, high heat capacity, low corrosion rate, and high boiling point have been reported for different compositions of the salt mixture (28,29,90–93). These results and the promising results in pyrolysis studies and thermal storage studies (28,84–87,89,90) make $ZnCl_2$:KCl:NaCl a promising candidate for the present study. Four compositions of the $ZnCl_2$:KCl:NaCl ternary system were chosen for experimental investigation, as described in Table 3.1.

The second alternative salt mixture was KCl:CuCl due to its relatively low melting point, as presented in **Paper II**. Very few studies have explored this binary system. In early studies, Sandonini showed the eutectic of binary KCl:CuCl at 66 mol% CuCl, with a melting point of 136°C (17). Fontana et al. studied the same composition as the eutectic mixture and reported an eutectic temperature of 150°C (94). In a later work, Etter et al.

(17) investigated a composition containing 66.7 mol% CuCl and presented this as a eutectic mixture with a melting point of 150°C. They reported that the low melting point gives a wide liquidus range, and no indication of decomposition was observed up to 800°C for 96 h. Etter et al. also reported that this binary system has low viscosity (17). Three compositions of the KCl:CuCl binary system close to the reported eutectic composition were selected for further study in **Paper II** (see Table 3.1)

Different binary eutectic systems of pure salts have been modeled using FactSage, but the lack of measured properties and experimental data for many of these systems is a distinct challenge (6). There is very little information about binary KCl:CuCl as a molten salt system, and more investigation needs to be performed. The only available phase diagram for this binary system was generated based on experimental data without calculating thermodynamic parameters. To study this binary system in depth, **Paper II** assessed the thermodynamic parameters and regenerated the phase diagram using FactSage.

Table 3.1. Compositions and the theoretical melting point of three eutectic molten salts of $ZnCl_2$:KCl:NaCl, and KCl:CuCl.

Chemical formula	**$ZnCl_2$**	**KCl**	**NaCl**	**CuCl**	**References**
Molar mass (g/mol)	136.32	74.55	58.44	98.99	(91)
Melting point (°C)	318	776	801	422	(95)
Boiling point (°C)	732	1420	1413	1490	(91)
Density (g/cm^3) at the melting point	2.38	1.52	1.55	3.75	(95)
Viscosity (cp) at the melting point	40	50	17	104	(37,95)
Molar fraction (wt%) of studied compositions					**Experimental melting point (°C) in literature**
Salt #1	60	20	20	-	203 (91)
Salt #2	59.5	21.9	18.6	-	199 (89)
Salt #3	52.9	33.7	13.4	-	210 (89)
Salt #4	44.3	41.9	13.8	-	199 (89)
Salt #5	-	32	-	68	151 (17)
Salt #6	-	34	-	66	150 (17)
Salt #7	-	36	-	64	151 (17)

3.2 Molten salt purification

In the majority of the molten salt applications mentioned above, the melt is in contact with other materials, which can lead to contamination. Some of these impurities are introduced to the salt during the process (ash/char formed from biomass in the current case), while others are the product of molten salt application (corrosion products from the salt's interaction with alloying elements) (96). The contaminants in the molten salts can change the salt's thermophysical properties, such as heat capacity and thermal conductivity. Some impurities can act as catalysts, leading to more corrosion in the system (97). Moreover, in many processes, the molten salt needs to be recycled and reused many times. Therefore, molten salt purification and removal of impurities are critical concerns for molten salt applications.

Electrochemical removal is an effective method that can be used to separate impurities and purify molten salt (98). Electrolysis in molten salts has been used to recover metals from ores (99,100) and later to remove elements from various molten salt systems (101–105). Cyclic voltammetry (CV) is an electrochemical technique employed in **Paper III** to investigate the reduction and oxidation processes of molecular species. The reduction potential of each element can be detected using this method, and the impurities can be reduced by electrodeposition (98). More details of the theoretical background can be found in **Paper III**.

In the ABC-Salt project, after leaving the hydro-pyrolysis unit (Figure 1.1), the spent molten salt (Salt #4 from **Paper I**) can be contaminated by biomass char/ash or corrosion products. Thus, it needs to be purified before recycling it back into the system. According to internal communication in the ABC-Salt project (106), the most probable impurities in the spent molten salt are compounds, including elements such as calcium (Ca), potassium (K), odium (Na), magnesium (Mg), aluminum (Al), manganese (Mn), zinc (Zn), iron (Fe), and copper (Cu). The reaction potential of these elements with respect to the standard hydrogen electrode is presented in Table 3.2. These data have been used to compare their electrode potential under standard conditions and to establish the electrochemical window vs. the proposed electrode for the interested system.

The main concern of the electrolysis process is removing impurities without decomposing molten salt. Therefore, finding the electrode potential of the molten salt species is the first step. Among Zn^{2+}, K^{+} and Na^{+}, which are the molten salt cations, Zn^{2+} has less negative electrode potential values, meaning that it is the most easily reduced element. By contrast, Cl^{-} has the most positive electrode potential value. The electrode potential values of Zn^{2+} and Cl^{-} therefore define the electrochemical window, meaning that theoretically, it is only

possible to remove the elements that have their electrode potential within the window without salt decomposition.

Table 3.2. The reduction potential of elements with respect to the standard hydrogen electrode (19).

Half reaction	$\boldsymbol{E^0/V}$	**Electrodeposition possibility (theoretically)**
$Ca^+ + e \leftrightarrow$Ca	-3.8	Impossible
$K^+ + e \leftrightarrow K$	-2.931	Salt species
$Na^+ + e \leftrightarrow Na$	-2.71	Salt species
$Mg^{2+} + 2e \leftrightarrow Mg$	-2.372	Impossible
$Al^{3+} + 3e \leftrightarrow Al$	-1.662	Impossible
$Mn^{2+} + 2e \leftrightarrow Mn$	-1.185	Impossible
$\boldsymbol{Zn^{2+} + 2e \leftrightarrow Zn}$	**-0.762**	**Salt species**
$Fe^{2+} + 2e \leftrightarrow$Fe	-0.447	Possible
$Fe^{3+} + 3e \leftrightarrow Fe$	-0.037	Possible
$Fe^{3+} + e \leftrightarrow Fe^{2+}$	0.771	Possible
$Cu^+ + e \leftrightarrow Cu$	0.521	Possible
$\boldsymbol{Cl_2(g) + 2e \leftrightarrow 2Cl^-}$	**1.358**	**Salt species**
$Mn^{3+} + e \leftrightarrow Mn^{2+}$	1.542	Impossible

Figure 3.1 shows the cyclic voltammogram of $ZnCl_2$ (15). At a lower potential, the sharp increase of cathodic current defines the nucleation process of the electroreduction of metal (Zn), which can be attributed to the deposition of Zn. On the other side of the electrochemical window, anodic current is observed, which is considered to be chlorine gas evolution. In the figure, the proposed elements in Table 3.2 are added to the voltammogram according to their electrode potential to show the possibility of impurity removal from the salt. **Paper III** assessed the removal possibility of these elements (introduced from CuCl, $FeCl_2$ and $FeCl_3$) from Salt #4. Although Mn^{2+} and Mn^{3+} are out

of the electrochemical window, the possibility of Mn^{4+} removal was assessed by adding MnO_2 to the molten salt[1].

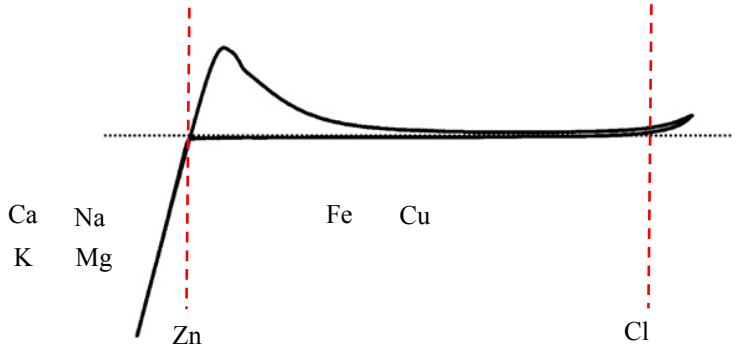

Figure 3.1. Schematic cyclic voltammogram of $ZnCl_2$ and some elements that can locate inside or outside the electrode potential window (15).

3.3 Modeling the salt mixture phase diagram

Calphad modeling of the binary KCl:CuCl molten salt and the liquid solution of hydrolyzed KCl is another part of this study (**Papers II** and **IV**). The Calphad (calculation of phase diagrams) method is a very important method for thermodynamic modeling and generation of the phase diagram for multicomponent systems. The method is based on a semi-empirical approach and requires a reliable basic amount of experimental data for modeling and describing thermodynamic properties. Such data allow extrapolation of the phase diagram and thermodynamic properties to regions where no experimental data are studied/available and more complicated systems (107).

Calphad is a sequential method, starting from simpler systems to more complicated cases. The temperature-dependent Gibbs energy for the various crystallography of the elements is required for phase diagram calculations. This is followed by reliable experimental data for binary systems. These data need to cover both the thermodynamic properties of the individual phases (e.g., heat capacity, enthalpies of formation or mixing, etc.) and the phase equilibria (e.g., transition temperatures, compositions, etc.). During the assessment, the

[1] The reduction potential of Mn^{4+} has not been found in literature.

Gibbs energies of the intermediate phases also needed to be modeled to determine the solubility of the elements in various phases. Consequently, the interaction parameters can be modeled for the defined system, which can predict the phase diagram.

The Gibbs free energy expression contains three parts for the liquid phase model, which can be written as Eq. 5.

$$G_m(T, x_i) = G^{ref} + G_{mix}^{ideal} + G^E \tag{5}$$

where G^{ref} is the contribution from pure components of the phase to the Gibbs energy, G_{mix}^{ideal} is the ideal mixing contribution, and x_i is the mole fraction of component i. G^E is the contribution due to non-ideal interactions between pure components, also known as the Gibbs excess energy of mixing. G^E is the most important parameter for representing the interaction of components, except for the entropy value increase contributed by the ideal mixture. G^E has several kinds of mathematical expressions that represent the interactions between constituents. The Redlich–Kister (RK) model is one of the most common models for binary systems (108), and it has been employed by the expression as Eq. 6:

$$G^E = x_{KCl}x_{CuCl}\sum_{\upsilon=0}^{n_{ij}} L^{(\upsilon)}(T))(x_{KCl} - x_{CuCl})^{\upsilon} \tag{6}$$

$L^{(\upsilon)}$ ($\upsilon = 0, 1, 2, \ldots$) are the RK interaction parameters between the two end members (109). It can be written in general form as a function of temperature in Eq. 7:

$$L_{ij}^{\upsilon} = A + BT + Ct\ln T + DT^2 + ET^3 + F/T \tag{7}$$

where A, B, C, D, E and F are constant parameters usually obtained through empirical or semi-empirical methods. A single parameter will always give a symmetrical contribution to the Gibbs energy of excess; thus, at least two RK coefficients are needed to describe a subregular solution. The composition dependence of the excess enthalpy is described by A and the excess entropy by B (109), which are considered and optimized in **Papers II** and **IV**.

The assessed thermodynamic data for binary or ternary systems were collected as thermodynamic databases in a proper software package that allows the prediction of properties and theoretical calculations for multicomponent systems in various compositions and conditions. FactSage has a vast database and calculation and manipulation modules, making it a powerful software for thermodynamic modeling (110). FactSage V.7.2 was applied in this study to set up the database and calculate the phase

diagrams. The in-house tool DataOptimizer (111) has been employed to optimize the parameters based on the experimental data.

Paper II models the thermodynamic properties of the KCl:CuCl molten salt system and generates a binary phase diagram for further theoretical studies. **Paper IV** used Calphad techniques to model the liquid phase of a hydrolyzed chloride solution. KCl has the most reliable and extended experimental data available in the literature, among other chloride systems studied in the current work. Therefore, the KCl–K_2O–HCl–H_2O reciprocal system was selected for this modeling. The thermodynamic parameters involved in the excess terms of the Gibbs energy phases were optimized considering the experimental data available from the literature. The phase diagrams and model parameters were derived from thermodynamic optimization.

4 Materials and Methods

This chapter describes the experimental conditions and setups for **Papers I–III**. **Paper II** is a collaborative paper, and the parts of the experiments performed by DLR[2] in Germany are not described here. **Paper IV** is based on modeling and simulation and does not include any experimental work.

4.1 Salt preparation

It was necessary to pre-dry the chemicals to remove residual crystal water due to the hygroscopic nature of the salts. The salts employed in the experiments, including $ZnCl_2$ (VWR, 98.3%), KCl (Sigma, ≥99.5%), NaCl (Sigma, ≥99.8%), and CuCl (VWR, ≥ 95%) were dried and kept in a heating cabinet at 200°C for at least 24 h in separate and closed beakers (see Figure 4.1). The dried salts were mixed mechanically to obtain the specific compositions listed in Table 4.1.

Figure 4.1. Beakers containing different salts kept inside the heating cabinet at a temperature of 200°C.

[2] Partner in ABC-Salt

*Table 4.1. Composition of the salts used for the experiments in **Papers I–III.***

Salt		Composition (mol%)	Paper
Salt #1	$ZnCl_2$:KCl:NaCl	60:20:20	I
Salt #2	$ZnCl_2$:KCl:NaCl	59.5:21.9:18.6	I
Salt #3	$ZnCl_2$:KCl:NaCl	52.9:33.7:12.4	I
Salt #4	$ZnCl_2$:KCl:NaCl	44.3:41.9:13.8	I, III
Salt #5	KCl:CuCl	32:68	II
Salt #6	KCl:CuCl	34:66	II
Salt #7	KCl:CuCl	36:64	II

The salts were in powder form at room temperature, and they were melted at elevated temperature under an inert atmosphere before starting the experiments.

4.2 Adding other chemicals

Although the salts listed in Table 4.1 are the main chemicals for the experiments, other chemicals were added to the salt mixture at different stages to investigate their effects on the molten salt characteristics in some experiments.

In **Paper I**, ZnO (Alfa Aesar, 99%) was added to $ZnCl_2$:KCl:NaCl (Salt #1: 60:20:20 mol%) at the stage of preparing the salt mixture to investigate its effect on the hydrolysis of the salt.

In **Paper III**, multiple chemicals were added to $ZnCl_2$:KCl:NaCl (Salt #4: 44.3:41.9:13.8 mol%) at high temperatures to investigate the removal of impurity elements by electrodeposition from the salt. The chemicals CuCl (VWR, ≥95%), $FeCl_2$ (Thermo Fisher, ≥99.99%), $FeCl_3$ (Sigma, ≥99.9%) and MnO_2 (Thermo Fisher, ≥99.9%) were added to the molten salt at 260°C in separate experiments.

4.3 Inert gas

All experiments were carried out in an inert atmosphere. Nitrogen (N_2) or argon (Ar) was bubbled through the molten salt in all experiments to remove residual water molecules from the molten salt and deoxygenate the melt. This procedure also helped to provide a homogeneous mixture of the molten salt (or molten salt and added chemicals) before starting the experiments. During the experiments, an inert gas flowed from the bottom or

top of the experimental setup to provide an inert atmosphere. The gas compositions used for the experiments were Ar (AGA, ≥99.99%) and N_2 (AGA, ≥99.999%).

4.4 Experimental setup and procedure

Four different setups were used for experimental work in **Papers I, II,** and **III**. The thermodynamic properties of four compositions of $ZnCl_2$:KCl:NaCl and three compositions of KCl:CuCl, including melting point, thermal stability, and hydrolysis, were investigated in **Papers I** and **II**. The most promising composition concluded from **Papers I** and **II** was chosen for further purification studies by electrolysis in **Paper III**.

All experiments were carried out at ambient pressure. An S-type thermocouple was employed to measure and control the temperature. Temperature calibration is necessary to minimize the systematic errors of the thermocouple. The thermocouple was calibrated using deionized ice and water, deionized boiling water, pure tin (Sn) (Aldrich, ≥99.8%) and pure Zn (Sigma, ≥99.9%). The measured temperatures were calibrated according to Table 4.2 using linear regression.

Table 4.2.Standard and measured calibration points for S-type thermocouple.

Sample	Deionized ice+water	Deionized boiling water	Pure tin	Pure zinc
Calibration point (°C)	0.0	100.0	231.9	419.5
Measured value (°C)	0.06	97.9	231.2	417.1
Relative error	-	2.1%	0.3%	0.57%

4.4.1 Melting point experiments

The melting points of the selected salt mixtures were measured experimentally using the cooling curve method described by Rahman et al.(112). A total of 120 g of the dry salt mixture was placed inside a nickel crucible (5.7 cm height and 6.1 cm inner diameter) and heated up to 250°C (in **Paper I**) and up to 170°C (in **Paper II**) in a vertical electrical resistance furnace to ensure complete melting. To minimize heat loss, the crucible was equipped with nickel radiation shields on top (see Figure 4.2). The molten salt was mixed for at least 1 h using a mechanical nickel stirrer (40 rpm) to ensure a homogenous mixture. The salt mixture was then cooled down slowly at a rate of 0.3 or 0.5°C/min. In some cases in **Paper I**, 0.1–0.15 g of a solid salt crystal ($ZnCl_2$:KCl:NaCl) was added to the molten salt right before solidification occurred to control undercooling. The cooling curve experiments were repeated several times by heating up the solidified salt and cooling it down again for each composition.

Figure 4.2. Experimental setup for the determination of melting points. The sample was placed in a nickel crucible and underwent controlled cooling under constant stirring. The experiments were performed under an inert atmosphere (Ar).

4.4.2 Thermal stability experiments

Thermogravimetric analysis (TGA) was performed to compare the thermal stability of all four compositions in **Paper I** and three compositions in **Paper II** as a function of temperature up to 500°C. For this purpose, 235 g of the dried salt mixture was prepared and compressed in a tubular nickel crucible (17 cm height and 5.1 cm inner diameter). The crucible containing the salt was suspended from a weight scale (MS8001S, Mettler Toledo, accuracy of 0.1 g) located above the furnace, as shown in Figure 4.3. The salt mixture was heated up to 500°C at a heating rate of 10°C/min and the weight change was recorded continuously with a sampling rate of two seconds during the experiments. LabView 8.2 (National Instrument) was used to monitor and record any weight changes, presenting the mass loss.

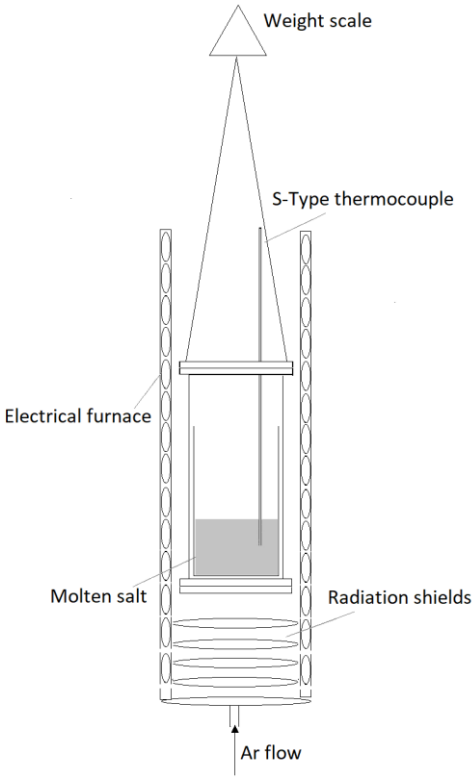

Figure 4.3. Schematic representation of the experimental setup for the TGA studies. The setup is hung from the weight scale, which records the weight. The temperature was measured using a type S thermocouple.

4.4.3 Hydrolysis experiments

Chlorides are widely used in many industries, and their hydrolysis is still a challenge. They are hygroscopic and have a high tendency to react with water to form highly corrosive acid HCl and metal oxide (96). To test whether the hydrolysis reactions occurred with the chlorides in this study, a series of hydrolysis experiments were performed in the setup depicted in Figure 4.4.

A total of 235 g of dried salt mixture was prepared in a nickel crucible, similar to the TGA experiment. The crucible was placed inside a sealed stainless steel vessel. The salt mixture was heated under an inert atmosphere (Ar flow) up to 230°C for the $ZnCl_2$:KCl:NaCl mixture in **Paper I** and up to 170°C for the KCl:CuCl mixture in **Paper II**. N_2 was bubbled through the molten salt for at least 12 h at a rate of 0.2 Nl/ min to ensure homogenous melts with no crystal water.

The salts were heated up, and the hydrolysis experiments started at 250°C. $H_2O(g)$ was added by bubbling 0.4 Nl/min N_2 through a closed, water-filled vessel. The water temperature was kept constant at a temperature of 46°C to ensure a water partial pressure of 10 kPa (10 vol%) (113). The gas consisting of N_2 and water vapor was then introduced to the melt through a nickel tube (diameter (d): 13 mm) placed one centimeter above the bottom of the molten salt (see **Papers I** and **II** for more details). Thus, the gas was released to the volume above the salt and left the sealed vessel through the stainless steel exhausting tube on top of the vessel. The exit gas was filtered using a high-voltage electrostatic filter (3–6 kV) to remove possible particles entrained in the gas stream. Finally, the filtered gas was continuously monitored by Fourier transform infrared spectroscopy (FTIR) at intervals of 50°C up to 500°C. The melt was kept at each temperature interval for at least 30 min to ensure the accuracy of the HCl level. The whole setup used in the lab is shown in Figure 4.5.

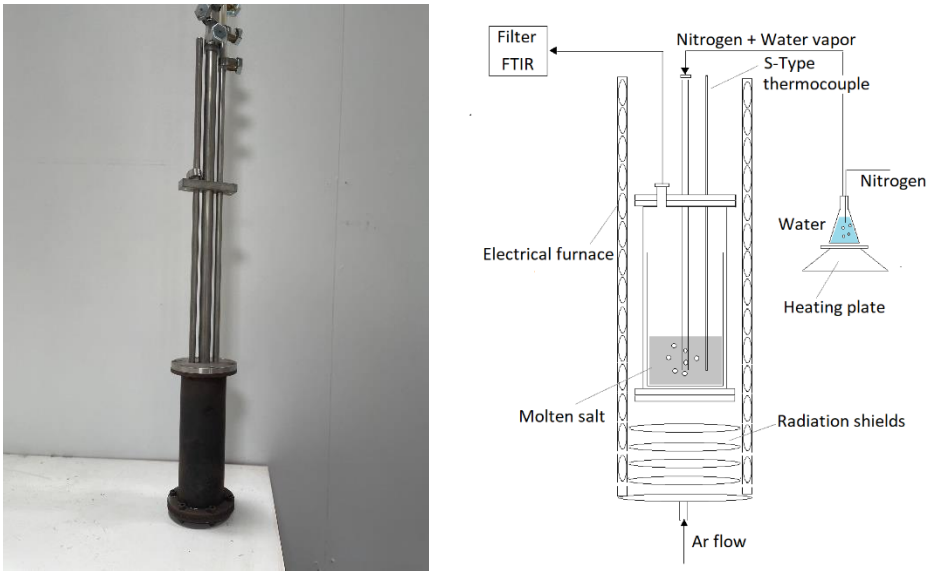

Figure 4.4. Experimental setup for hydrolysis studies. The inner crucible and feed tube are made of nickel, and the outer container is made of stainless steel.

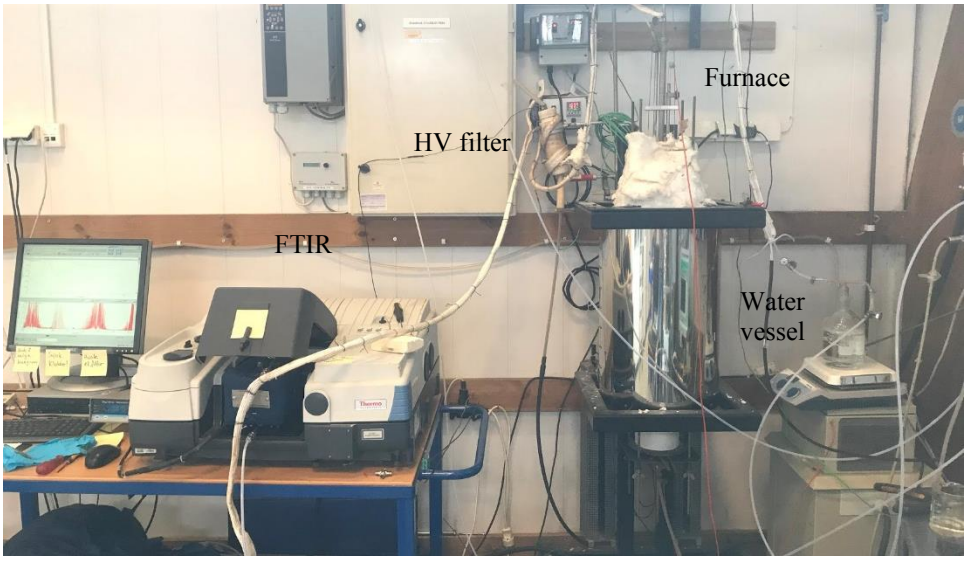

Figure 4.5. The entire experimental setup for hydrolysis investigation included furnace, high voltage filter, FTIR, water vessel, etc.

To investigate the effect of metal oxide on hydrolysis, the salt with the highest hydrolysis rate (Salt #1: $ZnCl_2$:KCl:NaCl, 44.3: 41.9:13.8 mol% in **Paper I**) was chosen as a suitable candidate. Two different amounts of dried ZnO powder, namely 5 wt% and 10 wt %, were added to the salt mixture at the stage of mixing the salt, and the same procedure was carried out for both ZnO concentrations.

4.4.4 Electrolysis experiments

According to the results from **Papers I and II**, the most promising salt mixture (Salt #4: $ZnCl_2$:KCl:NaCl mixture, 44.3–41.9–13.8 mol%) was chosen for further study. The selected salt mixture is a candidate for liquefying biomass and transferring it to the hydro-pyrolysis unit (500℃ and 30-50 bar) in the ABC–Salt process. The molten salt can be contaminated by ash/ char from the biomass conversion process. Therefore, the impurity elements need to be removed from the spent molten salt. In this study, electrolysis was employed to investigate the purification of the salt.

In total, 235 g of $ZnCl_2$:KCl:NaCl mixture (Salt #4) was prepared in a graphite crucible (12.5 cm height, 9.5 cm outer diameter, and 6.5 cm inner diameter) (shown in Figure 4.6) and located in the furnace where the salt mixture was heated to around 260℃. Ar was bubbled through the molten salt for at least 12 h. Then, 2 g of the impurity (in the form of CuCl, $FeCl_2$, $FeCl_3$, or MnO_4) was added to the molten salt, and Ar was bubbled at the

bottom of the mixture to stir the mixture for 1 h. During the experiments, the Ar flow was kept above the melt in the crucible to provide an inert atmosphere.

Figure 4.6. Crucibles used in different experiments from the left side: nickel crucible for melting point experiments, nickel crucible for TGA and hydrolysis experiments, and graphite crucible for electrolysis experiments.

CV and chronoamperometry were performed using an electrochemical measurement system (Autolab, PGSTAT302N) and controlled using Nova software version 2.1 for Windows. A graphite rod (6 mm diameter) and a Zn rod (3 mm diameter) were used as the working electrodes in CV and potentiostatic electrolysis, respectively. The reference electrode was a platinum (Pt) wire (0.5 mm diameter). The graphite crucible functioned as a counter electrode. The S-type thermocouple was located just above the molten salt surface during the experiments (see Figure 4.7).

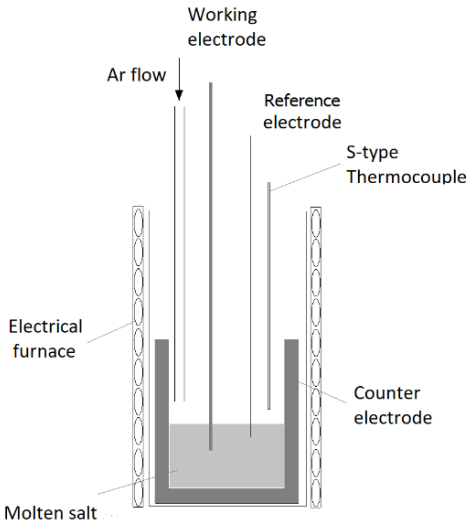

Figure 4.7. Schematic of the experimental setup for electrochemical salt purification using a graphite crucible as the counter electrode, Pt wire as the reference electrode, and graphite rod or Zn rod as the working electrode.

Electrolysis of the molten salt was carried out in four stages for each experiment:

1. CV was conducted before adding the impurities to analyze the pure salt mixture and detect the peaks related to the salt elements.
2. CV was conducted after adding the impurity to detect the new peak related to the impurity.
3. Potentiostatic electrolysis was performed using chronoamperometry to extract the impurity from the molten salt by applying constant potential.
4. CV was conducted after removing the impurities to assess the removal possibility and to compare the voltammograms before and after electrodeposition.

In step 3, after a time between 30 min and a few hours, the electrolysis was terminated, and the working electrode was removed from the melt. Then, the impurities attached to the working electrode were extracted from the molten salt. The applied potential value for each electrodeposition run was adjusted according to the cathodic peak in the cyclic voltammogram before a new run, as suggested by Kim et al. (98). This phenomenon is caused by a shift in the reference electrode potential, which in the present study is Pt.

The temperature was kept at 260°C for all experiments to ensure the liquid state of the salt. For every experiment with a new impurity, a newly prepared salt mixture was used. To minimize the ohmic drop in the CV, a slow scan rate was selected (20 mV/s). Moreover, a

short distance (1 cm) between the working and reference electrodes was kept during the experiments, as suggested by Saveant, and Oldham and Stevens (114,115). The geometric area of the graphite working electrode in contact with the molten salt was 3.8 cm^2 and the counter electrode was 94.4 cm^2.

The deposited compound from the third stage was analyzed using X-ray diffraction (XRD) (Bruker D8 Advance) to characterize the elements. However, the results for only one case (CuCl and molten salt) are presented because the results from the other cases show a lot of noise, which makes them difficult to interpret. This is probably because of the rapid oxidation of Fe and the presence of various ferric oxides.

4.5 Modeling

Apart from the experimental research, modeling studies were carried out to support the experimental results, particularly for hydrolysis studies. The modeling studies were in collaboration with GTT technologies in Germany through an exchange study during the PhD period. For all assessments, the FactSage software V.7.2 (110) and the in-house tool DataOptimizer (111) were used.

The phase diagram for the ternary system $ZnCl_2$:KCl:NaCl studied in **Paper I** was available from the literature (91), and the thermodynamic parameters were calculated for the system; however, no thermodynamic parameters were calculated for the binary KCl:CuCl system. Although there is a phase diagram for this system in the literature based on experimental data (17), no database was found for this solution. The experimental data, including liquidus temperature, eutectic temperature and composition, peritectic temperature, and melting enthalpy (assessed by DLR), which are reported in **Paper II,** were adopted to assess the calculation results in the binary phase diagrams. First, the related interaction parameters were determined, and then the binary system was optimized by employing the Redlich–Kister expression. The first and second terms of interaction parameters (L_i; i=0, 1) were optimized by using experimental results from liquidus line and eutectic in the wide temperature and composition ranges, as well as the accurately measured melting enthalpy. For the intermediate compound K_2CuCl_3 in the KCl:CuCl system, the standard entropy was optimized as well, while the enthalpy of formation was fixed, as shown in Table 5.3.

Paper I presents the experimental results of $ZnCl_2$:KCl:NaCl hydrolysis at an atmospheric pressure of up to 500°C. However, the operation pressure in the hydro-pyrolysis unit in the ABC-Salt project can be increased to 50 bar, which was not possible to examine in NMBU's laboratory. Thus, the FactSage employed and the FactPS and Factsalt databases were used to simulate the effect of increasing pressure on HCl formation.

Moreover, the effect of adding metal oxide to the molten salt was studied experimentally in **Paper I**. However, there is no database for the thermodynamic modeling of a liquid solution with chlorides and oxides over the complete composition space. To study the hydrolysis of chlorides and the effect of their oxide in the system, KCl was selected to be modeled in the solution together with water and its oxide (K_2O). For KCl, the hydrolysis reaction is given in Eq. 8.

$$2\mathrm{KCl} + H_2O \leftrightarrow 2HCl + K_2O \quad (8)$$

Generally, all the components in Eq.8 could be dissolved in the liquid solution and make a KCl–K_2O–HCl–H_2O reciprocal system which needs to be studied. However, because of the limited stability of K_2O, no experimental data for K_2O–KCl or K_2O–KOH was found from the literature, and it is assumed that it has an ideal contribution to the liquid solution, but its properties (standard enthalpy and entropy) are included. Therefore, KOH was added to the solution as an associate in the solution with the non-ideal contribution, and the complete system KCl–KOH–HCl–H_2O can be described as shown in Figure 4.8.

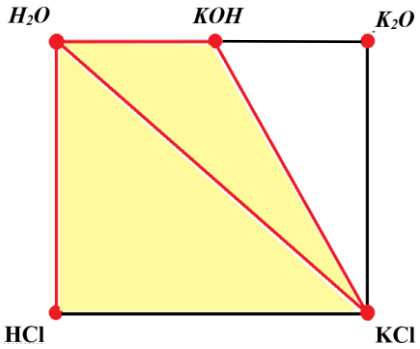

Figure 4.8. KCl–K_2O–HCl–H_2O reciprocal system using an associate solution model. Red lines: assessed quasi-binary systems; yellow area: composition space covered.

The order of the assessment was to first optimize the H_2O–KCl system with two end members in the liquid phase, H_2O and KCl. After optimizing all binary systems, H_2O–KCl was reassessed with five end members in the liquid phase, including H_2O, KCl, HCl, K_2O and KOH. Therefore, the optimized binary systems are H_2O–HCl, H_2O–KOH, KOH–KCl and finally H_2O–KCl. The data for the pure components of the liquid phase were taken from the Fact Pure Substances database. To maintain consistency, the data for pure solid KCl and CuCl were also adopted from the same source. The model parameters for the H_2O–HCl, H_2O–KOH, KOH–KCl and H2O–KCl binary systems were determined using various

types of thermodynamic data, that is, vapor pressure, solubility in water, melting, and boiling point, and heat capacity of the solution collected from the literature. The interaction parameters between components in every binary system in the liquid phase, including the first and second term ($A + B \cdot T$) of L^0 and L^1, were optimized, as reported in Table 5.3.

5 Results and Discussion

In this chapter, the most important outcomes from the experimental work (**Papers I–III**) and thermodynamic modeling work (**Papers II and IV**) are presented and discussed. The thermodynamic properties of the ternary system $ZnCl_2$:KCl:NaCl (**Paper I**) and the binary system KCl:CuCl (**Paper II**) were studied and compared. **Paper III** chose the most promising molten salt system from the first two papers for further purification studies, and the results from molten salt electrolysis are discussed in the current chapter. Moreover, the modeling results for HCl formation vs pressure, the thermodynamic modeling for generating the phase diagram for KCl:CuCl (**Paper II**), and the thermodynamic modeling of phase equilibria in the KCl–K_2O–HCl-H_2O reciprocal system (**Paper IV**) are presented and discussed.

5.1 Thermodynamic properties

The main aim of **Papers I** and **II** was to find the most promising salt mixture for the ABC-Salt process based on the thermodynamic properties that could make it suitable as a biomass liquefier. Melting point, thermal stability, and hydrolysis were the main properties that were studied for four compositions of $ZnCl_2$:KCl:NaCl and three compositions of KCl:CuCl.

Figure 5.1 presents three repetitions of the cooling curves for Salts #1 and 4 from the ternary system and Salts #5 and 6 from the binary system as some examples. The undercoolings represent the melting points of the salt mixtures. The cooling curves for the other salts showed similar trends but with other observed melting points (see Table 5.1).

Figure 5.2 presents the average value of the measured melting points of all seven compositions before and after calibrations of the thermocouple. Salts #1–4 (ternary $ZnCl_2$:KCl:NaCl) show similar melting point in the range of 202–205°C except for Salt #3, which had a slightly higher melting point around 212°C. Salts #5–7 (binary KCl:CuCl) exhibited much lower melting points around 146°C. Although the binary system had a lower melting point, the ternary system is still an interesting option as a biomass liquefier, since the acceptable melting point is around 200°C in the ABC-Salt project.

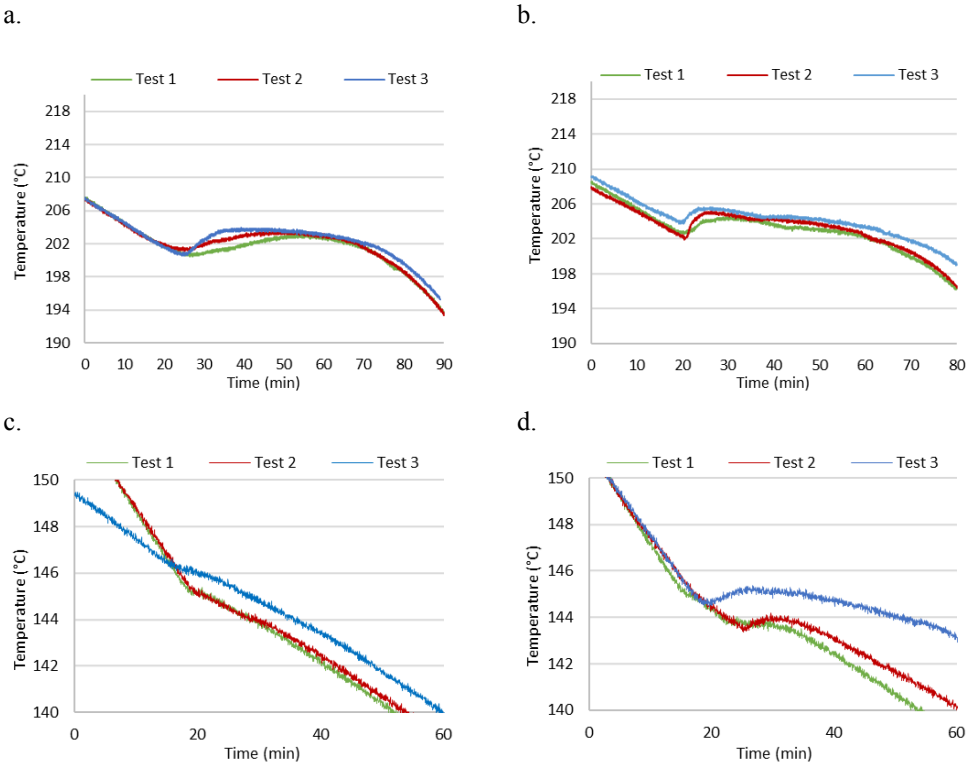

Figure 5.1. Cooling curves for the molten salts, including (a) Salt #1 (60:20:20mol%), (b) Salt #4 (44.3:41.9:13.8mol%), (c) Salt #5 (32-68mol%), and (d) Salt #6 (34:66mol%). For a and b, 0.1–0.15 g of solid salt crystal was added right before solidification to smooth the undercooling.

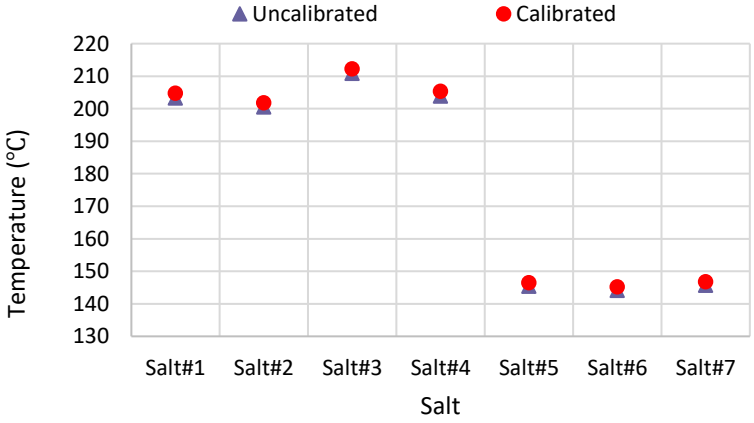

Figure 5.2. Experimental melting points for four compositions of $ZnCl_2$:KCl:NaCl (Salts #1–4) and three compositions of KCl:CuCl (Salts #5–7) before and after calibration of the thermocouple.

Figure 5.3 shows the mass loss as a function of temperature up to 500°C for Salts 1–7. All seven compositions are very stable, even at high temperatures of up to 500°C. However, the compositions of KCl:CuCl were more stable than the compositions of $ZnCl_2$:KCl:NaCl. Salts #5–7 did not show significant mass loss in TGA results, whereas Salt #1–4 lost a few percent of their mass. Salt #1 lost up to 2 wt% at 500°C. This composition started to lose mass at lower temperatures than the others. Salt #2 lost around 1% of the mass when the temperature reached 500°C and Salts #3 and 4 lost 0.5 and 0.2% of mass at the same temperature, respectively. Although $ZnCl_2$:KCl:NaCl had higher mass loss, it is still in the acceptable range for the ABC-Salt purpose.

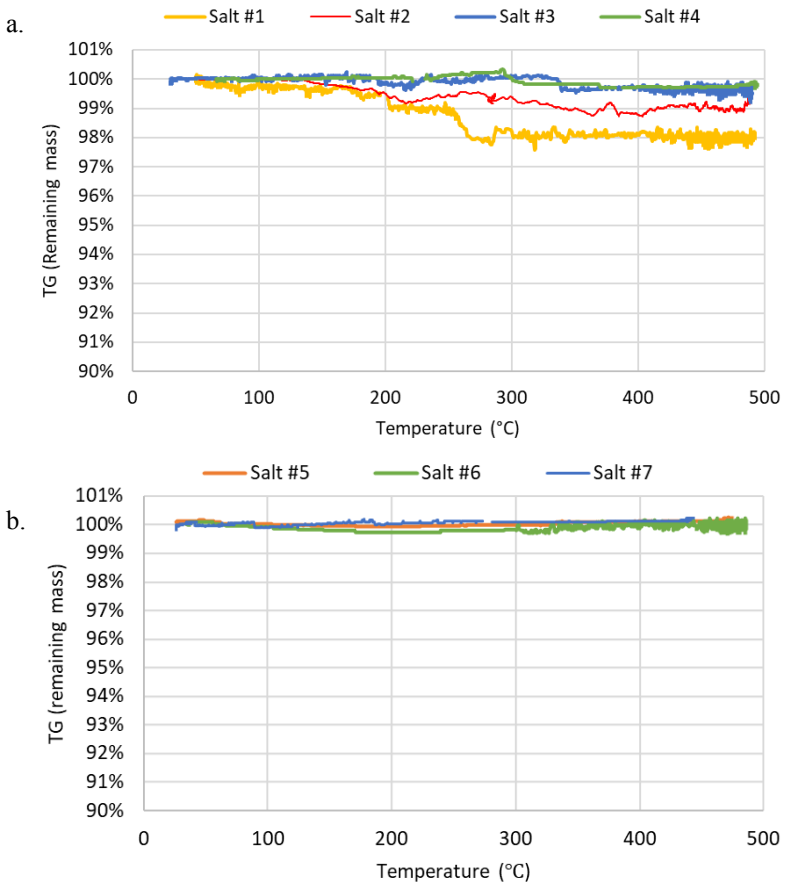

Figure 5.3. Mass loss as a function of temperature for (a) four compositions of $ZnCl_2$:KCl:NaCl (Salts #1–4) and (b) three compositions of KCl:CuCl (Salts #5–7).

5.2 Hydrolysis

Figure 5.4 shows the average HCl levels (including standard deviation for 30-min experimental duration for each interval) measured by FTIR-gas analysis from experiments with four $ZnCl_2$:KCl:NaCl compositions (Salts #1–4) and three KCl:CuCl compositions (Salts #5–7). As the figure shows, the HCl levels from $ZnCl_2$:KCl:NaCl hydrolysis were significantly higher than the levels from KCl:CuCl hydrolysis. For Salt #1–4, increasing temperature usually leads to more hydrolysis and thus higher HCl levels. For Salt #5-7, the HCl concentration is below the detection limit of FTIR. Among the salts from the ternary system, Salt #1 showed the highest level of HCl formation, reaching more than 4600 ppm_v at 500°C. Salts #2 and 3 produced low levels of HCl up to 350°C, as acid formation increased to more than 4000 ppm_v at 500°C. The HCl formation in Salt #4 was clearly lower than the others from the ternary system; HCl level was around zero at up to 350°C, whereas it dramatically increased to 1300 ppm_v at 500°C. Overall, hydrolysis occurred to a larger extent for the Zn-based salt, with higher Zn content yielding more HCl formation.

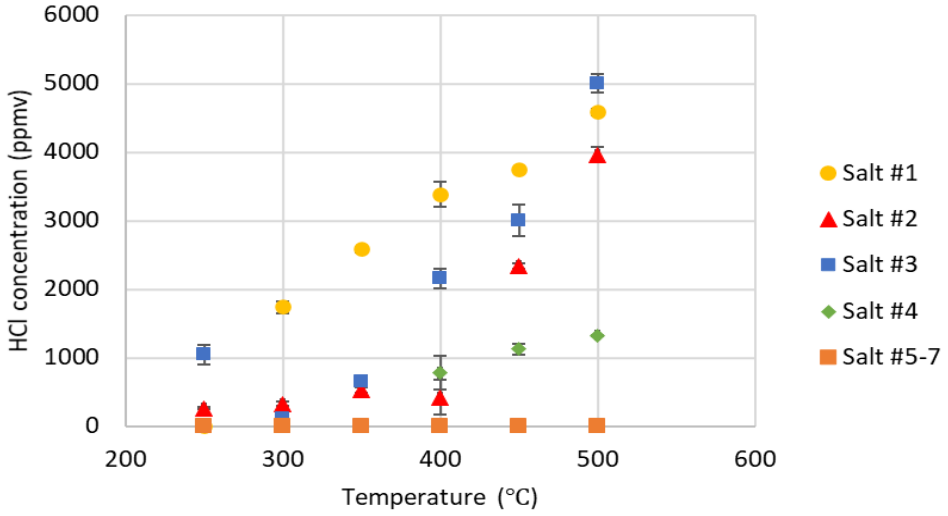

Figure 5.4. The average content of HCl in the exit gas in hydrolysis experiments as a function of temperature from 250 to 500°C when 10 vol% in N_2 is added to the molten salt (Salts #1–7).

To demonstrate HCl formation as a function of temperature for each interval, Figure 5.5 is provided as an example. It shows the HCl level for each temperature interval, from 250°C to 500°C, for Salt #1 (60:20:20 mol% $ZnCl_2$:KCl:NaCl). The temperature was kept constant for at least 30 min to ensure a stable level of HCl formation, as was obvious within each interval. As the figure shows, increasing the temperature led to higher HCl levels.

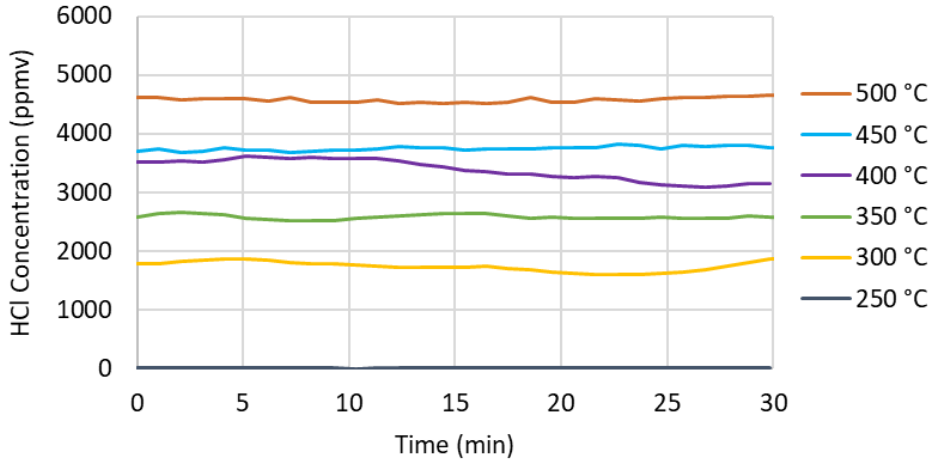

Figure 5.5. The content of HCl in the exit gas as a function of temperature from 250°C to 500°C for Salt #1.

To further investigate the mass loss and hydrolysis of the salts as a function of temperature, two compositions from the ternary system were modeled using FactSage. These results are not included in any of the papers, but they have been performed to gain a better understanding of the system. Salt #1 with maximum mass loss and hydrolysis (according to the experimental results) and Salt #4 as the most promising option among the other compositions were selected for further modeling. Figure 5.6 shows the estimated levels of HCl and $ZnCl_2$(g) formed through the hydrolysis of the salt with 10 vol% water present in the system. The figure shows that by increasing the temperature, more HCl and $ZnCl_2$(g) were formed, indicating a higher hydrolysis rate and higher vapor pressure of $ZnCl_2$ in both systems. The $ZnCl_2$ in gas form can be interpreted as mass loss in the system due to vaporization of the salt. The amount of HCl and $ZnCl_2$ in Salt #1 was higher than in Salt #4, which shows that the modeling results are in good agreement with the experimental results. In Salt #1, HCl formation started at 300°C, whereas for Salt #4, the level of HCl was still negligible at this temperature. Similar results were reported in the experimental part of the study.

a.

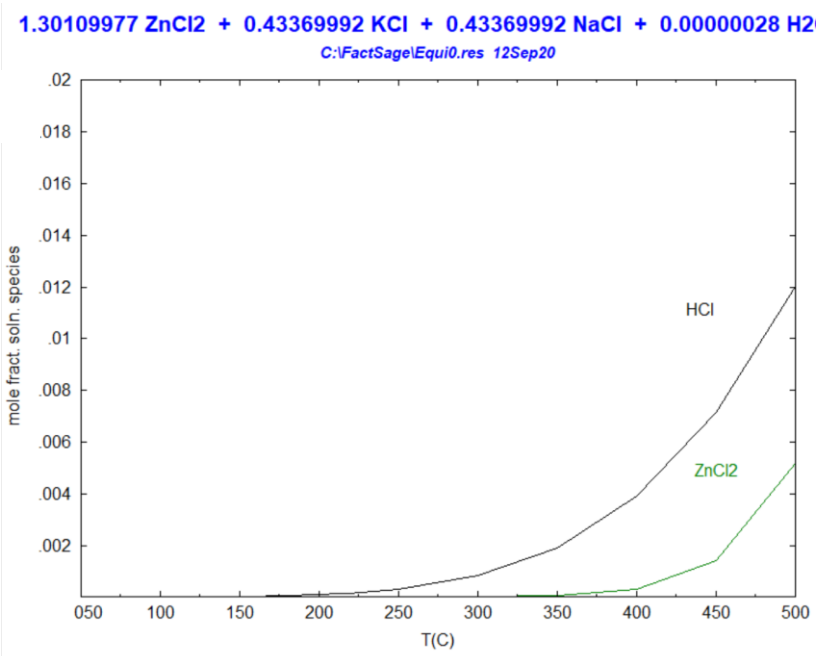

b.

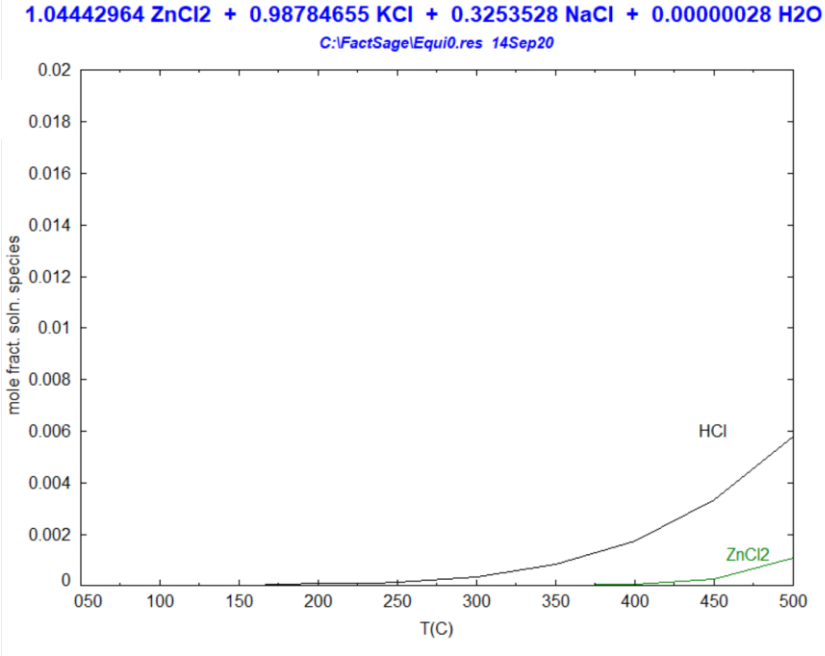

Figure 5.6. Composition of the gas phase (HCl and $ZnCl_2$) from hydrolysis of (a) Salt #1 (b) Salt #4 as a function of temperature up to 500°C modelled in FactSage.

The hydrolysis experiments were performed at ambient pressure due to limitations of the experimental setup. Hydro-pyrolysis is, by contrast, a high-pressure process that can suppress vapor pressure and HCl formation. Therefore, the hydrolysis rate could be lower than the values reported in this study. To study this hypothesis, the HCl and $ZnCl_2$(g) level of the same systems were modeled as a function of pressure up to 50 bar, but this time, at a constant temperature of 500°C. Figure 5.7 shows how the levels of formed acid (HCl) and $ZnCl_2$(g) was reduced by increasing the pressure. At 50 bar, the HCl level decreased by 83% in both systems, and $ZnCl_2$(g) was reduced to close to zero.

a.

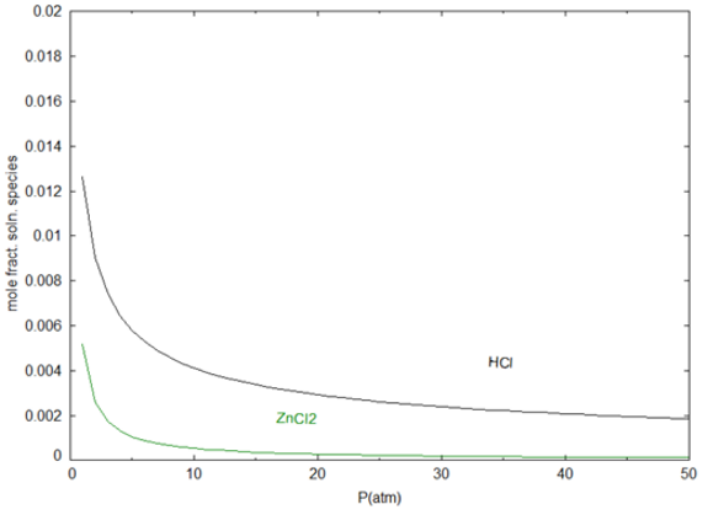

b.

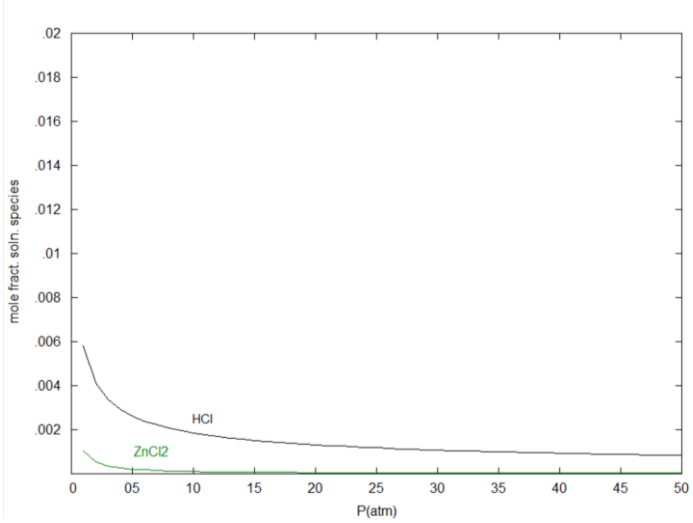

Figure 5.7. The variation of HCl and ZnCl2 gases as a function of pressure simulated with FactSage for (a) Salt #1 and (b) Salt #4.

Since $ZnCl_2$ shows the most significant contribution to HCl formation in hydrolysis studies, the Gibbs free energy of hydrolysis reactions of the single salts $ZnCl_2$, KC, NaCl, and CuCl were simulated in HSC chemistry (116). The hydrolysis reactions are described in Eqs. 9–12, and the simulated Gibbs free energy of these reactions are depicted in Figure 5.8. The ΔGs for all salts are well above zero up to even higher than 500°C, which means that hydrolysis is not thermodynamically favored at relevant process temperatures. However, all reactions are in equilibrium, and hydrolysis leads to the formation of gaseous products. The produced compounds will be constantly removed from the system and will decrease vapor pressure. It will tend to drive the reaction in the right direction and increase HCl production (117) and the experimental results confirm this. Since $ZnCl_2$ has the minimum Gibbs energy among the other compounds, it is assumed that this chloride plays the main role in molten salt hydrolysis. However, a higher HCl level in Salt #1 hydrolysis, which contains a higher amount of $ZnCl_2$ compared to the other salts (see Table 4.1), can strengthen this hypothesis.

$$ZnCl_2 + 2H_2O(g) \leftrightarrow ZnO + 2HCl(g) \quad (9)$$

$$KCl + 2H_2O(g) \leftrightarrow KOH + HCl(g) \quad (10)$$

$$NaCl + 2H_2O(g) \leftrightarrow NaOH + 2HCl(g) \quad (11)$$

$$2CuCl + H_2O(g) \leftrightarrow Cu_2O + 2HCl(g) \quad (12)$$

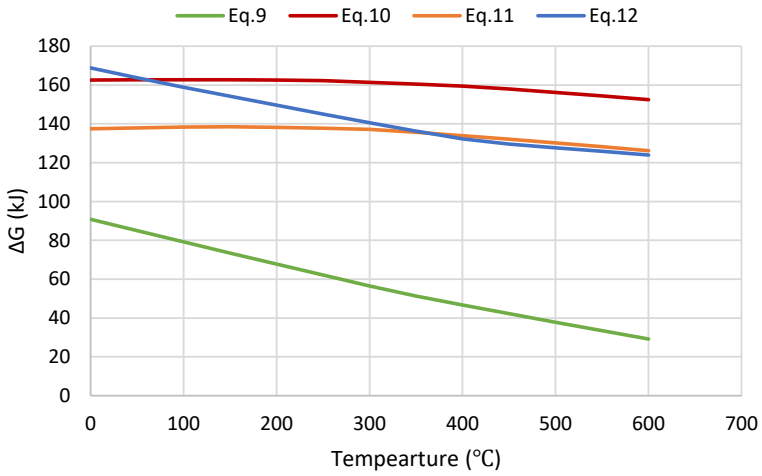

Figure 5.8. Gibbs free energy of hydrolysis reactions of $ZnCl_2$, NaCl, and KCl (Eqs. 9–12) in the range of 0 to 600°C.

To compare the hydrolysis reaction of these two groups of molten salts, their two main components $ZnCl_2$ and CuCl were considered in further simulations. KCl and NaCl had lower concentrations in salt mixtures, and their hydrolysis reactions also had higher Gibbs energy. This makes them less critical components for hydrolysis reactions. Therefore, the hydrolysis reactions for the single salts $ZnCl_2$ and CuCl were simulated with FactSage using the FactPS database. The equilibrium partial pressures above a mixture of 1 mol of salt and 1 mol of H_2O is shown in Figure 5.9. For both salts, the hydrolysis product HCl is the dominating gas species besides H_2O below 400°C. However, the equilibrium partial pressure of HCl at 200°C is nearly three orders of magnitude lower for CuCl than for $ZnCl_2$. The HCl partial pressure forming in contact of $ZnCl_2$ with water at 200°C (0.3 mbar) is observed for CuCl only at 420°C, indicating a significant increase in hydrolysis resistance.

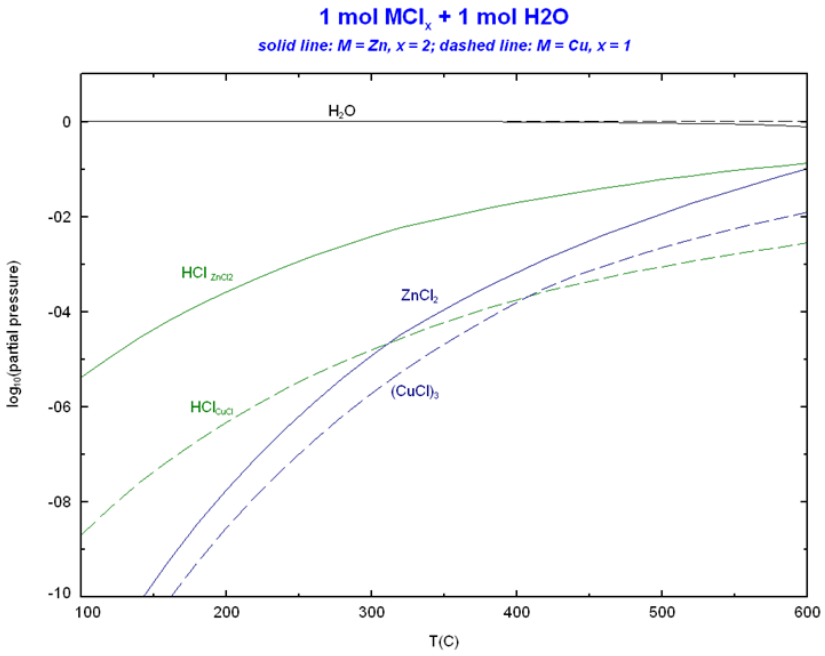

Figure 5.9. Partial pressure of most dominant gas phase species in equilibrium between 1 mol of water and 1 mol of $ZnCl_2$ (solid lines) or 1 mol of CuCl (dashed lines).

According to the simulations in *Figure 5.8*, $ZnCl_2$ is the critical component in hydrolysis, and a higher concentration of this salt in molten salt compositions (Salt #1) leads to a higher rate of hydrolysis and more HCl formation, as shown in Figure 5.4.

To reduce the hydrolysis rate of molten salts, the effect of adding metal oxide was considered. Salt #1 (with the highest level of HCl formation) was chosen to investigate the

effect that adding ZnO to the salt has on hydrolysis. Eq. 13 shows the chemical reaction of ZnO with HCl:

$$ZnO + 2HCl(g) \leftrightarrow ZnCl_2 + H_2O(g) \quad (13)$$

Figure 5.10 shows the effect of adding 5 wt% and 10 wt% ZnO to Salt #1 at different temperatures. The figure shows that ZnO can significantly decrease HCl formation at temperatures of 400°C and lower. However, it is not very effective at higher temperatures. According to the presented results, adding 5 wt% and 10 wt% ZnO to the salt mixture can reduce the HCl level by more than 96% and 99% at 350°C.

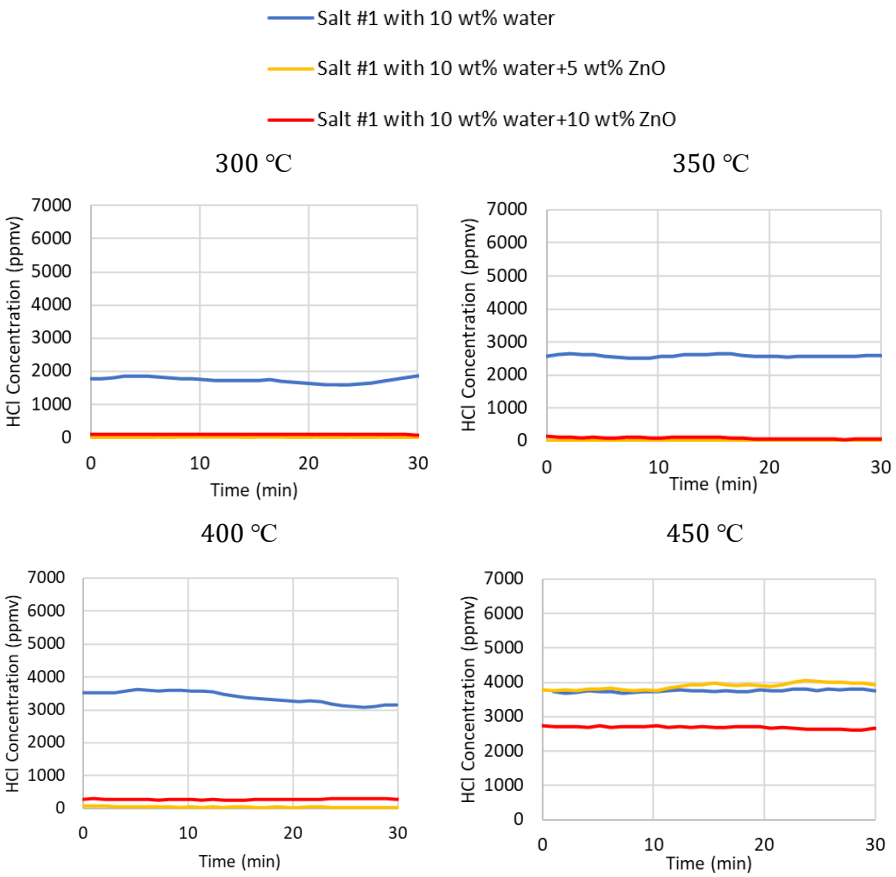

Figure 5.10. The content of HCl in the exit gas in FTIR for Salt #1 by adding 5 and 10 wt% ZnO and comparing to Salt #1 at a temperature range of 300–450°C.

Table 5.1 summarizes the investigated properties of the seven compositions from the $ZnCl_2$:KCl:NaCl and KCl:CuCl molten salt systems. In the ternary system (Salts #1–4),

Salt #4 can be considered the best candidate for ABC-Salt from the $ZnCl_2$:KCl:NaCl system due to the relatively low melting point and significantly lower mass loss and HCl formation. The results show that the binary system KCl:CuCl has an even lower melting point and higher thermal stability. Furthermore, no hydrolysis was observed, which makes it the most promising alternative for the liquefaction of biomass. However, during the experiments, one important drawback of this salt mixture was observed, which makes it less attractive than Salt #4.

Table 5.1. Thermochemical properties of Salts #1–7.

Salt	***$ZnCl_2$:KCl:NaCl/ KCl:CuCl***	***Melting point (℃)***	***Mass loss at 500 ℃***	***HCl level at 500 ℃ (ppm_v)***
Salt #1	60:20:20	205	2%	4600
Salt #2	59.5:21.9:18.6	203	1%	4000
Salt #3	52.9:33.7:13.4	212	0.5%	5000
Salt #4	44.3:41.9:13.8	205	0.2%	1300
Salt #5	32:68	146.6	~0	ND
Salt #6	34:66	145.2	~0	ND
Salt #7	36:64	146.8	~0	ND

The appearance of the experimental setup in contact with KCl:CuCl shows the high corrosiveness of this salt. Figure 5.11 shows the cooling curve experimental setup, including the nickel radiation shields, the crucible containing molten salt, and the stainless-steel setup after one transition temperature experiment. In this experiment, the salt mixture was heated up to 350°C, and after a few hours, it was cooled down slowly at a rate of 0.5°C/min. The process was carried out under an inert atmosphere (Ar flow) and repeated three times. As the figure shows, the stainless steel stirrer at the middle of the setup was broken due to high corrosion. Other researchers working with the same salt have had the same concerns, and they used fused silica and borosilicate crucibles for their experiments to avoid the corrosion issue (17,94). The corrosive nature of KCl:CuCl can be better understood using the FactPS database in FactSage: a 1:1:1 mixture of KCl:CuCl:Ni forms 0.5 mol of $KNiCl_3$, 0.5 mol of KCl, 0.5 mol of Ni, and 1 mol of Cu, while a 1:1:1 mixture

of KCl:CuCl:Fe forms in equilibrium 0.5 mol of K_2FeCl_4, 1 mol of Cu and 0.5 mol of Fe. This indicates that in both cases, Cu has a tendency to transfer chlorine to the nickel crucible and steel setup. According to these thermochemical considerations, another interesting construction material in the presence of the KCl:CuCl mixture can be copper, which needs to be studied. However, this is beyond the scope of the present work.

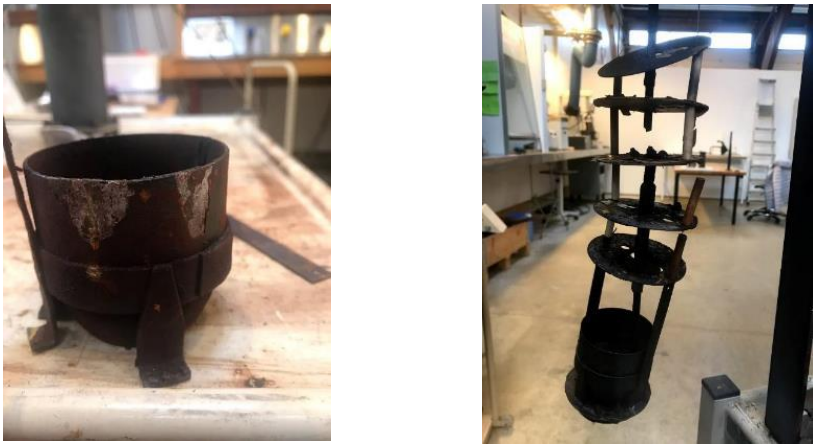

Figure 5.11. The corrosion of the nickel crucible containing molten salt and nickel stainless steel setup containing KCl:CuCl molten salt after an experiment in a temperature range of 50–350°C under an inert atmosphere.

Consequently, despite the promising properties of KCl:CuCl (Table 5.1), this salt is not considered the best alternative as a biomass liquefier in ABC-Salt. Therefore, Salt #4 from the ternary system $ZnCl_2$:KCl:NaCl was chosen as the candidate for further studies and salt purification in **Paper III**. However, even though the corrosiveness of KCl:CuCl makes it less relevant to the ABC-Salt concept, it is still a very interesting molten salt system due to its thermodynamic properties obtained from experimental studies. Moreover, there is very little information about this molten salt system in the literature, and more investigation needs to be performed. Therefore, thermodynamic assessment of KCl:CuCl was performed, and its phase diagram and interaction parameters were calculated in **Paper II** (see Chapter 5.4).

5.3 Salt purification

According to the results in chapter 5.1 and 5.2, Salt #4 was chosen for further salt purification. The spent salt was simulated by adding the impurities CuCl, $FeCl_2$, $FeCl_3$, and MnO_2 (concluded from Table 3.2) to the molten salt, and electrolysis was employed to study the deposition of impurities from the molten salt. A series of CV and potentiostatic

electrolysis experiments were carried out to investigate the reduction potential of the elements (salt and impurities) and to remove the added impurities.

Figure 5.12 shows the CV of pure Salt #4 at 260°C before adding any impurity chemicals. The cathodic current at -0.5 V represents the electroreduction of the metal. Among the metal elements existing in the salt, Zn(II) is the most easily reduced element, and the cathodic peak is assumed to represent Zn electrodeposition from $ZnCl_2$. Na and K have more negative electrode potentials, and their reduction was not observed in this experiment. By reversing the sweep direction, an anodic peak was observed. On the other side of the voltammogram, the anodic current observed at 1.4 V represents chlorine gas evolution. The potential intervals of -0.5 and 1.4 V define the electrochemical window for the salt mixture (1.9 V). However, Nitta et al. showed almost the same voltammogram for pure $ZnCl_2$ molten salt with a 1.7 V electrochemical window using a Zn electrode (15).

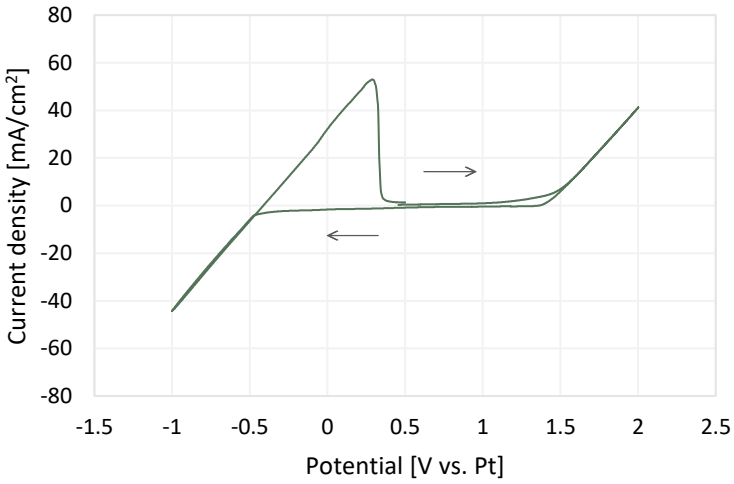

Figure 5.12. Cyclic voltammogram of $ZnCl_2$:KCl:NaCl recorded on a Zn electrode at 260°C.

Figure 5.13 compares the voltammograms before and after attempting to remove impurities from the salt. The figure shows the CV results after adding 2 g of impurities and one or two levels of purification for four different impurities (CuCl, $FeCl_2$, $FeCl_3$, and MnO_2). In all experiments, new anodic and cathodic peaks were observed in the voltammogram after adding chemicals, indicating the presence of impurities in the molten salt.

In Figure 5.13a, the cathodic peak at a potential of -0.04 V represents the bulk deposition of Cu in the molten salt. However, the other new peaks appeared at -1.2 and -0.8 V, likely because of the underpotential deposition of sodium. This is a well-known process when the

alkali metal is in contact with graphite (118). The constant potential through potentiostatic electrolysis was then applied for some time (detailed in Table 5.2) to remove impurities. Purifications 1 and 2 show the voltammogram after one and two steps of impurity removal. The redox peak height of Cu^{+} clearly decreased in purification 1 and almost diminished in purification 2. This can be interpreted as all Cu(I) from CuCl being reduced from the molten salt by potentiostatic electrolysis.

In Figure 5.13b and c, the new redox peaks were detected after adding $FeCl_2$ and $FeCl_3$. There was one couple of cathodic and anodic current peaks between 0.2 and 1 for $FeCl_2$ and between 0 and 1.2 for $FeCl_3$ presenting the redox peak for Fe ion existence. The first purification in both systems showed significant impurity removal by reducing peak heights. After the second round of impurity removal, in purification 2, the redox peaks were still visible in the case of $FeCl_2$, representing the existence of impurity in the molten salt. However, in the other case ($FeCl_3$), no peaks were detected, indicating almost complete purification of the salt.

In Figure 5.13d, the case is slightly different. In the very early CV experiment, the voltammogram of the pure salt shifted toward a negative direction (compared to Figure 5.12) and the reduction of Zn started at a more negative potential around -1 V. However, the electrochemical window was still 1.9 V. This can occur due to the instability of the reference electrode. After adding MnO_2, redox peaks, including cathodic peak at -0.6 and anodic peak at -0.25 V, represent the presence of impurity (Mn^{4+}) in the melt. After potentiostatic electrolysis for some time (Table 5.2), the heights of the peaks were reduced, which is interpreted as the impurity reduction from the molten salt. No significant removal was observed in more electrolysis rounds.

a.

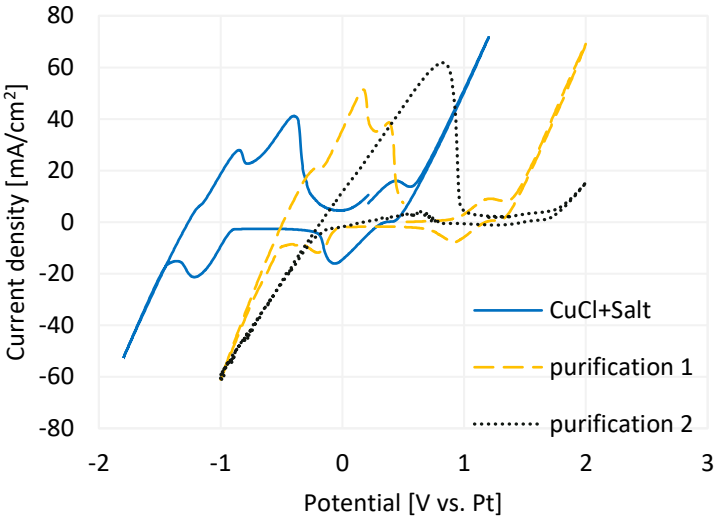
Current density [mA/cm²]
80
60
40
20
0
-20
-40
-60
-80
-2
-1
0
1
2
3
Potential [V vs. Pt]
CuCl+Salt
purification 1
purification 2

b.

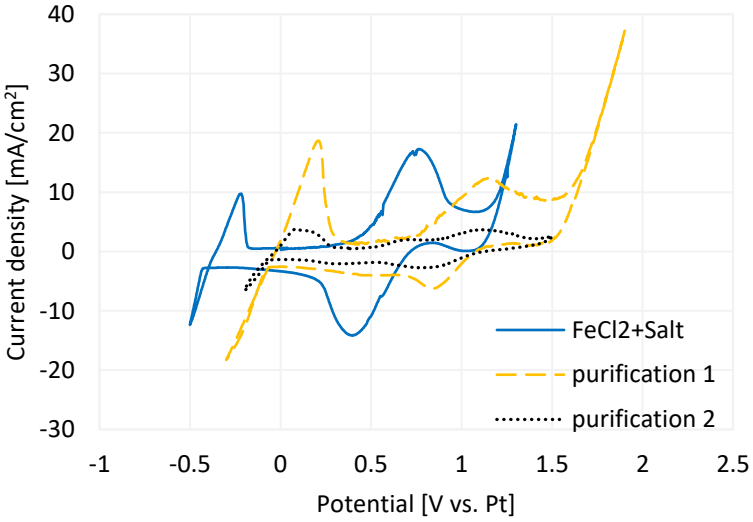
Current density [mA/cm²]
40
30
20
10
0
-10
-20
-30
-1
-0.5
0
0.5
1
1.5
2
2.5
Potential [V vs. Pt]
FeCl2+Salt
purification 1
purification 2

c.

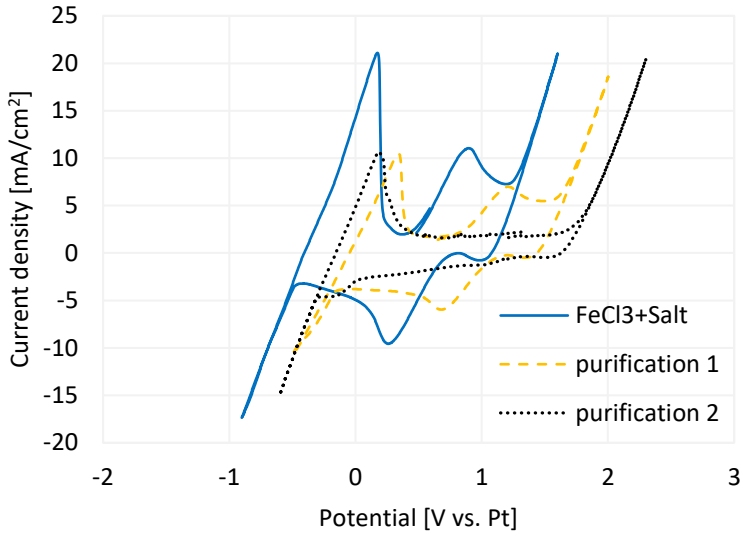

d.

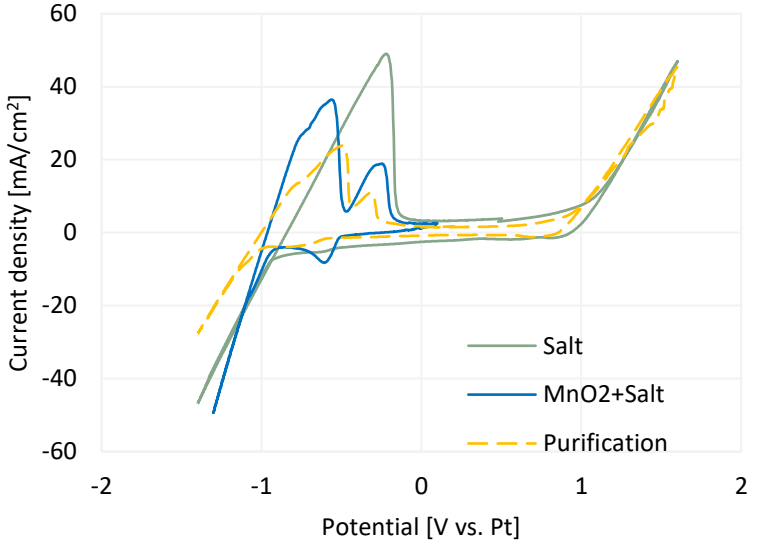

Figure 5.13. Cyclic voltammogram of $ZnCl_2$:KCl:NaCl containing (a) CuCl (b) $FeCl_2$ (c) $FeCl_3$ and (d) MnO_2 before and after each potentiostatic electrolysis run.

Table 5.2. The applied potential and the duration of potentiostatic electrolysis in a few rounds to remove impurities (Cu^{+}, Fe^{2+}, Fe^{3+} and Mn^{4+}) from Salt #4 melt at 260°C.

	Potentiostatic round 1			**Potentiostatic round 2**			**Potentiostatic round 3**		
Added impurity	Applied potential (V)	Time (min)	Effective	Applied potential (V)	Time (min)	Effective	Applied potential (V)	Time (min)	Effective
CuCl	0.1	30	yes	0.9	60	yes	-	-	-
$FeCl_2$	0.7	90	yes	1.1	90	yes	1.15	90	no
$FeCl_3$	0.2	60	yes	1	90	yes	-	-	-
MnO_2	-0.55	90	yes	-0.8	90	no	-	-	-

The reduced elements from the molten salt in some cases (in which CuCl and MnO_2 were added as impurities) deposited on to the surface of the working electrode as shown in Figure 5.14. However, in the other cases (in which $FeCl_2$ and $FeCl_3$ were added as impurities), no metal was observed on the surface of the working electrode. Since the CV results showed impurity removal from the salt, the idea of precipitation of the impurities was assumed. Therefore, the graphite crucible was broken after the solidification of the melt, as shown in Figure 5.15. The figure shows two layers of substances. The dark layer at the bottom indicates the separated impurity, which is settled at the bottom of the crucible, while the layer at the top is the salt, which has turned to a brownish color, most likely due to the presence of Fe ions.

a. b.

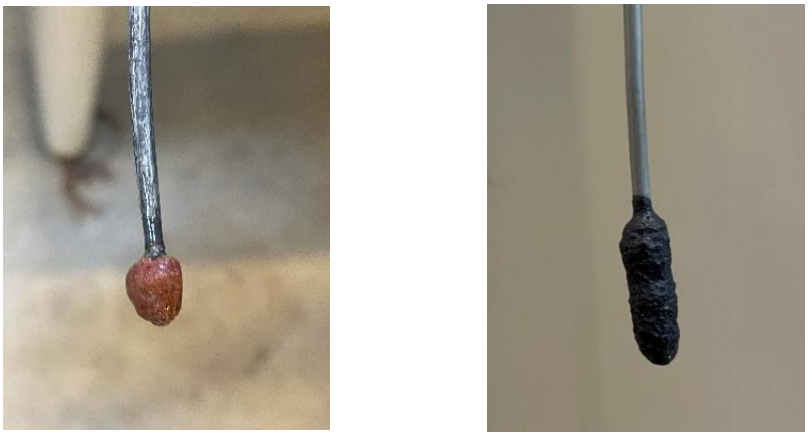

Figure 5.14. The deposited (a) Cu from CuCl and (b) Mn from MnO_2 in the molten salt after electrodeposition.

Figure 5.15. The cross section of the crucible after 2.5 h electrodeposition of Fe from $FeCl_3$ in $ZnCl_2$:KCl:NaCl showing two separate layers: molten salt on top and Fe compound at the bottom.

The deposited materials, shown in Figure 5.14 and Figure 5.15, were analyzed using X-ray diffraction (XRD). Figure 5.16 exhibits the XRD results for extracted components from CuCl and Salt #4 (shown in Figure 5.14.a). The XRD spectra exhibited the strongest diffraction peaks of Cu, indicating that the main chemical composition of the obtained electrodeposits was Cu. The other peaks were mostly noises due to the presence of some molten salt in the extracted metal. The same analysis was carried out for the other three deposited materials, but the results were too noisy, most likely due to the existence of oxides and moisture.

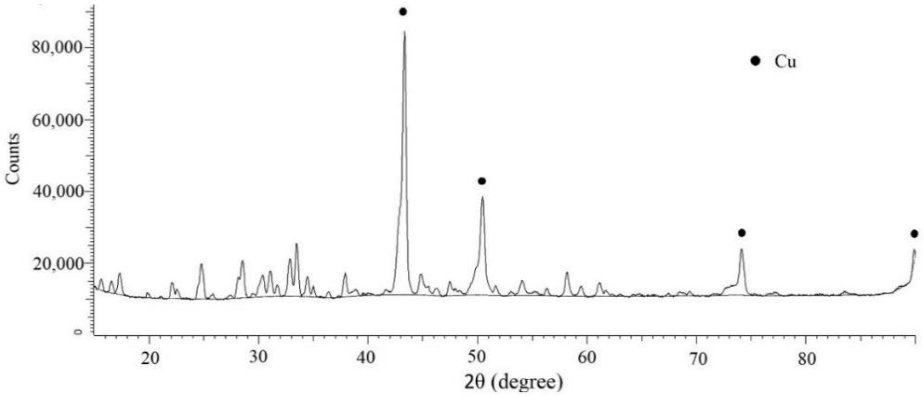

Figure 5.16. XRD pattern of copper electrodeposits obtained from $ZnCl_2$:KCl:NaCl containing CuCl (0.8 wt%) at 260°C.

5.4 Phase diagram generation

This chapter presents the modeling results and generated phase diagrams for the binary system KCl:CuCl and the liquid solution of hydrolyzed KCl. The experimental results from the current study and the literature, as well as the FactPS database, were used to optimize the thermodynamic parameters involved in the excess term of the Gibbs energy phases. The phase diagrams and model parameters were derived from thermodynamic optimization.

Based on the experimental results reported in **Paper II**, binary KCl:CuCl was thermodynamically assessed. The RK expression was employed to optimize the L_i(i=0,1) parameters in Eq. 6. For the intermediate compound K_2CuCl_3, the standard entropy was optimized as well, while the enthalpy of formation was fixed, as shown in Table 5.3. Figure 5.17 shows the phase diagram of the binary system KCl:CuCl evaluated and calculated based on the experimental data. The calculated eutectic point of the system was located at 145.9°C and 64.9 mol% CuCl, and the peritectic temperature was obtained at 241.2°C. The experimental data from the current study and from the literature (17) are included in the phase diagram to compare with the modeled results. Etter et al. identified higher eutectic and peritectic temperatures (50 and 245°C respectively), whereas Sandonini reported lower eutectic temperatures around 136°C (17).

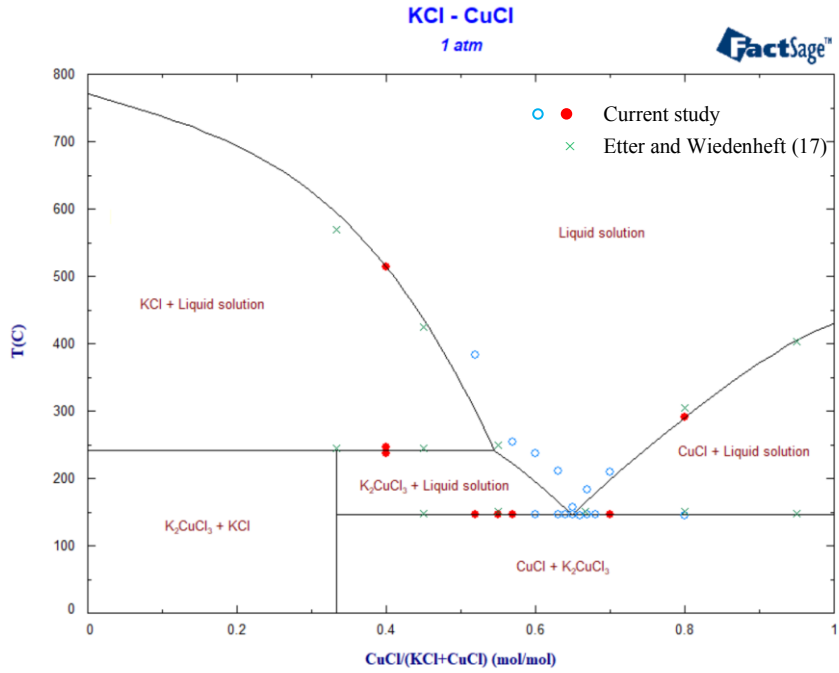

Figure 5.17. Calculated phase diagram of KCl:CuCl in comparison with experimental data generated in the present work (red points have been used in optimization), as well as from Etter and Wiedenheft (17) *(green crosses).*

To the best of the authors' knowledge, there is no theoretical study regarding chloride hydrolysis in the presence of water. The aim of **Paper IV** was to study the simulation of chlorides in the presence of water and chloride oxide. Although it would have been very interesting to model the hydrolysis of $ZnCl_2$ according to the described results, the available data for this salt and its binary systems were very limited, making the simulation very complicated. Therefore, KCl was selected for this part of the study due to the available experimental data in the literature. Furthermore, salt is a very popular salt in molten salt systems and is a part of both the studied systems ($ZnCl_2$:KCl:NaCl and KCl:CuCl).

The interaction parameters of the systems including L_i(i=0,1) parameters for H_2O–HCl, H_2O–KOH and H_2O–KCl liquid solutions and KCl–KOH for both liquid and solid solutions, are optimized and presented in Table 5.3. The standard enthalpy and entropy for KCl are also optimized and presented in the table. These data were employed in the phase diagram module in FactSage 7.2 to calculate the phase diagrams of the quasi-binary systems. The calculated phase diagrams are shown in Figure 5.18. It is obvious that the experimental points employed in the literature meet the calculated liquidus in all phase diagrams.

Table 5.3. Optimized thermodynamic parameters of KCl:CuCl system and H_2O–HCl, H_2O–KOH, KOH–KCl and H_2O–KCl systems using the Redlich–Kister model.

System	***Phase type***	***Phase name***	***Thermodynamic parameters***
KCl, CuCl	Solution	Liquid	$L^0 = -27373\frac{J}{mol} + 3.94\frac{J}{mol\ K}T$ $L^1 = -15416\frac{J}{mol} + 25.57\frac{J}{mol\ K}\ T$
K_2CuCl_3	compound	Solid	$\Delta H^{298}_{K_2CuCl_3} = -1018294\frac{J}{mol\ K}$ $S^{298}_{K_2CuCl_3} = 247.92\frac{J}{mol\ K}$
H_2O–HCl	Solution	Liquid	$L^0 = -44928+110.82\ T$ $L^1 = -11618 + 131.32\ T$
H_2O–KOH	Solution	Liquid	$L^0 = -47375 + 2.33\ T$ $L^1 = -5545 + 16.94\ T$
KCl–KOH	Solution	Liquid	$L^0 = 3296 - 8.78\ T$ $L^1 = 5714 - 1.26\ T$
		Solid	$L^0 = 8331 - 0.40\ T$ $L^1 = -12551 + 13.38\ T$
H_2O–KCl	Solution	Liquid	$L^0 = 10443 - 26.23\ T$ $L^1 = -10478 - 21.71\ T$
KCl	Solution	Liquid	$H^{298}_{KCl} = -421103$ $S^{298}_{KCl} = 88.02$ $Cp^{<1044K}_{KCl(liquid)} = 70.957\ + 0.002528\ T$

a.

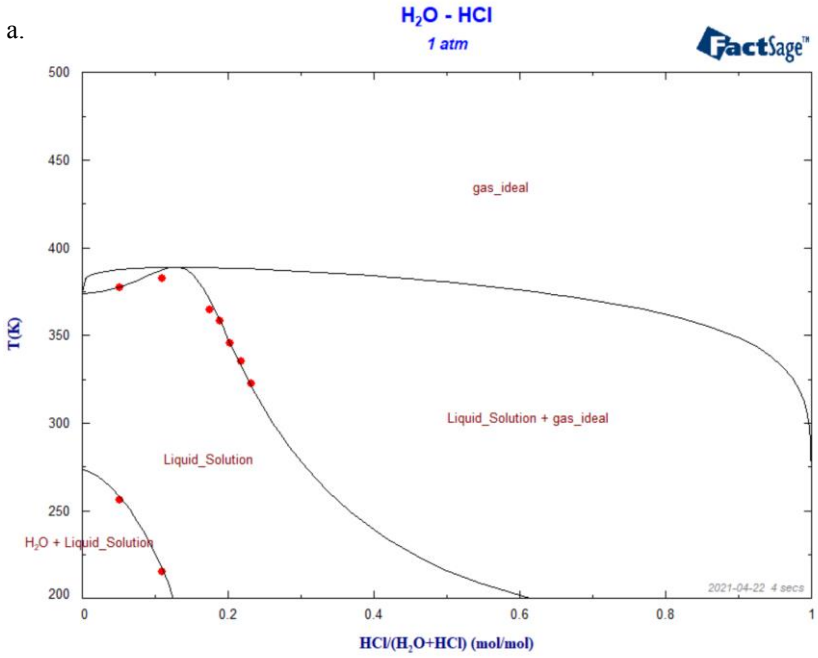
H2O - HCl
1 atm
FactSage
gas_ideal
Liquid_Solution + gas_ideal
Liquid_Solution
H2O + Liquid_Solution
T(K)
HCl/(H2O+HCl) (mol/mol)
2021-04-22 4 secs

b.

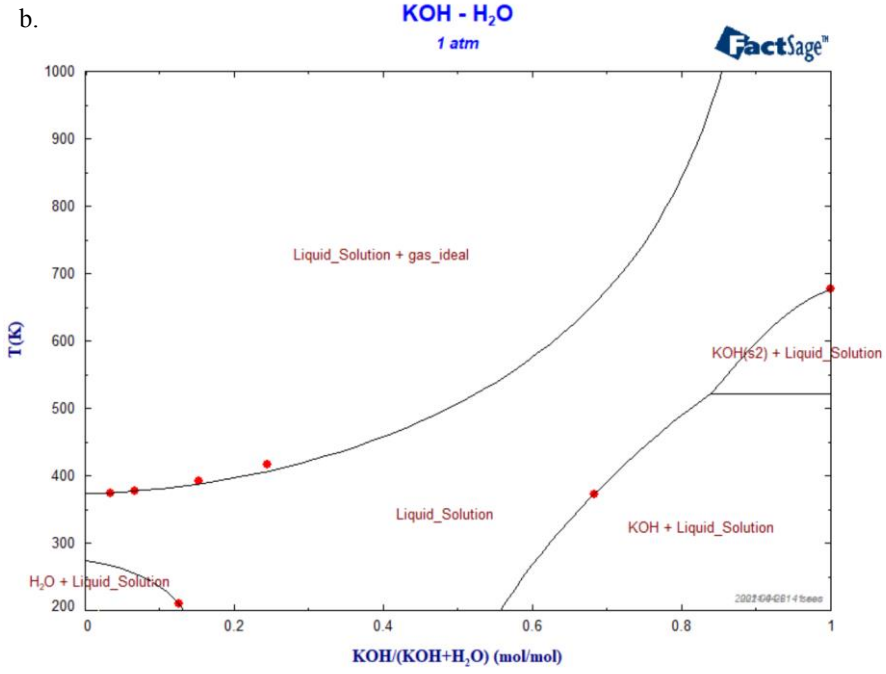
KOH - H2O
1 atm
FactSage
Liquid_Solution + gas_ideal
KOH(s2) + Liquid_Solution
Liquid_Solution
KOH + Liquid_Solution
H2O + Liquid_Solution
T(K)
KOH/(KOH+H2O) (mol/mol)

c.

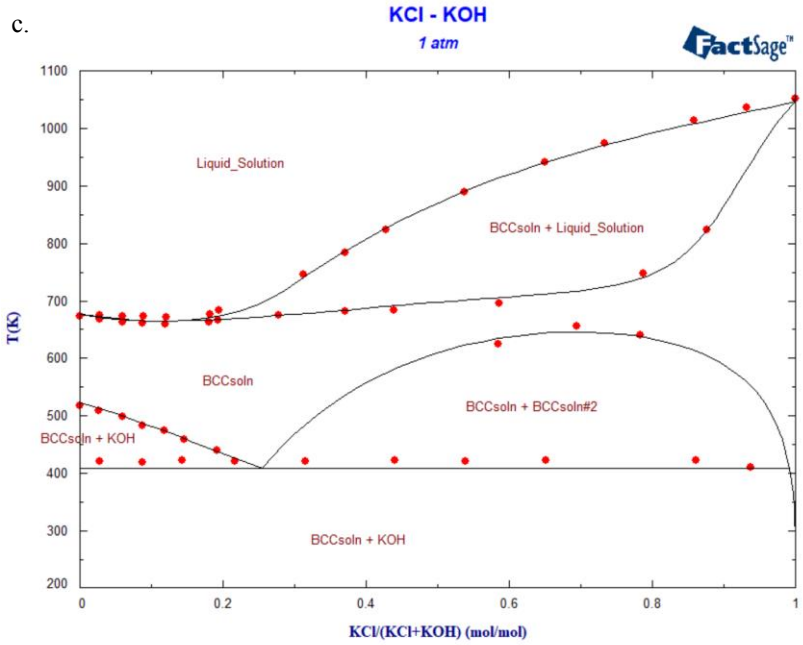

d.

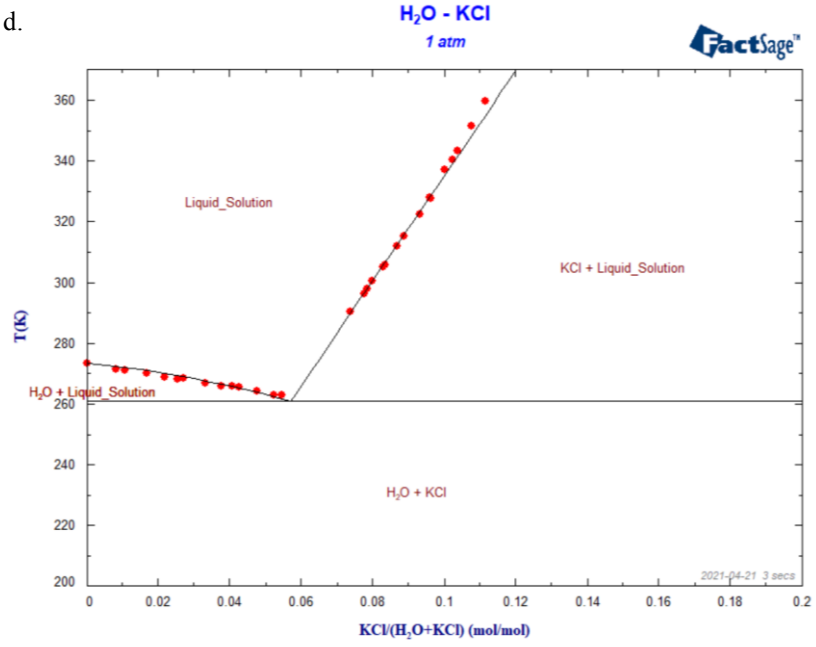

Figure 5.18. Phase diagram for binary systems. Lines: The present model results. Red points: Experimental data a. H_2O–KCl b. H_2O–HCl c. H_2O–KOH d. KCl–KOH solution.

6 Conclusion

This study aims to find a promising molten salt system for the ABC-Salt project based on its thermodynamic properties. ABC-Salt has the purpose of producing middle distillate refined from the lignocellulosic waste stream in molten salt through liquefaction, hydro-pyrolysis, and deoxygenation. The reason for employing molten salts is that biomass is soluble in molten salt. Thus, the feed can be liquefied, which makes it pumpable to the high-pressure hydro-pyrolysis unit. Further, the rapid heating of biomass in molten salts can enhance product quality. The proper molten salt system must have good transport properties and a low melting point of around 200°C. This temperature is high enough to liquefy biomass and low enough to avoid producing many chars. Moreover, the molten salt must have high thermal stability to avoid decomposition, since the temperature in the hydro-pyrolysis unit can reach 500°C. Hydrolysis is another issue that needs to be investigated. Biomass contains a large amount of moisture that can react with the salt and produce highly corrosive acids, such as HCl, which can ruin the construction materials.

According to the literature, two molten salt systems have been found interesting for ABC-Salt purposes, and they have been studied and compared in the present study. Four compositions of $ZnCl_2$:KCl:NaCl (Salts #1-4) (**Paper I**) and three compositions of KCl:CuCl (Salts #5–7) (**Paper II**) were studied experimentally. The results showed that although KCl:CuCl had the most promising properties, it was a highly corrosive salt that ruined the setup. Therefore, Salt #4 (44.3:41.9:13.8mol%), with a melting point of 205°C, 0.2% mass loss, and a low level of HCl formation (no HCl below 350°C and 1300 ppm_v at 500°C), was selected as the best candidate for the ABC-Salt project. The experimental results in **Paper I** also show that adding ZnO to the salt mixture has a significant effect on inhibiting hydrolysis, especially at temperatures below 450°C. Further, FactSage modeling results show that high pressure (up to 50 bar) in the hydro-pyrolysis unit can suppress HCl formation and $ZnCl_2$ evaporating, which decreases the hydrolysis level, vapor pressure, and mass loss.

In terms of economic and environmental aspects, Salt #4 for the ABC-Salt project needs to be recycled in the system and reused many times. The spent molten salt can be contaminated by char and ash when it leaves the hydro-pyrolysis unit. Thus, it needs to be purified and recycled into the system. In this study, the electrodeposition of Cu, Fe, and Mn was investigated by adding four compounds—CuCl, $FeCl_2$, $FeCl_3$ and MnO_2—to Salt #4. CV and amperochronometry were employed to study the electrochemical removal of impurities. The results showed that Cu was successfully removed from the salt after 120

min of electrolysis. The extracted impurity was analyzed using XRD, and the Cu element was confirmed. In other cases, Fe(III) was removed from the salt after 150 min of electrolysis; however, Fe(II) was not fully recovered from the salt after 270 min. In these cases, the deposited elements were settled at the bottom of the crucible. Mn(IV) was successfully extracted from the molten salt; however, after 90 min of electrolysis, no more purification was observed. These results in **Paper III** provide the primary results of molten salt purification through electrolysis.

Apart from the experimental work, the lack of some theoretical data related to the KCl:CuCl molten salt system and chloride hydrolysis as a single liquid phase led the current study to perform modeling using Calphad techniques. These modeling results can be used in further studies to enable thermodynamic calculations.

Although the KCl:CuCl system was pretermitted from the ABC-Salt project due to its high corrosivity, other materials, such as copper, might be an interesting crucible and construction material in the presence of KCl:CuCl mixtures. This molten salt system was still an interesting system due to its low melting point (146°C), high thermal stability (no mass loss up to 500°C), and low hydrolysis level. Since no thermodynamic parameters were calculated for this system, and no database was found for the KCl:CuCl solution, Calphad modeling was performed in **Paper II**, and FactSage was employed to assess the thermodynamic parameters and generate the phase diagram. Temperature-dependent Gibbs energy expressions for the liquid solution and the intermediate K_2CuCl_3 solid compound were derived. This optimization is a necessary first step for further studies to enable thermodynamic calculations of practical interest for biomass liquefaction, copper electrodeposition from salts, or solvent metallurgy.

The hydrolysis of chlorides is still a challenge, since they have a high tendency to react with water and generate HCl gas and metal oxide. In **Paper IV**, the thermodynamic properties of KCl hydrolysis in the liquid phase were modeled in FactSage. In addition to KCl, H_2O and HCl, the hydroxide KOH and an oxide (here only K_2O) were also included. The results show that the associate model in the present thermodynamic framework can represent the properties of the liquid phase in all binary sub-systems (H_2O–HCl, H_2O–KOH, H_2O–KCl, KOH–K_2O, KOH–KCl). Consequently, the entire KCl–K_2O–H_2O–HCl reciprocal system was modeled for the first time using a single subregular model in FactSage.

7 Identified Gaps for Future Studies

The main focus of this work was the investigation of the thermodynamic properties of molten salts suitable for biomass liquefaction in ABC-Salt. Two molten salt systems were studied experimentally and theoretically. However, there are other binaries, ternary, and even quaternary systems that have not been studied well before and can be interesting for the same purpose.

The hydrolysis of molten salt is a serious challenge that has been studied for two chloride systems in the current work. However, it would be interesting to investigate the hydrolysis levels of the other molten salts. The effect of adding metal oxide was examined in the current study for the ternary system to inhibit hydrolysis. Investigating the effects of various metal oxides on their molten salt hydrolysis can be studied and examined in future works.

KCl:CuCl was found to be a corrosive molten salt in contact with stainless steel and nickel materials. However, its thermodynamic properties make it an interesting molten salt for many applications. Future studies could use other materials (for instance copper or fused silica) for instruction setup and study the corrosion rate of this salt in contact with various setup materials.

Electrolysis experiments could be carried out in a sealed setup to avoid environmental contamination. These experiments used Zn and graphite electrodes and were carried out at 260°C. The higher temperature led to Zn electrode contribution in the deposition process. However, other electrodes can be tried for further study and compared with electrolysis efficiency at various temperatures. The current study used a Pt wire as quasi reference electrode. These experiments were mainly qualitative experiments to test whether purification of molten $ZnCl_2$:KCl:NaCl is possible through electrolysis. However, quantitative analysis can be considered for future work in which the same system is studied, but with the use of more stable electrodes such as Ag/Ag^+.

Since hydrolysis was the main focus of the current study, the hydrolysis of KCl in liquid solution was modeled using the Calphad method. It could be very interesting to model the hydrolysis of $ZnCl_2$ since this salt was mainly responsible for the ternary system hydrolysis. The lack of experimental data for the binary systems of H_2O-$ZnCl_2$, H_2O-ZnO and $ZnCl_2$-ZnO makes this modeling very complicated. Therefore, practical studies to provide experimental data for these systems can make it possible to model the hydrolysis of $ZnCl_2$.

8 References

1. Nunes V, Queirós C, Lourenço M, Santos F, Nieto de Castro C. Molten salts as engineering fluids – A review: Part I. Molten alkali nitrates. Appl Energy. 2016;183:603–11. Available from: https://www.sciencedirect.com/science/article/pii/S0306261916313058
2. Iwadate Y. Chapter 260 - Structures and properties of rare-earth molten salts. In: Bünzli J-CG, Pecharsky VK, editors. Including actinides. Elsevier; 2014. p. 87–168. (Handbook on the Physics and Chemistry of Rare Earths; vol. 44). Available from: https://www.sciencedirect.com/science/article/pii/B9780444627117002607
3. Sato Y. Fundamentals of molten salt thermal technology. by Soc Molten-Salt Therm Tech, Agne. 1993;45.
4. Nunes V, Santos F, Lopes M, De Castro CN. 17 Accurate measurement of physicochemical properties on ionic liquids and molten salts. Molten salts and ionic liquids: Never the twain? John Wiley \& Sons; 2010.
5. Lovering DG. An introduction to molten salt technology. In: Lovering DG, editor. Molten salt technology. Boston, MA: Springer US; 1982.
6. Myers PD, Goswami DY. Thermal energy storage using chloride salts and their eutectics. Appl Therm Eng. 2016;
7. Ellabban O, Abu-Rub H, Blaabjerg F. Renewable energy resources: Current status, future prospects and their enabling technology. Renew Sustain Energy Rev. 2014;39:748–64. Available from: https://www.sciencedirect.com/science/article/pii/S1364032114005656
8. Kousksou T, Bruel P, Jamil A, El Rhafiki T, Zeraouli Y. Energy storage: Applications and challenges. Sol Energy Mater Sol Cells. 2014;120:59–80. Available from: https://www.sciencedirect.com/science/article/pii/S0927024813004145
9. S. Nygård H, Olsen E. Review of thermal processing of biomass and waste in molten salts for production of renewable fuels and chemicals. Int J Low-Carbon Technol. 2012;7(4):318–24.
10. Lovering DG. Molten salt technology. Springer; 2014.
11. Demirbas A, Arin G. An overview of biomass pyrolysis. Energy sources. 2002;24(5):471–82.
12. Bridgwater A, Meier D, Radlein D. An overview of fast pyrolysis of biomass. Org Geochem. 1999;30(12):1479–93. Available from: https://www.sciencedirect.com/science/article/pii/S0146638099001205
13. Ding W, Gomez-Vidal J, Bonk A, Bauer T. Molten chloride salts for next generation CSP plants: Electrolytical salt purification for reducing corrosive impurity level. Sol Energy Mater Sol Cells. 2019;199:8–15.
14. Maksoud L, Bauer T. Experimental investigation of chloride molten salts for thermal energy storage applications. In: 10th International Conference on Molten Salt. 2015. p. 273–80.
15. Nitta K, Nohira T, Hagiwara R, Majima M, Inazawa S. Physicochemical properties of ZnCl 2 -NaCl-KCl eutectic melt. Electrochim Acta. 2009;54(21):4898–902.
16. Manga VR, Swinteck N, Bringuier S, Lucas P, Deymier P, Muralidharan K.

Interplay between structure and transport properties of molten salt mixtures of ZnCl2-NaCl-KCl: A molecular dynamics study. J Chem Phys. 2016;144(9).
17. Etter DE, Wiedenheft CJ. The study of KCl-CuCl eutectic fused salt as a potential intermediate temperature heat transfer and storage medium. Sol Energy Mater. 1980;2(4):423–31.
18. Guo S, Zhang J, Wu W, Zhou W. Corrosion in the molten fluoride and chloride salts and materials development for nuclear applications. Prog Mater Sci. 2018;97:448–87.
19. Lide DR. CRC handbook of chemistry and physics. 85th ed. CRC press; 2004. 2–55 p.
20. Britannica TE of E. salt. Available from: https://www.britannica.com/science/salt-acid-base-reactions
21. Anderson W. Organic vs. inorganic chemistry. 2021. Available from: https://schoolworkhelper.net/organic-vs-inorganic-chemistry/
22. Guidotti RA, Masset PJ. Primary batteries–reserve systems | thermally activated batteries: Lithium. In: Garche J, editor. Encyclopedia of Electrochemical Power Sources. Amsterdam: Elsevier; 2009. p. 141–55. Available from: https://www.sciencedirect.com/science/article/pii/B9780444527455001210
23. Pauling L. The nature of the chemical bond. Application of results obtained from the quantom mechanics and from a theory of paramagnetic susceptibility to the structure of molecules. J Am Chem Soc. 1931;53(4):1367–400.
24. Pauling L. The nature of the chemical bond. 3rd ed. Oxford University Press; 1960. 98–100 p.
25. Ouellette RJ, Rawn JD. Organic chemistry: Structure, mechanism, synthesis. Academic Press; 2018.
26. Kulakovskaya T V, Vagabov VM, Kulaev IS. Inorganic polyphosphate in industry, agriculture and medicine: Modern state and outlook. Process Biochem. 2012;47(1):1–10. Available from: https://www.sciencedirect.com/science/article/pii/S1359511311003850
27. Dupont J. From molten salts to ionic liquids: a “nano” journey. Acc Chem Res. 2011;44(11):1223–31.
28. Vignarooban K, Xu X, Wang K, Molina EE, Li P, Gervasio D, et al. Vapor pressure and corrosivity of ternary metal-chloride molten-salt based heat transfer fluids for use in concentrating solar power systems. Appl Energy. 2015;159:206–13.
29. Ding W, Bonk A, Bauer T. Molten chloride salts for next generation CSP plants: Selection of promising chloride salts & study on corrosion of alloys in molten chloride salts. In: Solarpaces 2018: International Conference on Concentrating Solar Power and Chemical Energy Systems. 2019.
30. Caraballo A, Galán-Casado S, Caballero Á, Serena S. Molten salts for sensible thermal energy storage: A review and an energy performance analysis. Energies. 2021;14(4). Available from: https://www.mdpi.com/1996-1073/14/4/1197
31. Gheribi AE, Torres JA, Chartrand P. Recommended values for the thermal conductivity of molten salts between the melting and boiling points. Sol Energy Mater Sol Cells. 2014;126:11–25. Available from: https://www.sciencedirect.com/science/article/pii/S0927024814001597
32. Janz G. High-temperature calibration quality data: Molten salts and metals. Mater Sci Forum. 1991;73:707–14.
33. Cornwell K. The thermal conductivity of molten salts. J Phys D Appl Phys. 1971;4(3):441.

34. Li Y, Xu X, Wang X, Li P, Hao Q, Xiao B. Survey and evaluation of equations for thermophysical properties of binary/ternary eutectic salts from NaCl, KCl, MgCl2, CaCl2, ZnCl2 for heat transfer and thermal storage fluids in CSP. Sol Energy. 2017;152:57–79. Available from: https://www.sciencedirect.com/science/article/pii/S0038092X17301792
35. Williams DF, Toth LM, Clarno KT. Assessment of Candidate Molten Salt Coolants for the Advanced High Temperature Reactor (AHTR). United States. Department of Energy; 2006.
36. Wang T, Mantha D, Reddy RG. Novel low melting point quaternary eutectic system for solar thermal energy storage. Appl Energy. 2013;102:1422–9. Available from: https://www.sciencedirect.com/science/article/pii/S0306261912006411
37. Pedersen S. Viscosity, structure and glass formationin the AlCl3-ZnCl2 system. NTNU; 2001.
38. Zhang C, Simpson M. Density of molten salt mixtures of eutectic LiCl-KCl containing UCl3, CeCl3, or LaCl3. J Nucl Fuel Cycle Waste Technol. 2017;15(2):117–24.
39. Wei X, Peng Q, Ding J, Yang X, Yang J, Long B. Theoretical study on thermal stability of molten salt for solar thermal power. Appl Therm Eng. 2013;54(1):140–4. Available from: https://www.sciencedirect.com/science/article/pii/S135943111300063X
40. Fathollahnejad H, Tsao B-H, Ponnappan R, Jacobson D. Post-test corrosion analysis of high-temperature thermal energy storage capsules. J Mater Eng Perform. 1993;2(1):125–34.
41. Forsberg CW, Peterson PF, Zhao H. High-temperature liquid-fluoride-salt closed-Brayton-cycle solar power towers. J Sol Energy Eng. 2007;129(2):141–6.
42. Druding L. Use of molten salts as a solvent in thin layer chromatography. Anal Chem. 1963;35(11):1744.
43. Fischer S, Leipner H, Thmmler K, Brendler E, Peters J. Inorganic molten salts as solvents for cellulose. Cellulose. 2003;10(3):227–36.
44. Fernandez A, Lasanta M, Perez F. Molten salt corrosion of stainless steels and low-Cr steel in CSP plants. Oxid Met. 2012;78(5):329–48.
45. Cabeza LF. Advances in thermal energy storage systems: methods and applications. Elsevier Science; 2014.
46. Bauer T, Pfleger N, Laing D, Steinmann W-D, Eck M, Kaesche S. 20 - High-temperature molten salts for solar power application. In: Lantelme F, Groult H, editors. Molten Salts Chemistry. Oxford: Elsevier; 2013. p. 415–38. Available from: https://www.sciencedirect.com/science/article/pii/B9780123985385000202
47. Bauer T, Pfleger N, Breidenbach N, Eck M, Laing D, Kaesche S. Material aspects of Solar Salt for sensible heat storage. Appl Energy. 2013;111:1114–9. Available from: https://www.sciencedirect.com/science/article/pii/S0306261913003681
48. Vignarooban K, Xu X, Arvay A, Hsu K, Kannan AM. Heat transfer fluids for concentrating solar power systems - A review. Applied Energy. 2015.
49. Raade JW, Padowitz D. Development of molten salt heat transfer fluid with low melting point and high thermal stability. J Sol Energy Eng. 2011;133(3):031013.
50. Bradshaw RW, Meeker DE. High-temperature stability of ternary nitrate molten salts for solar thermal energy systems. Sol Energy Mater. 1990;21(1):51–60. Available from:

https://www.sciencedirect.com/science/article/pii/016516339090042Y
51. Zhao CY, Wu ZG. Thermal property characterization of a low melting-temperature ternary nitrate salt mixture for thermal energy storage systems. Sol Energy Mater Sol Cells. 2011;95(12):3341–6. Available from: https://www.sciencedirect.com/science/article/pii/S0927024811004478
52. Wang T, Mantha D, Reddy RG. Thermal stability of the eutectic composition in LiNO3–NaNO3–KNO3 ternary system used for thermal energy storage. Sol Energy Mater Sol Cells. 2012;100:162–8. Available from: https://www.sciencedirect.com/science/article/pii/S0927024812000104
53. Peng Q, Ding J, Wei X, Jiang G. Thermodynamic investigation of the eutectic mixture of the Li-NO3-NaNO3-KNO3-Ca(NO3)2 system. Int J Thermophys. 2017;38(9):1–10.
54. An X-H, Cheng J-H, Su T, Zhang P. Determination of thermal physical properties of alkali fluoride/carbonate eutectic molten salt. In: AIP Conference Proceedings. 2017. p. 070001.
55. Vidal JC, Klammer N. Molten chloride technology pathway to meet the US DOE sunshot initiative with Gen3 CSP. AIP Conf Proc. 2019;2126(1).
56. Wei X, Song M, Wang W, Ding J, Yang J. Design and thermal properties of a novel ternary chloride eutectics for high-temperature solar energy storage. Appl Energy. 2015;156:306–10. Available from: https://www.sciencedirect.com/science/article/pii/S030626191500851X
57. Du L, Tian H, Wang W, Ding J, Wei X, Song M. Thermal stability of the eutectic composition in NaCl-CaCl2-MgCl2 ternary system used for thermal energy storage applications. Energy Procedia. 2017;105:4185–91. Available from: https://www.sciencedirect.com/science/article/pii/S1876610217309918
58. Du L, Ding J, Tian H, Wang W, Wei X, Song M. Thermal properties and thermal stability of the ternary eutectic salt NaCl-CaCl2-MgCl2 used in high-temperature thermal energy storage process. Appl Energy. 2017;204:1225–30. Available from: https://www.sciencedirect.com/science/article/pii/S0306261917303380
59. Li P, Molina E, Wang K, Xu X, Dehghani G, Kohli A, et al. Thermal and transport properties of NaCl–KCl–ZnCl2 eutectic salts for new generation high-temperature heat-transfer fluids. J Sol Energy Eng. 2016;138(5).
60. Serrano-ópez R, Fradera J, Cuesta-López S. Molten salts database for energy applications. Chem Eng Process - Process Intensif. 2013;73:87–102.
61. Jerden J. Molten salt thermophysical properties database development: 2019 update. 2019.
62. Barnes J, Coutts R, Horne T, Thai J. Characterisation of Molten Salts for application in molten salt reactors. PAM Rev Energy Sci Technol. 2019;6.
63. Briant RC, Weinberg AM. Molten fluorides as power reactor fuels. Nucl Sci Eng. 1957;2(6):797–803. Available from: https://doi.org/10.13182/NSE57-A35494
64. Ladkany S, Culbreth W, Loyd N. Molten salts and applications I: molten salt history, types, thermodynamic and physical properties, and cost. J Energy Power Eng. 2018;12:507–16.
65. Stern KH. High temperature properties and decomposition of inorganic salts part 3, nitrates and nitrites. J Phys Chem Ref Data. 1972;
66. Hoshi A, Mills DR, Bittar A, Saitoh TS. Screening of high melting point phase change materials (PCM) in solar thermal concentrating technology based on CLFR. Sol Energy. 2005;79(3):332–9.
67. Venkatesetty H, Lefrois R. Thermal energy storage for solar power plants. In: 11th

Intersociety Energy Conversion Engineering Conference. 1976. p. 606–12.
68. Kearney D, Herrmann U, Nava P, Kelly B, Mahoney R, Pacheco J, et al. Assessment of a molten salt heat transfer fluid in a parabolic trough solar field. J Sol Energy Eng Trans ASME. 2003;
69. Williams D. Assessment of candidate molten salt coolants for the NGNP/NHI heat-transfer loop. 2006.
70. Reilly HE, Kolb GJ. An evaluation of molten-salt power towers including results of the Solar Two project. Sandia National Laboratories, Albuquerque, NM. 2001.
71. Palacios A, Barreneche C, Navarro ME, Ding Y. Thermal energy storage technologies for concentrated solar power A review from a materials perspective. Renew Energy. 2020;156:1244–65.
72. Alva G, Lin Y, Fang G. An overview of thermal energy storage systems. Energy. 2018;144:341–78. Available from: https://www.sciencedirect.com/science/article/pii/S036054421732056X
73. Olsen E, Tomkute V. Carbon capture in molten salts. Energy Sci Eng. 2013;1(3):144–50.
74. Moorhouse J. Transport biofuels. 2021. Available from: https://www.iea.org/reports/transport-biofuels
75. Resende FLP. Recent advances on fast hydropyrolysis of biomass. Catal Today. 2016;269:148–55. Available from: https://www.sciencedirect.com/science/article/pii/S0920586116300025
76. Tian B, Xu L, Jing M, Liu N, Tian Y. A comprehensive evaluation on pyrolysis behavior, kinetics, and primary volatile formation pathways of rice husk for application to catalytic valorization. Fuel Process Technol. 2021;214:106715. Available from: https://www.sciencedirect.com/science/article/pii/S0378382020310067
77. Bridgwater A V. Principles and practice of biomass fast pyrolysis processes for liquids. J Anal Appl Pyrolysis. 1999;51(1):3–22. Available from: https://www.sciencedirect.com/science/article/pii/S0165237099000054
78. Bridgwater A V. Renewable fuels and chemicals by thermal processing of biomass. Chem Eng J. 2003;91(2):87–102. Available from: https://www.sciencedirect.com/science/article/pii/S1385894702001420
79. Bridgwater A V, Peacocke GVC. Fast pyrolysis processes for biomass. Renew Sustain Energy Rev. 2000;4(1):1–73. Available from: https://www.sciencedirect.com/science/article/pii/S1364032199000076
80. Tan EC, Marker TL, Roberts MJ. Direct production of gasoline and diesel fuels from biomass via integrated hydropyrolysis and hydroconversion process—A techno-economic analysis. Environ Prog Sustain Energy. 2014;33(2):609–17.
81. Elliott DC. Historical developments in hydroprocessing bio-oils. Energy & Fuels. 2007;21(3):1792–815.
82. Singh NR, Delgass WN, Ribeiro FH, Agrawal R. Estimation of liquid fuelyields from biomass. Environ Sci Technol. 2010;44(13):5298–305.
83. Marker TL, Felix LG, Linck MB, Roberts MJ. Integrated hydropyrolysis and hydroconversion (IH2) for the direct production of gasoline and diesel fuels or blending components from biomass, part 1: Proof of principle testing. Environ Prog Sustain Energy. 2012;31(2):191–9.
84. Sada E, Kumazawa H, Kudsy M. Pyrolysis of lignins in molten salt media. Ind Eng Chem Res. 1992;31(2):612–6.
85. Kudsy M, Kumazawa H. Pyrolysis of kraft lignin in the presence of molten ZnCl2-

KCl mixture. Can J Chem Eng. 1999;77(6):1176–84.
86. Yasunishi A, Tada Y. Wood pyrolysis in molten-salt. Kagaku Kogaku Ronbunshu. 1985;Vol. 11(3):346–9.
87. Nygård HS, Olsen E. Effect of salt composition and temperature on the thermal behavior of beech wood in molten salt pyrolysis. Energy Procedia. 2014;58:221–8.
88. Wang Y, Wei L, Li K, Ma Y, Ma N, Ding S, et al. Lignin dissolution in dialkylimidazolium-based ionic liquid–water mixtures. Bioresour Technol. 2014;170:499–505.
89. Xu X, Dehghani G, Ning J, Li P. Basic properties of eutectic chloride salts NaCl-KCl-ZnCl2 and NaCl-KCl-MgCl2 as HTFs and thermal storage media measured using simultaneous DSC-TGA. Sol Energy. 2018;162:431–41.
90. Jiang H, Ai N, Wang M, Ji D, Ji A. Experimental study on thermal pyrolysis of biomass in molten salt media. Electrochemistry. 2009;77(8):730–5.
91. Robelin C, Chartrand P. Thermodynamic evaluation and optimization of the (NaCl + KCl + MgCl 2 + CaCl2 + ZnCl2) system. J Chem Thermodyn. 2011;43:377.
92. Manga VR, Bringuier S, Paul J, Jayaraman S, Lucas P, Deymier P, et al. Molecular dynamics simulations and thermodynamic modeling of NaCl–KCl–ZnCl2 ternary system. Calphad. 2014;46:176–83.
93. Li C-J, Li P, Wang K, Emir Molina E. Survey of properties of key single and mixture halide salts for potential application as high temperature heat transfer fluids for concentrated solar thermal power systems. AIMS Energy. 2014;2(2):133–57.
94. Fontana CM, Gorin E, Kidder GA, Meredith CS. Chlorination of methane with copper chloride melts. Ternary system, CuCl–CuCl 2 –KCl, and its equilibrium chlorine pressures. Ind Eng Chem. 1952;44(2):369–73.
95. Handbook M salts. No Title. Janz, George J. 2013.
96. Ong T-C, Sarvghad M, Lippiatt K, Griggs L, Ryan H, Will G, et al. Review of the solubility, monitoring, and purification of impurities in molten salts for energy storage in concentrated solar power plants. Renew Sustain Energy Rev. 2020;131:110006. Available from: https://www.sciencedirect.com/science/article/pii/S1364032120302975
97. Gomez-Vidal JC, Tirawat R. Corrosion of alloys in a chloride molten salt (NaCl-LiCl) for solar thermal technologies. Sol Energy Mater Sol Cells. 2016;157:234–44. Available from: https://www.sciencedirect.com/science/article/pii/S0927024816301593
98. Kim G-Y, Jang J, Paek S, Lee S-J. Electrochemical removal of rare earth element in LiCl-KCl molten salt. Sci Technol Nucl Install. 2020;2020.
99. Simka W, Puszczyk D, Nawrat G. Electrodeposition of metals from non-aqueous solutions. Electrochim Acta. 2009;54(23):5307–19. Available from: doi.org/10.1016/j.electacta.2009.04.028
100. Inman D, White S. The production of refractory metals by electrolysis of molten salts design factors and limitations. J Appl Electrochem. 1978;8(5):375–90.
101. Khalaghi B, Kvalheim E, Tokushige M, Teng L, Seetharaman S, Haarberg GM. Electrochemical behaviour of dissolved iron chloride in KCl+LiCl+NaCl melt at 550ºC. ECS Trans. 2014;64(4):301.
102. Castrillejo Y, Bermejo MR, Barrado E, Martínez AM. Electrochemical behaviour of erbium in the eutectic LiCl–KCl at W and Al electrodes. Electrochim Acta. 2006;51(10):1941–51. Available from:

https://doi.org/10.1016/j.electacta.2005.07.004
103. Castrillejo Y, Fernández P, Medina J, Hernández P, Barrado E. Electrochemical extraction of samarium from molten chlorides in pyrochemical processes. Electrochim Acta. 2011;56(24):8638–44. Available from: https://doi.org/10.1016/j.electacta.2011.07.059
104. Chen GZ, Fray DJ, Farthing TW. Direct electrochemical reduction of titanium dioxide to titanium in molten calcium chloride. Nature. 2000;407(6802):361–4.
105. Yasuda K, Nohira T, Ito Y. Effect of electrolysis potential on reduction of solid silicon dioxide in molten CaCl2. J Phys Chem Solids. 2005;66(2):443–7. Available from: https://doi.org/10.1016/j.jpcs.2004.06.037
106. Bialik M. Personal communication. Sr Res Assoc RISE Bioeconomy.
107. Kroupa A. Modelling of phase diagrams and thermodynamic properties using Calphad method – Development of thermodynamic databases. Comput Mater Sci. 2013;66:3–13. Available from: https://www.sciencedirect.com/science/article/pii/S0927025612000699
108. Li X, Wu S, Wang Y, Xie L. Experimental investigation and thermodynamic modeling of an innovative molten salt for thermal energy storage (TES). Appl Energy. 2018;212:516–26. Available from: https://www.sciencedirect.com/science/article/pii/S0306261917317841
109. Lukas HL, G. Fries S, Sundman B. Computational thermodynamics, the Calphad method. New York: United States of America by Cambridge University Press, New York; 2007.
110. Bale CW, Chartrand P, Degterov SA, Eriksson G, Hack K, Ben Mahfoud R, et al. FactSage thermochemical software and databases. Calphad. 2002;26(2):189–228. Available from: https://www.sciencedirect.com/science/article/pii/S0364591602000354
111. Reis BH. Development of a novel thermodynamic database for salt systems with potential as phase change materials [PhD thesis]. Brandenburgische Technische Universität Cottbus - Senftenberg; 2021.
112. Rahman MS, Guizani N, Al-Khaseibi M, Ali Al-Hinai S, Al-Maskri SS, Al-Hamhami K. Analysis of cooling curve to determine the end point of freezing. Food Hydrocoll. 2002;Vol. 16(6):653–9.
113. Sonntag RE, Borgnakke C. Introduction to engineering thermodynamics. 2nd ed. Hoboken, N.J: Wiley; 2007.
114. Savéant J-M. Elements of molecular and biomolecular electrochemistry: an electrochemical approach to electron transfer chemistry. John Wiley & Sons; 2006.
115. Oldham KB, Stevens NP. Uncompensated resistance. 2. The effect of reference electrode nonideality. Anal Chem. 2000;72(17):3981–8.
116. Roine A, Lamberg P, Mansikka-aho J, Björklund P, Kentala J-P, Talonen T. HSC chemistry. Outotec Research Oy; 2006.
117. Olsen E, Hansen M, S. Nygård H. Hydrolysis of molten CaCl2-CaF2 with additions of CaO. AIMS Energy. 2017;5:873–86.
118. Adhoum N, Bouteillon J, Dumas D, Poignet JC. Electrochemical insertion of sodium into graphite in molten sodium fluoride at 1025°C. Electrochim Acta. 2006;51(25):5402–6. Available from: https://doi.org/10.1016/j.electacta.2006.02.019

9 Papers

Paper I

Niazi, Sepideh; Olsen, Espen; Nygård, Heidi S. "Hydrolysis of eutectic compositions in the $ZnCl_2$: KCl: NaCl ternary system and effect of adding ZnO." Journal of Molecular Liquids 317 (2020): 114069. https://doi.org/10.1016/j.molliq.2020.114069.

Paper II

Niazi, Sepideh; Bonk, Alexander; Hanke, Andrea; to Baben, Moritz; Reis, Bruno, Olsen, Espen; Nygård, Heidi S. "Thermal stability, hydrolysis and thermodynamic properties of molten KCl-CuCl." Materialia 21 (2022): 101296.
https://doi.org/10.1016/j.mtla.2021.101296.

Paper III

Niazi, Sepideh; Olsen, Espen; Nygård, Heidi S. "Electrochemical removal of Cu, Fe and Mn from molten $ZnCl_2$:KCl:NaCl". Submitted to Journal of Separation and Purification Technology.

Paper IV

Niazi, Sepideh; Nygård, Heidi S.; Reis, Bruno; to Baben, Moritz. "Thermodynamic modeling of KCl-H_2O and its binary subsystems including H_2O-HCl, KOH-H_2O and KCl-KOH". Submitted to CALPHAD Journal.

Paper I

Niazi, Sepideh; Olsen, Espen; Nygård, Heidi S. "Hydrolysis of eutectic compositions in the $ZnCl_2$: KCl: NaCl ternary system and effect of adding ZnO." Journal of Molecular Liquids 317 (2020): 114069.
https://doi.org/10.1016/j.molliq.2020.114069.

Journal of Molecular Liquids 317 (2020) 114069

Contents lists available at ScienceDirect

Journal of Molecular Liquids

journal homepage: www.elsevier.com/locate/molliq

Hydrolysis of eutectic compositions in the $ZnCl_2$:KCl:NaCl ternary system and effect of adding ZnO

Sepideh Niazi *, Espen Olsen, Heidi S. Nygård

Faculty of science and technology, Norwegian University of Life Science (NMBU), Ås, Norway

ARTICLE INFO

Article history:
Received 4 June 2020
Received in revised form 11 August 2020
Accepted 13 August 2020
Available online 22 August 2020

Keywords:
Molten salts
$ZnCl_2$:KCl:NaCl
Hydrolysis
Eutectics

ABSTRACT

Molten salt systems have been considered as proper liquefiers, solvents and transfer media due to their transport and thermodynamic properties. Employing molten salts to liquify biomass could be performed to make it pumpable and transfer it more easily through thermochemical conversion processes to e.g. bio-oil. The first challenge for this application is to find a salt with relatively low melting point. It needs to be low enough to avoid producing ash or char and at the same time high enough to liquify biomass. The selected molten salt requires high thermal stability to avoid salt decomposition at high temperatures and make salt recycling possible. Another challenge is minimising the hydrolysis rate of the molten salt in contact with water molecules originated from the biomass, because this can lead to undesired formation of highly corrosive acids. $ZnCl_2$:KCl:NaCl is a promising molten salt with relatively low melting point, high thermal stability and good properties in contact with biomass. The objective of this work is to investigate the properties of the eutectic mixtures of $ZnCl_2$:KCl:NaCl that are of importance for thermochemical conversion of biomass. Four compositions of $ZnCl_2$:KCl:NaCl are investigated, including Salt #1: 60: 20: 20, Salt #2: 59.5: 21.9: 18.6, Salt #3: 52.9: 33.7: 13.4 and Salt #4: 44.3: 41.9:13.8 in mole fraction. Salt #4 is found to exhibit the best properties, with low melting point, the highest thermal stability and the lowest hydrolysis rate. Salt #1 had the highest hydrolysis rate. However, addition of ZnO showed a marked, limiting effect on the hydrolysis, especially at temperatures below 400 °C.

1. Introduction

Molten salts have been used in various applications since the 19th century and their technologies are still under development [1,2]. One of the molten salt usages which has attracted a lot of attention in recent years is their role in the emerging renewable energy applications such as thermochemical conversion of biomass. In the late 20th century, molten salts were employed to develop pyrolysis of biomass in a few studies. The results showed that using molten salts could improve the yield production of for example phenolic compounds [3–5]. This is indicating that the molten salt could have catalytic effects. Another possible advantage is that the heating rate of biomass particles in molten salts is found to be higher than in inert atmosphere [6] or in a fluidized sand bed [7].

Some challenging technical issues are still unresolved, for example feeding the solid biomass into the reaction unit. The complexity of this increases for high pressure reactor such as hydro pyrolysis. Problems such as plugging, clogging, leakages, and uneven flow all lead to low production rate and poor quality. Liquifying biomass before feeding it into the high-pressure pyrolysis reactor can resolve the mentioned problem. It can facilitate pumping of the biomass and thus give better control of the feeding system.

Molten salts are considered as promising biomass liquefiers since they can maximize the liquid fraction in the fast pyrolysis process downstream. Other advantages of employing molten salts are the solubility of biomass in molten salts [8,9], high thermal conductivity of the molten salt and the possibility of using solar energy to heat and melt the salt. The molten salt is also a heat carrier and a possible catalyst in the follow up hydro-pyrolysis step of the process [3]. Additionally, they have favourable transport properties, i.e. low viscosity which leads to rapid enclosing of the biomass particles [2]. Molten salts can be recycled after removing char and ash.

The salt criteria for biomass liquefaction are in many ways similar to those of high-temperature phase change materials (PCM) for thermal energy storage. Favourable properties of a proper fluid are high heat capacity, high conductivity, low vapor pressure, high boiling point, low viscosity and low cost [10–12]. Moreover, the selected molten salt needs to liquefy the biomass at mild conditions and have a melting point around 200 °C. This temperature is low enough to avoid producing by-products such as ash or char and high enough to liquify biomass. The selected molten salt requires high thermal stability to avoid salt decomposition at high temperatures and make salt recycling possible. It is also important that the salts do not react chemically with constituents from

* Corresponding author.
E-mail address: sepideh.niazi@nmbu.no (S. Niazi).

https://doi.org/10.1016/j.molliq.2020.114069

the biomass particles and also provide minimum corrosion to metal pipes and containers. Hydrolysis is a possible reaction due to the presence of water in biomass. Water may react with the salts and form highly corrosive gases such as HCl or HF, if chlorides or fluorides are used, respectively. Therefore, the minimum rate of hydrolysis is a considerable issue for this study.

According to the mentioned favourable properties, different groups of molten salts have been considered as possible candidates to liquify biomass:

- Fluorides are thermally stable at high temperatures (>700 °C) [13], but they also have high melting points (>400 °C) [14].
- Carbonate salts are not chemically stable at high temperatures [15].
- Hydroxides show potential for dissolving biomass, but they will form stable carbonates in contact with carbon that need to be regenerated [16].
- Nitrites are not stable and oxidize at temperature higher than 350 °C [12].
- Nitrate mixtures are very common in solar energy systems [17], but they are very oxidizing and will not be stable in direct contact with carbon containing materials such as biomass [18]. Moreover, limited global reserves of nitrate salts is another drawback [19].
- Ionic metal chloride salts have potential due to high boiling points, abundant natural reserves and low cost compared to nitrates and nitrites [10,20]. They have low melting points and high thermal stability limits (>800 °C) [14].

Among all above groups, chlorides have the most essential properties for biomass liquefaction including low melting points and high thermal stability. Although many chlorides have been investigated in the literature for several applications, a eutectic mixture of $ZnCl_2$, NaCl and KCl is one of the most promising candidates for the present purpose. This ternary mixture is non-toxic, non-flammable, has a melting point around 200 °C and is stable at even higher temperatures compared to other ternary mixtures [21]. NaCl and KCl are available in large amounts. They have high heat capacities and low vapor pressures, but too high melting points (>750 °C). However, when a cubic ionic chloride such as NaCl or KCl with a high melting point is mixed with tetrahedral covalent chloride such as $ZnCl_2$ with a lower melting point in a particular proportion, a eutectic mixture is formed with a substantially lower melting point [10,14]. All three single melts ($ZnCl_2$, KCl and NaCl) have high stability even at high temperatures and the ternary salt system has low vapor pressure in temperature range of interest (0.7 atm at 800 °C) which is very promising [10,22]. Low vapor pressure (<1 atm) at high temperature, low melting point (~200 °C), high thermal conductivity, high heat capacity, low corrosion rate and high boiling point have been reported for different compositions of this salt mixture [5,14,23–25]. These results and the promising results in pyrolysis studies and thermal storage studies make $ZnCl_2$:KCl:NaCl as a promising candidate for this study [3–7,10,21,26].

Robelin and Chartrand have reported the thermodynamically modelled phase diagram of $ZnCl_2$:KCl:NaCl [23]. Moreover, the melting points of some compositions of this ternary chloride were investigated experimentally by a few researchers. Nitta et al. reported the eutectic temperature for $ZnCl_2$:KCl:NaCl = 60:20:20 (in mole fraction) to be around 203 °C [26]. Xu et al. carried out Differential Scanning Calorimetry (DSC) on three eutectic compositions of the salt [21]. The theoretical and experimental melting point of four eutectic compositions of the ternary salt reported in literature are given in Table 1. There are some variations for the reported melting points, and these will therefore be verified experimentally in the present study.

Table 1
Four different $ZnCl_2$:KCl:NaCl compositions and their melting points found in literature.

Salt	Molar composition (mol%)			Melting point (°C)	
	$ZnCl_2$	KCl	NaCl	Theoretical	Experimental
#1	60	20	20	–	203 (26)
#2	59.5	21.9	18.6	213 (23)	198.7 (21)
#3	52.9	33.7	13.4	204 (23)	210.3 (21)
#4	44.3	41.9	13.8	229 (23)	199.4 (21)

2. Thermodynamic modelling

Although thermodynamic and transport properties of the ternary composition of $ZnCl_2$:KCl:NaCl are investigated in some studies, there are no studies regarding hydrolysis in the case of presence of moisture. Moisture is one of the most common detrimental impurities in molten chlorides [1] since chlorides such as $ZnCl_2$ are strongly hygroscopic. Although this salt is normally kept at high temperatures to avoid absorbing moisture, small amounts of water may induce hydrolysis of the salt. It can react with the chlorine anion and lead to the formation of HCl, which is a highly corrosive gas [14,27]. In the case where a chloride molten salt is in contact with water containing feedstock such as lignocellulosic biomass, this may aggravate the corrosion rate of process equipment [28].

The hydrolysis reactions for the single salts $ZnCl_2$, KCl and NaCl are described by Eqs. (1)–(4) [18]. The Gibbs free energy of the reactions (simulated with HSC Chemistry), are well above zero up to 1000 °C as depicted in Fig. 1. It means that hydrolysis is not thermodynamically favoured at relevant process temperatures. However, all reactions are in equilibrium and the hydrolysing halides form gaseous compounds. The formed compounds will be constantly removed from the system and decrease the vapor pressure and it will tend to drive the reactions towards HCl production [29].

$$ZnCl_2 + 2H_2O(g) \leftrightarrow Zn(OH)_2 + 2HCl(g) \quad (1)$$

$$ZnCl_2 + H_2O(g) \leftrightarrow ZnO + 2HCl(g) \quad (2)$$

$$NaCl + H_2O(g) \leftrightarrow NaOH + HCl(g) \quad (3)$$

$$KCl + H_2O(g) \leftrightarrow KOH + HCl(g) \quad (4)$$

In order to reduce the hydrolysis rate of molten salts, the effect of adding a metal oxide was recently investigated. Olsen et al. reported that adding CaO to molten $CaCl_2$:CaF lowers the tendency for hydrolysis [29]. For the present study ZnO is considered as a potential oxide to reduce the hydrolysis rate. According to Eq. (5) and Fig. 1, ZnO can theoretically react with the produced HCl and hence reduce the levels of HCl in the exit gas [2].

$$ZnO + 2HCl(g) \leftrightarrow ZnCl_2 + H_2O(g) \quad (5)$$

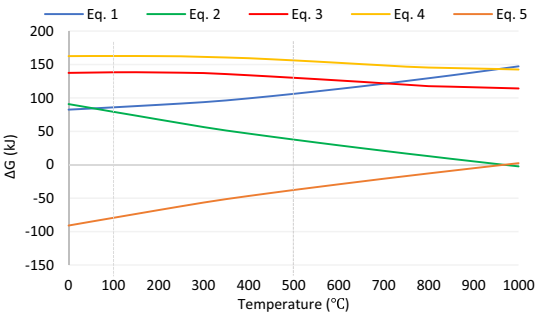

Fig. 1. Gibbs free energy of hydrolysis reactions of $ZnCl_2$, NaCl, KCl (Eqs. (1)–(4)) and the reaction of ZnO with HCl (Eq. (5)) in the range of 0 to 1000 °C. The relevant range of temperature for biomass liquefaction is 100–500 °C.

In addition to hydrolysis reaction, direct oxidation reaction of $ZnCl_2$ can also form ZnO and release chlorine [30,31]. In this case, dissolved oxygen in the biomass may react with molten $ZnCl_2$ and play a role of hydrolysis inhibitor by forming ZnO.

3. Experimental details

Four different compositions of $ZnCl_2$:KCl:NaCl as described in Table 1 have been studied. Experiments to measure melting points, thermal stability and hydrolysis were performed. Afterwards, the hydrolysis process has been studied and the effect of ZnO on hydrolysis rate has been investigated.

3.1. Materials and setup

It was necessary to pre dry the chemicals in order to remove residual crystal water due to the hygroscopic nature of the salts (especially $ZnCl_2$). $ZnCl_2$ (VWR, 98.3%), KCl (Sigma, ≥99.5%), NaCl (Sigma, ≥99.8%) and ZnO (Alfa Aesar, 99%), were dried and kept in a muffle furnace at 200 °C for at least 24 h in separate and closed beakers.

In all experiments, dried salts were mixed and prepared in a nickel crucible. The reactor setup containing the nickel crucible was heated in a vertical electrical tube furnace with radiation shields at the bottom part to minimize the heat loss. LabView 8.2 (National Instrument) was used to monitor and record the measurements. Ar gas was passed through the furnace from the bottom to provide inert atmosphere during the experiments. A type S thermocouple was immersed in the salt for monitoring and recording the salt temperature profile during all experiments. All experiments were carried out at ambient pressure. Since hydropyrolysis of biomass is carried out in high pressure units, it is not possible to conduct such experiments with the existing experimental setup.

Although the mentioned requirements and conditions are common for all experiments, the measurement methods and set up details vary for melting point, thermal stability and hydrolysis, and these are further are described in following sections.

3.2. Melting point experiments

The melting point of the selected molten salt is one of the main issues since the idea is to perform the liquefaction step at mild conditions (~200 °C, atmospheric pressure). To verify the reported melting points from the literature, the melting points were measured experimentally by using the cooling curve method [32]. 120 g of dry salt mixture was placed inside a nickel crucible (with the height of 5.7 cm and the inner diameter of 6.1 cm) and heated up to 250 °C in a vertical electrical resistance furnace to ensure complete melting. The crucible was equipped with radiation shields above to minimize heat loss (see Fig. 2). A mechanical nickel stirrer (40 rpm) was used to mix the molten salt for at least one hour to ensure a homogenous mixture. Then the salt mixture was cooled down slowly at a rate of 0.3 or 0.5 °C/min. In some cases, 0.1–0.15 g of a solid salt crystal ($ZnCl_2$:KCl:NaCl) was fed through a seeding pipe right before the solidification occurred. This was performed in order to reduce undercooling. The melting point experiments were repeated several times by heating up the solidified salt and cooling down again for each composition.

3.3. Thermal stability experiments

Thermogravimetric analysis (TGA) was performed to compare the thermal stability of all four compositions as a function of temperature up to 500 °C. For this purpose, 235 g of dried salt mixture was placed in a tubular nickel crucible with the height of 17 cm and the inner diameter of 5.1 cm. The mixture was compressed as much as possible in order to remove the trapped air and minimize the possible experimental errors, as suggested by Xu et al. [21]. A weight scale which was connected to a computer was located above the furnace and the crucible containing the salt was hanged from the weight scale to record the weight change continuously during the experiment (see Fig. 3). The salt mixture was heated up to 500 °C at a heating rate of 10 °C/min.

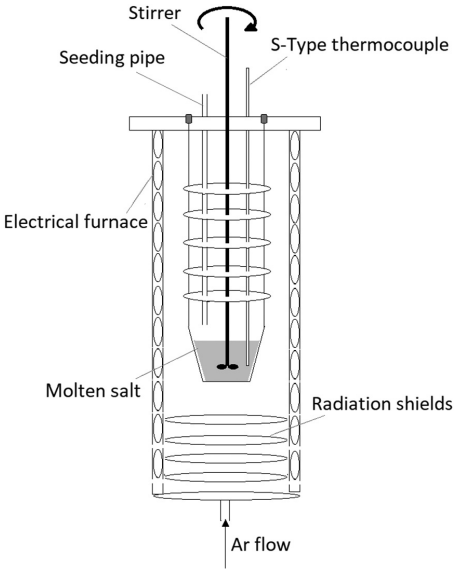

Fig. 2. Schematic representation of the experimental setup for determination of melting points. The sample is placed in a nickel crucible and undergoes controlled cooling under constant stirring. The experiments were performed under inert atmosphere (Ar).

3.4. Hydrolysis experiments

The possible side reactions of the four $ZnCl_2$:KCl:NaCl mixtures were investigated with emphasize on hydrolysis reactions. Hydrolysis reactions could give HCl formation, which is a highly corrosive and undesirable gas.

In order to test whether the hydrolysis reactions occur, a series of hydrolysis experiments were performed in the setup depicted in Fig. 4. 235 g of dried salt mixture was prepared in a nickel crucible similar to the TGA experiment crucible described in Section 3.2. It was placed inside a sealed stainless-steel vessel. The salt mixture was heated up to 230 °C under inert atmosphere (Ar flow). To ensure homogenous melts and to ensure that all initial crystal water was removed, N_2 was bubbled through the molten salt for at least 12 h at the rate of 0.2 Nl/min while monitoring the gas composition escaping from the system. Experiments were not started before no HCl was detected.

The hydrolysis experiments started from 250 °C. H_2O (g) was added by bubbling 0.4 Nl/min N_2 through a closed, water filled vessel placed on a hot plate with temperature control. The water temperature was kept at a constant value of 46 °C, to ensure a water partial pressure of 10 kPa (10 vol%) [33]. Heated gas lines (around 170 °C) which include PTFE (Teflon) tubes covered by heating elements, were employed throughout the whole system to avoid vapor condensing. The gas consisting of N_2 and water vapor was then added to the molten salt. This was performed by bubbling one centimetre above the bottom of the molten salt by an immersed nickel tube as a part of the sealed vessel. Thus, the gas will flow to the top of the molten salt bath and then being released to the volume above the salt and leave the vessel from the top through the stainless-steel exhausting tube. The exit gas was passed through a high voltage electrostatic filter (3–6 kV) to remove possible

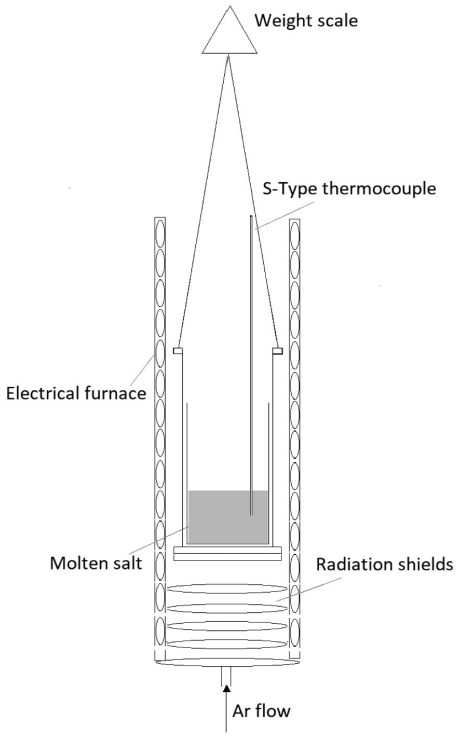

Fig. 3. Schematic representation of the experimental setup for TGA studies. The setup is hanged from the weight scale which records the weight. The temperature is measured by a type S thermocouple.

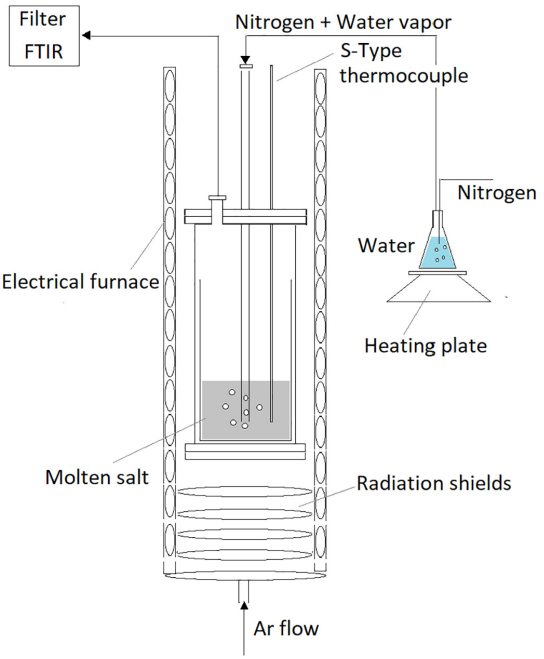

Fig. 4. Schematic representation of the experimental setup for hydrolysis studies. The inner crucible and the feed tube are made of nickel, and the outer container is made of stainless steel. The melt temperature is measured by a type S thermocouple.

particles entrained in the gas stream. High voltage was supplied from a power supply (Spellman SL300). Afterwards, the filtered gas was analysed by Fourier Transform Infrared spectroscopy (FTIR). The FTIR unit (Thermo Nicolet 6700) was equipped with a 2 m gas cell running the commercial Fire Science method (Thermo Fisher). The gas escaping from the system was continuously monitored by FTIR from the beginning. During the experiments, the salt temperature was increased in intervals of 50 °C up to 500 °C. The melt was kept at each temperature interval for at least 30 min to get an approximate stable level of HCl.

In order to investigate the effect of ZnO on hydrolysis, the salt with the highest hydrolysis rate was chosen as a suitable candidate. The same setup and procedure as the hydrolysis experiments were used. Two different amounts of dried ZnO powder, namely 5 wt% and 10 wt %, were added to the chosen salt (Salt #1) at the stage of preparing the salt mixture and the same procedure was carried out for both ZnO concentrations.

4. Results and discussion

4.1. Eutectic composition and melting point experiments

Fig. 5 shows the cooling curves of four selected compositions of $ZnCl_2$:KCl:NaCl. For Salt #1, 2 and 4 three parallels were conducted while for Salt #3 there were two parallels. In the cases of Salt #1, 3 and 4 the molten salt was seeded just before solidification to smooth undercooling while for Salt #2 this was not necessary because no large undercooling was observed even without seeding. The results from the cooling curves for Salt #3 show two occasions of undercooling and superheating, indicating that this composition is in fact not a true eutectic composition. However, this is not crucial for the biomass liquefaction, as long as the liquefaction temperature is above the highest melting point. In the cooling curves for Salt #4 small shoulders are observed which were recorded very quickly after the first undercooling.

Temperature calibration is necessary in order to minimize the systematic errors of the thermocouple. The thermocouple was calibrated using deionized ice and water, deionized boiling water, pure tin and pure zinc. The measured melting points based on cooling curves were calibrated according to Table 2 using linear regression.

Fig. 6 presents the average value of the measured melting points for all four compositions, before and after calibrating calculations. The data shows almost similar melting points for Salt #1, #2 and #4, in the range between 202 °C and 205 °C. However, the melting point for the non-eutectic composition #3 is relatively higher (the first transition temperature around 217 °C and the second one around 212 °C). These values are closer to the experimental melting points from literature [21] rather than the values based on the reported phase diagram [23] listed in Table 1. The difference of theoretical analysis with the measured value may be due to various reasons. Uncertainty of salt properties of individual salts in theoretical analysis and impurities in the salts in experimental values can be the most relevant explanation.

4.2. Thermal stability

Fig. 7 shows the mass loss as a function of temperature for the selected compositions of $ZnCl_2$:KCl:NaCl. According to the TGA results, the mass loss is relatively small when the temperature is below 500 °C. Salt #1 (60:20:20 mol%) started to lose mass earlier than the others, and totally lost 2% of mass when the temperature reached 500 °C. In Salt #2 (59.5:21.9:18.6 mol%) around 1% mass loss was observed at the same temperature, while Salt #3 (52.9:33.7:13.4 mol%) and #4 (44.3:41.9:13.8) presented the lowest mass loss at 500 °C,

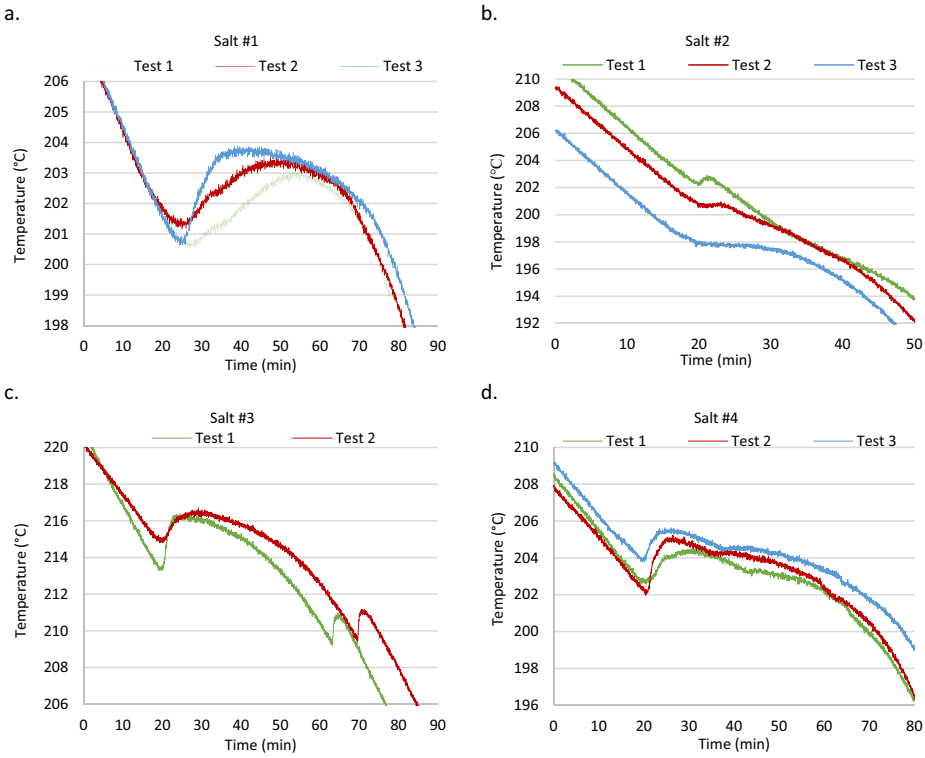

Fig. 5. Cooling curves for the molten salts including a. Salt #1 (60:20:20 mol%) b. Salt #2 (59.5:21.9:18.6 mol%) c. Salt #3 (52.9:33.7:13.4 mol%) d. Salt #4 (44.3:41.9:13.8 mol%). For a, c and d the cooling rate is 0.3 and 0.1–0.15 g of solid salt crystal was added right before the solidification to smooth the undercooling. For case b the cooling rate is 0.5 °C/min and no salt crystal was added.

with around 0.5% and 0.2%, respectively. The results show that by decreasing the concentration of $ZnCl_2$ and increasing the concentration of KCl in the salt mixture, the thermal stability is strengthened.

Nitta et al. have reported similar results. They carried out TG-DTA (Thermogravimetry/Differential Thermal Analysis) curves of three selected compositions, $ZnCl_2$:KCl:NaCl, 55:22.5:22.5, 60:20:20 and 65:17.5:17.5, in mole fraction [26]. For all the TG curves, no weight decrease was observed up to 350 °C. Xu et al. carried out TGA simultaneously on three eutectic compositions of the salt [21]. They have investigated the melting points and reported slight mass loss, less than 1%, with the increase of the temperature up to 400 °C. The current study goes a bit higher temperature up to 500 °C, because these temperatures are more relevant for hydropyrolysis of biomass.

4.3. Hydrolysis experiments

Fig. 8 shows the level of HCl formation for each temperature interval, from 250 °C to 500 °C, for the four selected compositions of $ZnCl_2$:KCl:NaCl. As the figures show, increasing temperature usually leads to higher HCl levels. Salt #1 produces very low levels of HCl (~0 ppmv) at 250 °C, however, they increase dramatically by increasing temperature and reach more than 4500 ppmv at 500 °C. Salt #2 has lower levels of HCl in all temperature intervals and produces low amounts of HCl below 400 °C. Then it increases to more than 2300 ppmv at 450 °C and around 4000 ppmv at 500 °C. Salt #3 shows unstable HCl level production more or less in all intervals but still higher level of HCl at temperature above 400 °C and form around 2000, 3000 and 5000 ppmv at 400, 450 and 500 °C,

Table 2
Standard and measured calibration points for S-type thermocouple.

Sample	Deionized ice+ water	Deionized boiling water	Pure tin	Pure zinc
Calibration point (°C)	0.0	100.0	231.9	419.5
Measured value (°C)	0.06	97.9	231.2	417.1
Relative error	–	2.1%	0.3%	0.57%

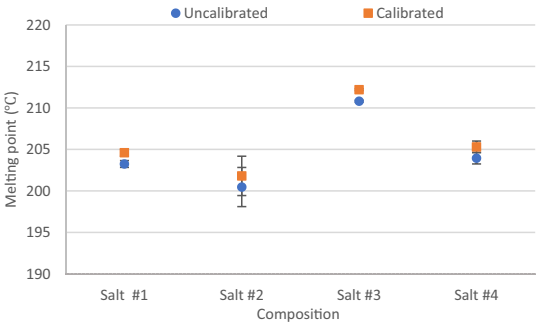

Fig. 6. Experimental melting points for four compositions of $ZnCl_2$:KCl:NaCl before and after calibration.

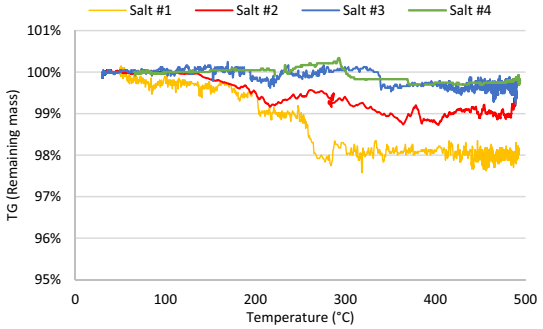

Fig. 7. Mass loss as a function of temperature for four different compositions of $ZnCl_2$:KCl:NaCl.

respectively. The formation of HCl in Salt #4 is clearly less than the other salt compositions and almost no HCl formation was observed at 350 °C and lower. The first sign of HCl formation was at 400 °C around 1000 ppmv and increased to 1300 ppmv at 500 °C.

The average value of the HCl formation for each composition and each temperature interval was calculated and shown in Fig. 9. For all compositions, similar trends were observed, and the maximum amount of HCl are detected at the highest temperatures. In Salt #1 with the highest amount of $ZnCl_2$ and lowest amount of KCl (60:20:20 mol% $ZnCl_2$:KCl:NaCl), HCl forms readily at and above 300 °C. Salt #4 (44.3:41.9:13.8 mol% $ZnCl_2$:KCl:NaCl), with the lowest amount of $ZnCl_2$ in the composition, shows the lowest levels of HCl at almost all temperatures, with almost no HCl below 400 °C.

Addition of ZnO to Salt #1 raises the temperature for onset of hydrolysis. HCl formation started above 400 °C and again the HCl formation increased with higher temperature. The results in Fig. 10 show that adding 5 and 10 wt% ZnO to Salt #1 can reduce the levels of HCl from 1700, 2600 and 3400 ppmv to less than 300 ppmv at temperatures below 400 °C while these were not very effective at higher temperatures. Adding 10% ZnO decreases the HCl formation at 450 °C more than 1000 ppmv, however no positive effects were observed in higher temperatures with adding 5% ZnO.

5. Conclusion

The properties of molten $ZnCl_2$:KCl:NaCl including melting points, thermal stability and hydrolysis have been studied experimentally. Four different compositions were chosen: Salt #1: 60:20:20 mol%, Salt #2: 59.5:21.9:18.6 mol%, Salt #3: 52.9:33.7:13.4 mol%, Salt #4: 44.3:41.9:13.8 mol% $ZnCl_2$:KCl:NaCl. These four compositions have been considered to be candidate molten salts for biomass liquefaction, with sufficiently low melting point around 200 °C.

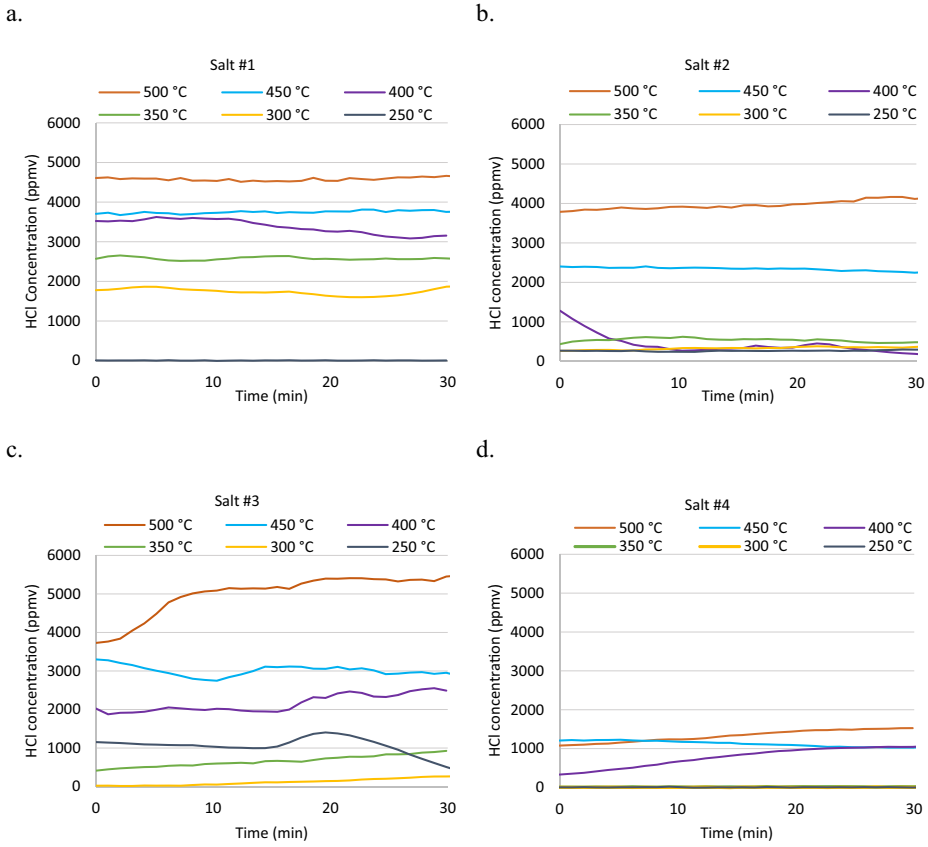

Fig. 8. The content of HCl in the exit gas as a function of temperature from 250 °C to 500 °C when 10 vol% water in N_2 is added to a: Salt #1 (60:20:20 mol%) b: Salt #2 (59.5:21.9:18.6 mol%) c: Salt #3 (52.9:33.7:13.4 mol%) and d: Salt #4 (44.3:41.9:13.8 mol%) $ZnCl_2$:KCl:NaCl.

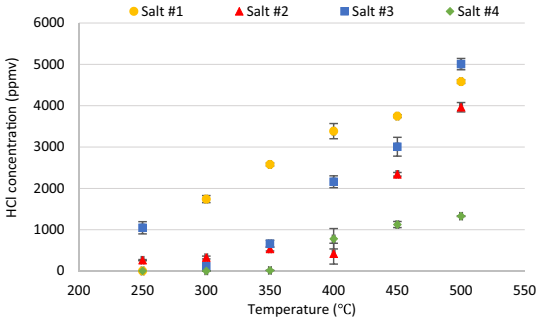

Fig. 9. The average content of HCl in the exit gas as a function of temperature from 250 °C to 500 °C when 10 vol% water in N_2 is added to Salt #1 - #4.

The melting point experiments for Salt #3 indicated that this composition is not a true eutectic composition. However, this is not considered as an issue in this study as long as the biomass liquefaction temperature is above its melting point. The other compositions had melting points in the range of 203–205 °C. TGA was employed to analyse the thermal stability of all compositions up to 500 °C. In the cyclic short-term thermal stability experiments, Salt #1 showed the highest mass loss around 2% at 500 °C. The mass loss for the other mixtures decreased with lower concentration of $ZnCl_2$ in the mixture and the weight loss for Salt #4 was negligible. Hydrolysis reactions are of special importance since these could form undesired and corrosive gases such as HCl. The results show that molten chlorides react with water vapor and form HCl. Furthermore, the reaction is quite temperature dependent. Lower amounts of $ZnCl_2$ in the mixture leads to lower rates of hydrolysis and Salt #4 shows the minimum amount of HCl compared to the other compositions. The experiments have been performed at ambient pressure due to limitations of the experimental setup. Hydro pyrolysis is, on the other hand, a high-pressure process which can supress vapor pressure and HCl formation. Therefore, the hydrolysis rate could be lower than reported values in this study. Moreover, addition of ZnO to Salt #1 shows a significant reduction effect on HCl production especially at the lower temperatures.

In total, Salt #4 seems to have the most promising properties relevant for thermochemical conversion of biomass. It has a relatively low melting point (~205 °C), the highest thermal stability (~0.2% mass loss at 500 °C) and exhibit the least tendency to form HCl during hydrolysis experiments. In order to avoid HCl formation completely, it is advised to keep the reaction temperatures below 400 °C and/or add ZnO as a hydrolysis inhibitor.

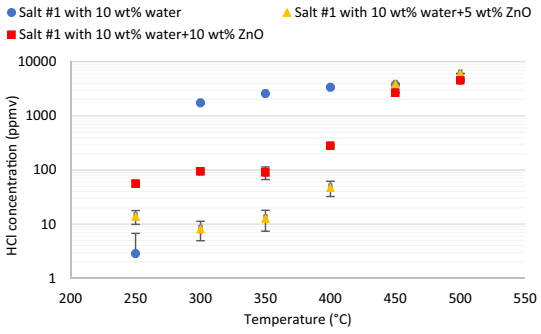

Fig. 10. The content of HCl in the exist gas for Salt #1 by using 0%, 5% and 10% ZnO.

CRediT authorship contribution statement

Sepideh Niazi: Conceptualization, Data curation, Formal analysis, Investigation, Methodology, Software, Validation, Visualization, Writing - original draft, Writing - review & editing. **Espen Olsen:** Conceptualization, Methodology, Supervision, Validation, Writing - review & editing. **Heidi S. Nygård:** Conceptualization, Funding acquisition, Methodology, Project administration, Resources, Supervision, Validation, Writing - review & editing.

Declaration of competing interest

All experiments have been carried out at the Norwegian University of Life Sciences (NMBU). Laboratories and financial supports for this project have been supplied by European union's Horizon 2020 Research and Innovation programme under grant agreement number 764089.

Acknowledgments

This project has received funding from the European union's Horizon 2020 - Research and Innovation Framework Programme under grant agreement number 764089.

References

[1] S. Guo, J. Zhang, W. Wu, W. Zhou, Corrosion in the molten fluoride and chloride salts and materials development for nuclear applications, Prog. Mater. Sci. 97 (2018) 448–487.
[2] D.G. Lovering, An introduction to molten salt technology, in: D.G. Lovering (Ed.), Molten Salt Technology, Springer US, Boston, MA, 1982.
[3] E. Sada, H. Kumazawa, M. Kudsy, Pyrolysis of lignins in molten salt media, Ind. Eng. Chem. Res. 31 (2) (1992) 612–616.
[4] M. Kudsy, H. Kumazawa, Pyrolysis of kraft lignin in the presence of molten $ZnCl_2$-KCl mixture, Can. J. Chem. Eng. 77 (6) (1999) 1176–1184.
[5] H. Jiang, N. Ai, M. Wang, D. Ji, A. Ji, Experimental study on thermal pyrolysis of biomass in molten salt media, Electrochemistry 77 (8) (2009) 730–735.
[6] A. Yasunishi, Y. Tada, Wood pyrolysis in molten-salt, Kagaku Kogaku Ronbunshu 11 (3) (1985) 346–349.
[7] H.S. Nygård, E. Olsen, Effect of salt composition and temperature on the thermal behavior of beech wood in molten salt pyrolysis, Energy Procedia 58 (2014) 221–228.
[8] Y. Wang, L. Wei, K. Li, Y. Ma, N. Ma, S. Ding, et al., Lignin dissolution in dialkylimidazolium-based ionic liquid–water mixtures, Bioresour. Technol. 170 (2014) 499–505.
[9] P. O'Connor, J.A. Moulijn, M. Makkee, S. Daamen, R.M. de Almeida, Process for the Conversion of Cellulose in Hydrated Molten Salts, US8846902B2, United States, 2014.
[10] K. Vignarooban, X. Xu, K. Wang, E.E. Molina, P. Li, D. Gervasio, et al., Vapor pressure and corrosivity of ternary metal-chloride molten-salt based heat transfer fluids for use in concentrating solar power systems, Appl. Energy 159 (2015) 206–213.
[11] R. Serrano-ópez, J. Fradera, S. Cuesta-López, Molten salts database for energy applications, Chem Eng Process - Process Intensif 73 (2013) 87–102.
[12] L.F. Cabeza, Advances in Thermal Energy Storage Systems: Methods and Applications, Elsevier Science, 2014.
[13] H. Fathollahnejad, B.-H. Tsao, R. Ponnappan, D. Jacobson, Post-test corrosion analysis of high-temperature thermal energy storage capsules, J. Mater. Eng. Perform. 2 (1) (1993) 125–134.
[14] W. Ding, A. Bonk, T. Bauer, Molten chloride salts for next generation CSP plants: selection of promising chloride salts & study on corrosion of alloys in molten chloride salts, SOLARPACES 2018: International Conference on Concentrating Solar Power and Chemical Energy Systems, 2019.
[15] S. Kuravi, J. Trahan, D.Y. Goswami, M.M. Rahman, E.K. Stefanakos, Thermal energy storage technologies and systems for concentrating solar power plants, Prog. Energy Combust. Sci. 39 (4) (2013) 258–319.
[16] J.K. Maund, D.M. Earp, Fuels from biomass by conversion in molten salts, Research in Thermochemical Biomass Conversion, Springer, Dordrecht 1988, pp. 542–556.
[17] B. D'Aguanno, M. Karthik, A.N. Grace, A. Floris, Thermostatic properties of nitrate molten salts and their solar and eutectic mixtures, Sci Reports 8 (2018), 10485.
[18] A. Roine, P. Lamberg, J. Mansikka-aho, P. Björklund, J.-P. Kentala, T. Talonen, HSC Chemistry. Outotec Reseaqrch Oy, 2006.
[19] N.S. Patel, V. Pavlík, M. Boča, High-temperature corrosion behavior of superalloys in molten salts–a review, Crit Rev Solid State Mater Sci 42 (1) (2017) 83–97.
[20] A. Hoshi, D.R. Mills, A. Bittar, T.S. Saitoh, Screening of high melting point phase change materials (PCM) in solar thermal concentrating technology based on CLFR, Sol. Energy 79 (3) (2005) 332–339.
[21] X. Xu, G. Dehghani, J. Ning, P. Li, Basic properties of eutectic chloride salts NaCl-KCl-$ZnCl_2$ and NaCl-KCl-$MgCl_2$ as HTFs and thermal storage media measured using simultaneous DSC-TGA, Sol. Energy 162 (2018) 431–441.

[22] C.-J. Li, P. Li, K. Wang, E. Emir Molina, Survey of properties of key single and mixture halide salts for potential application as high temperature heat transfer fluids for concentrated solar thermal power systems, AIMS Energy 2 (2) (2014) 133–157.
[23] C. Robelin, P. Chartrand, Thermodynamic evaluation and optimization of the (NaCl + KCl + $MgCl_2$ + $CaCl_2$ + $ZnCl_2$) system, J. Chem. Thermodyn. 43 (2011) 377.
[24] V.R. Manga, S. Bringuier, J. Paul, S. Jayaraman, P. Lucas, P. Deymier, et al., Molecular dynamics simulations and thermodynamic modeling of NaCl–KCl–ZnCl2 ternary system, Calphad 46 (2014) 176–183.
[25] V.R. Manga, N. Swinteck, S. Bringuier, P. Lucas, P. Deymier, K. Muralidharan, Interplay between structure and transport properties of molten salt mixtures of $ZnCl_2$-NaCl-KCl: a molecular dynamics study, J. Chem. Phys. 144 (9) (2016).
[26] K. Nitta, T. Nohira, R. Hagiwara, M. Majima, S. Inazawa, Physicochemical properties of $ZnCl_2$-NaCl-KCl eutectic melt, Electrochim. Acta 54 (21) (2009) 4898–4902.
[27] L. Maksoud, T. Bauer, Experimental investigation of chloride molten salts for thermal energy storage applications, 10th International Conference on Molten Salt 2015, pp. 273–280.
[28] W. Ding, A. Bonk, T. Bauer, Corrosion behavior of metallic alloys in molten chloride salts for thermal energy storage in concentrated solar power plants: a review, Front. Chem. Sci. Eng. 12 (2018) 564–576.
[29] E. Olsen, M.S. Hansen, H. Nygård, Hydrolysis of molten $CaCl_2$-CaF_2 with additions of CaO, AIMS Energy 5 (2017) 873–886.
[30] Y.S. Li, Y. Niu, W.T. Wu, Accelerated corrosion of pure Fe, Ni,Cr and several Fe-based alloys induced by $ZnCl_2$-KCl at 450 °C in oxidizing environment, Mater. Sci. Eng. A 345 (1–2) (2003) 64–71.
[31] Y.S. Li, M. Spiegel, Models describing the degradation of FeAl and NiAl alloys induced by ZnCl2KCl melt at 400–450 °C, Corros. Sci. 46 (8) (2004) 2009–2023.
[32] M.S. Rahman, N. Guizani, M. Al-Khaseibi, S. Ali Al-Hinai, S.S. Al-Maskri, K. Al-Hamhami, Analysis of cooling curve to determine the end point of freezing, Food Hydrocoll. 16 (6) (2002) 653–659.
[33] R.E. Sonntag, C. Borgnakke, Introduction to Engineering Thermodynamics, 2nd ed. Wiley, Hoboken, N.J, 2007.

Paper II

Niazi, Sepideh; Bonk, Alexander; Hanke, Andrea; to Baben, Moritz; Reis, Bruno; Olsen, Espen; Nygård, Heidi S. "Thermal stability, hydrolysis and thermodynamic properties of molten KCl-CuCl." Materialia 21 (2022): 101296. https://doi.org/10.1016/j.mtla.2021.101296.

Materialia 21 (2022) 101296

Contents lists available at ScienceDirect

Materialia

journal homepage: www.elsevier.com/locate/mtla

Thermal stability, hydrolysis and thermodynamic properties of molten KCl-CuCl

Sepideh Niazi [a,*], Alexander Bonk [b], Andrea Hanke [b], Moritz to Baben [c], Bruno Reis [c], Espen Olsen [a], Heidi S. Nygård [a]

[a] Faculty of Science and Technology, Norwegian University of Life Science (NMBU), Ås, Norway
[b] German Aerospace Center (DLR), Institute of Engineering Thermodynamics, Stuttgart 70569, Germany
[c] GTT-Technologies, Kaiserstraße 103, Herzogenrath 52134, Germany

ARTICLE INFO

Keywords:
Molten salts
KCl-CuCl
Modelling
Phase diagram
Calphad

ABSTRACT

KCl-CuCl is known as an inorganic salt mixture with a particularly low melting point, below 200 °C. There are very few studies published investigating this binary system. In this study KCl-CuCl is considered as a candidate for liquifying biomass as a pre-step before a high pressure and temperature (40–50 bar, 450–500 °C) hydro-pyrolysis process. Its low melting point makes it a good candidate to liquify biomass at mild conditions (low temperature and pressure) and avoid producing char and ash. Thermal stability and stability against hydrolysis have been measured for compositions close to the eutectic composition up to 500 °C. The results show that KCl-CuCl is thermally stable, and no mass loss was observed up to 500 °C. Moreover, it is chemically stable in contact with water and no HCl was detected in hydrolysis experiments.

In addition, the modelling of the system was studied. Although there is a phase diagram for this system in the literature based on the experimental data, no thermodynamic parameters have been calculated for this system and no database was found for KCl-CuCl solution. Therefore, Calphad modelling of the binary KCl-CuCl molten salt is performed in this study and FactSage is employed to assess the thermodynamic parameters and generate the phase diagram. For this purpose, a series of experiments have been carried out to investigate transition points and thermodynamic properties of mixtures between 40 and 80 mol% of CuCl by cooling curve and differential scanning calorimetry. The intermediate compound K_2CuCl_3 is considered stoichiometric, and its Gibbs energy modelling relies on ab initio calculated enthalpy of reaction from the base salts and optimization of the standard entropy. The liquid solution is modelled with a subregular solution model using Redlich-Kister polynomials. The phase diagram of the system is generated based on thermodynamic data and experimental results. The results show that the predicted eutectic point of the binary system is located at $T = 145.9$ °C and 64.9 CuCl mol%. The calculated results are in excellent agreement with the measured values. The high thermal stability and stability against hydrolysis qualify eutectic KCl-CuCl mixtures as promising molten salt for biomass liquefaction. However, corrosion limits the choice of possible reactor materials.

1. Introduction

Inorganic molten salts have been used in many different industries and for various purposes for hundreds of years. Molten salt mixtures have been used for many years as bath for alloy heat treatment and metal production such as aluminium, titanium, etc. Chlorides, fluorides, and hydroxides are considered as very good solvents for solid-state synthesis [1]. Molten salts have also been used as coolant nuclear and non-nuclear applications such as fission power plants, fusion or hybrid reactors, hydrogen production, long distance heat transport, nuclear fuel reprocessing, chemical industry, oil refineries, shale oil processing, etc.[2,3]. They are commonly used as Heat Transfer Fluid (HTF) as well as Thermal Energy Storage (TES) due to higher operation temperature, high heat capacity, wide range of thermal stability, low vapour pressure and low cost [4,5].

However, they have been investigated in many applications, there are still a lot of interest and potential to study molten salt in new approach. In the last decades, they have attracted a lot of attention to improve the production efficiency in renewable energy sectors due to their thermochemical properties [6]. Molten salts are employed as electrolytes in batteries which are a category of high energy density and high-power density batteries. In Concentrated Solar Power plants (CSP) molten salts are the preferred technology for TES and they are still under

* Corresponding author.
E-mail address: Sepideh.niazi@nmbu.no (S. Niazi).

https://doi.org/10.1016/j.mtla.2021.101296
Received 26 November 2021; Accepted 3 December 2021
Available online 8 December 2021

development [7]. Since molten salts have the various applications, any studies on molten salts properties can be useable for many applications and industries. One of the recent applications of molten salts in renewable energy sectors is thermochemical conversion of biomass in molten salt for the purpose of pyrolysis which needs more studies[8]. The studies' results shows that molten salts could not only have a catalytic effect, but biomass is solubilized in molten salts effectively liquifying the biomass and could improve the yield production [9,10]. This resolves the challenge of feeding solid biomass to high-pressure reactors. Liquified biomass can be simply pumped to the hydro pyrolysis section [11]. It avoids problems such as plugging, clogging, leakages, and uneven flow in solid feeding systems which all lead to low production rate and poor quality [12]. Biomass liquefying in molten salts is still under developments and needs more studies. The selected molten salt for this purpose should be able to liquify the biomass at mild conditions. The ideal candidate has a melting point below 200 °C at atmospheric pressure, low vapour pressure, high conductivity, and low cost. It also needs to have a high thermal stability up to 500 °C which is the hydro-pyrolysis unit temperature. It is important that the salt does not react with the biomass in the high pressure and temperature reactor. Then, it will be possible to recycle the salt and reuse it in a circular system. Since biomass contains moisture, the salt requires to have very low hydrolysis rate because reaction with water may form highly corrosive gases such as HCl [12,13].

This study has the first aim to candidate a molten salt system and investigates its properties based on the required criteria which can be important for any other applications. To find the proper salt which has all the mentioned criteria, many groups of salts including fluorides, carbonates, hydroxides, nitrates, nitrites and chlorides have been considered as possible candidates [12]. It was found that fluorides have high melting points (>400 °C)[13]. Carbonate salts are not chemically stable at high temperatures [14]. Hydroxides will form stable carbonates in contact with carbon that need to be regenerated [15]. Nitrites are not stable and oxidize at temperatures higher than 350 °C [5]. Nitrate mixtures are very common in solar energy systems [16], but they are very oxidizing and will not be stable in direct contact with carbon containing materials such as biomass [17]. Finally, it was found that chlorides have the most essential properties which are needed for a biomass liquefaction process such as low melting points, high thermal stability, abundant natural reserve and low cost [13,18,19]. In the previous work, ternary $ZnCl_2$-KCl-NaCl was studied experimentally [12]. This ternary system with low melting point and high thermal stability is considered as a promising biomass liquefier.

However, $ZnCl_2$ has a high tendency to react to ZnO and HCl in the presence of water and therefore requires the addition of ZnO to decrease the hydrolysis rate. Precipitation of solid ZnO particles on the other hand does not only increase viscosity but can also lead to abrasive wear during pumping. Therefore, in this study another chloride system, binary KCl-CuCl, has been studied as alternative possibly combining the low melting point with high thermal and chemical stability. Through the literature review, KCl-CuCl compositions were identified with low melting points and chosen for further study. There are very few works having studied the binary system KCl-CuCl. Early studies of the KCl-CuCl binary system by Sandonnini showed a eutectic present at 66 mol% CuCl with a melting point of 136 °C[20]. Fontana et al. showed the same compositions as eutectic mixture with eutectic temperature of 150 °C [21] . Later work, Etter et al.[20] reported 66.7 mol% CuCl as eutectic mixture with melting point of 150 °C. They reported that the low melting point gives a wide liquidus range and no indication of decomposition was observed up to 800 °C for 96 h. Etter et al. also reported that this binary system has a low viscosity. Some researchers considered KCl-CuCl for optical processes due to their large free exciton binding energies [22] but there is very little information about this as molten salt system and more investigation needs to be performed. Since there are no thermodynamic model for this binary system in the literature, thermodynamic reassessment of this binary system was another interest of present work. Although, Etter et al. generated the phase diagram of the system [20], there is no information regarding interaction parameters and thermodynamic properties of intermediate compounds. The current studies have the second aim to assess the interaction parameters for the first time for KCl–CuCl using FactSage. These parameters are needed for further theoretical studies in many applications, e.g. on the chemical stability in the presence of water during biomass liquefaction but also for other applications such as electrodeposition of Cu from salts [23] or the behaviour of CuCl in solvometallurgy [24].

Therefore, this study contains two parts: Firstly, an experimental study to identify the salt properties such as thermal stability, hydrolysis, transition temperatures (melting point, liquidus, solidus temperatures and peritectic line) and melting enthalpy. Secondly, thermodynamic modelling to optimize the parameters of the liquid solution and regenerate the phase diagram in FactSage.

2. Experimental details

Three compositions of KCl-CuCl including 32–68 mol%, 34–66 mol% and 36–64 mol% are selected. The composition 34-66 mol% was considered as a potential eutectic composition according to the literature [20]. Two other mixtures (32-68 mol% and 36-64 mol%) were chosen very close to the introduced eutectic composition to survey the hypothesis. To increase precision of the model and phase diagram, several compositions in close proximity to the potential eutectic point, have been defined to identify the transition temperatures such as liquidus, eutectic and peritectic temperatures. In addition, the melting enthalpy for one composition has been measured to be used as input for the modelling part.

2.1. Materials and setup

Pre-drying of the salts is necessary, due to the hygroscopic nature of the salts. To remove the moisture, KCl (Sigma Aldrich, ≥99.5%) and CuCl (VWR, ≥95%) were dried and stored in a muffle furnace at 200 °C for at least 24 h in separate and closed glass beakers. Before the experiments the dried salts were mixed well in the chosen composition and prepared in a nickel crucible. All experiments were carried out at ambient pressure. The measurement methods and set up details vary for thermal stability, hydrolysis and transition temperatures and are described in the relevant sections.

2.2. Thermal stability experiments

Thermogravimetric analysis (TGA) was performed to identify the thermal stability of the KCl-CuCl binary system as a function of temperature up to 500 °C. This set of experiments aims to investigate the mass variation of the salt by increasing the temperature. Any mass variation can be interpreted as salt oxidation (mass gain) or salt decomposition (mass loss) respectively which can be related to low thermal stability of the salt. For these experiments, 235 g of dried salt mixture was placed in a tubular nickel crucible with the height of 17 cm and an inner diameter of 5.1 cm. The mixture was compressed as much as possible to remove trapped air and minimize the possible experimental errors (related to thermal conductivity and non-uniform temperature), as suggested by Xu et al. [25]. The reactor setup containing the nickel crucible was heated in a vertical electrical tube furnace with radiation shields at the bottom part to minimize the heat loss. LabView 8.2 (National Instrument) was used to monitor and record the measurements. A purge gas of Ar (AGA, 4.0, >99.99%) was passed through the furnace from the bottom to provide inert atmosphere during the experiments. A type S thermocouple was immersed in the salt for monitoring and recording the salt temperature profile during all the experiments. The weight change was recorded using a weight scale (MS8001S, Mettler Toledo, accuracy of 0.1 g) which was connected to a computer located above the furnace. The crucible containing the salt is attached to the scale using a hanging geometry and the weight change was recorded continuously during the

experiment (schematic of the experimental setup shown in Fig. 1). The salt mixture was heated up to 500 °C at a heating rate of 10 °C/min.

2.3. Hydrolysis experiments

No study was found in literature which investigated the hydrolysis rate of the KCl-CuCl binary system. Since chlorides are usually hygroscopic salts, even small amounts of water can react with the salt. The chlorine ions and hydrogen can form highly corrosive HCl which may alter the equipment in the long term. In the case where biomass is in contact with the salt, water molecules from the biomass can cause hydrolysis.

The hydrolysis reactions for the single salts $ZnCl_2$ and CuCl have been simulated with FactSage using the FactPS database and Equilib module. The equilibrium partial pressures above a mixture of 1 mol of the salt and 1 mol of H_2O is shown in Fig. 2. For both salts, the hydrolysis product HCl is the dominating gas species besides H_2O below 400 °C. However, the equilibrium partial pressure of HCl at 200 °C is nearly three orders of magnitude lower for CuCl than for $ZnCl_2$. The HCl partial pressure forming in contact of $ZnCl_2$ with water at 200 °C (0.3 mbar) is observed for CuCl only at 420 °C, indicating a significant increase in hydrolysis resistance.

In order to test whether the hydrolysis reactions will occur, a series of hydrolysis experiments were performed for three compositions. Around 235 g of dried salt mixture was prepared in a nickel crucible and placed inside a sealed stainless-steel vessel as depicted in Fig. 3. The salt mixture was heated up to 170 °C under inert atmosphere (Ar flow). N_2 was bubbled through the molten salt for at least 12 h at the rate of 0.2 Nl/min to ensure homogenous melts and to ensure that all initial crystal water was removed. The hydrolysis experiments started around 200 °C which is above the melting point of the salt mixture to ensure that the salt was melted completely. The setup is the same setup as for the ternary $ZnCl_2$-KCl-NaCl system which is described in the last study in detail[12]. Gaseous H_2O was introduced by bubbling N_2 through a closed, water filled vessel at constant temperature of 46 °C to ensure a water partial pressure of 10 kPa (10 vol%), in accordance with the

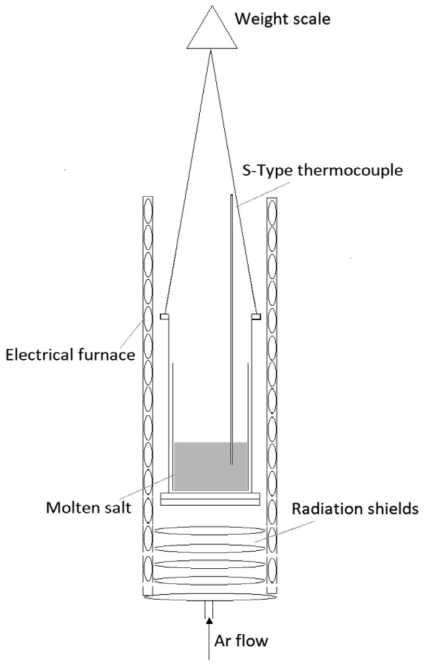

Fig. 1. Schematic representation of the experimental setup for TGA studies. The setup is hanged from the weight scale which records the weight. The temperature is measured by a type S thermocouple.

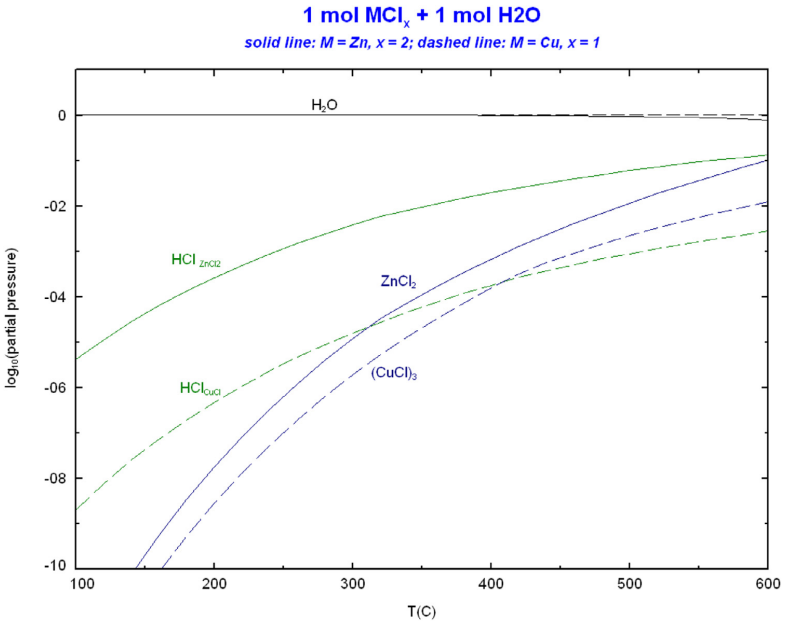

Fig. 2. Partial pressure of most dominant gas phase species in equilibrium between 1 mol of water and 1 mol of $ZnCl_2$ (solid lines) or 1 mol of CuCl (dashed lines).

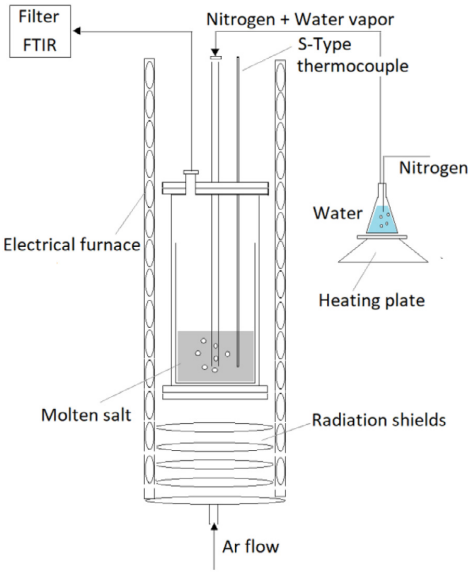

Fig. 3. Schematic representation of the experimental setup for hydrolysis studies. The inner crucible and the feed tube are made of nickel, and the outer container is made of stainless steel. The melt temperature is measured by a type S thermocouple.

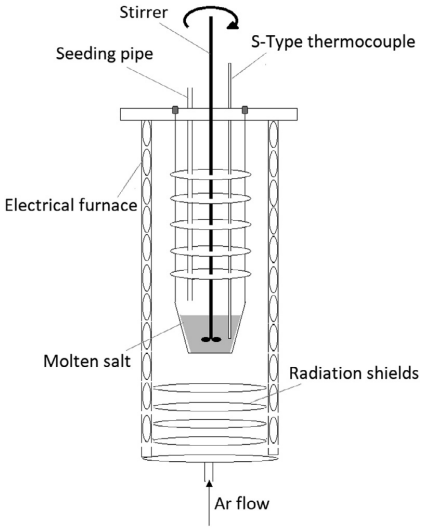

Fig. 4. Schematic representation of the experimental setup for determination of melting points by cooling curve method. The sample is placed in a nickel crucible and undergoes controlled cooling under constant stirring. The experiments were performed under inert atmosphere (Ar).

method introduced by Olsen et al.[26]. Heated gas lines which include PTFE (Teflon) tubes, were employed in the whole system. They were equipped with heating elements (H 900 °C, Tyco Thermal Controls) and kept at a constant temperature of 170 °C to avoid condensation of water in the lines. The gas consisting of 10 vol% water vapour and 90 vol% N_2 was bubbled through the molten salt from the bottom of the crucible. The gas will flow to the top of the molten salt and leave the crucible to a high voltage filter to remove residual particles and finally to a Fourier Transform Infrared spectrometer (FTIR) to be analysed. The FTIR unit (Thermo Nicolet 6700) was equipped with a 2 m gas cell running the commercial Fire Science method (Thermo Fisher). The gas was continuously analysed by FTIR. During the experiments, the salt temperature was increased in intervals of 50 °C up to 500 °C. The melt was kept at each temperature interval for at least 30 min to record the formed HCl concentration for a period of time.

2.4. Transition temperatures and melting enthalpy

The melting point of the selected molten salt is one of the most crucial properties, since the liquefaction step during biomass conversion should be at mild conditions (e.g. below 200 °C, atmospheric pressure). Moreover, transition temperatures are the main input for phase diagram reassessment. To verify the reported transition temperatures from the literature, two different methods were used including cooling curve [27] and Differential Scanning Calorimetry (DSC). In the first method, 120 g of dry salt mixture was placed inside a nickel crucible (with a height of 5.7 cm and an inner diameter of 6.1 cm) and heated up in a vertical electrical resistance furnace to ensure complete melting. The crucible was equipped with radiation shields above to minimize heat loss (Fig. 4). A mechanical nickel stirrer (40 rpm) was used to mix the molten salt for at least one hour to ensure a homogenous mixture. Then the salt mixture was cooled down slowly at a rate of 0.5 °C/min while stirring. The experiments were repeated 2-3 times by heating up the solidified salt and cooling down again for each composition.

The cooling curve method was employed for 5 compositions of the mixture while DSC (Netzsch DSC 204) experiments were conducted over a wider range of compositions. To decrease the experimental error, 1 g-batches of each salt mixtures was prepared in a glovebox (Argon-filled) by mortaring for 15 min. Compositions of KCl-CuCl with a CuCl-content of 52, 55, 57, 60, 63, 65, 67 and 70 mol% were produced. For each composition 10-15 mg of salt was weighed into a gold-coated steel crucible (Netzsch), which was hermetically sealed. The crucible types were used to reduce both, the uptake of moisture during transfer of the salt to the DSC, and the chance of corrosion of the crucible with the salt. Subsequently, the DSC measurement was carried out with a heating rate of 5 °C/min under a flow of N_2-purge gas. Multiple thermal cycles were recorded to ensure high reproducibility, and the second or third cycle were used for evaluation unless stated otherwise. The onset and offset of the melting peaks and the melting enthalpy were analysed using the Proteus Analysis Software package.

The heat capacity of two KCl-CuCl mixtures was measured following the guidelines of the ASTM E1269. The same setup in terms of salt preparation, crucible type and equipment were used for the measurements, but the heating rate was slightly higher (10 °C/min). The second heating cycle was used for evaluation of the heat capacity from a series of three measurements. A blank crucible and a sapphire disc were used as reference measurements successively and the salt mass was reduced to 15 mg. The error of measurement was identified to be in the order of 10% due to the relatively large mass of crucibles (>1 g), compared to the low samples mass (~15 mg).

2.5. Thermodynamic modelling

Beside the experimental work, a thermodynamic assessment of the KCl–CuCl binary system was performed to model the Gibbs energy of all stable phases in the system, following the Calphad technique [28]. For the assessment, the FactSage software [29] and the in-house tool DataOptimizer [30] have been used. The Gibbs free energy expression contains three parts for the liquid phase model which can be written as

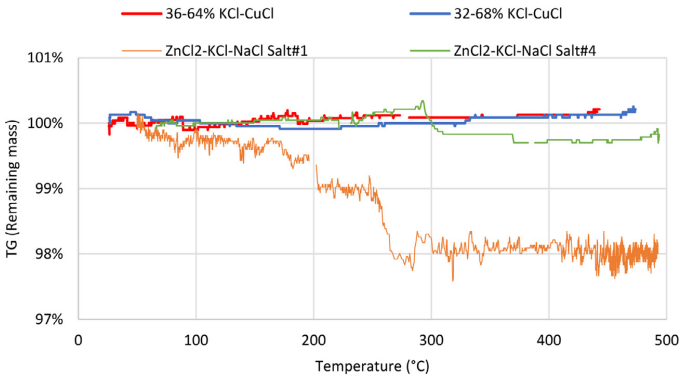

Fig. 5. Mass loss as a function of temperature for three different compositions of KCl-CuCl in comparison to salt #1 (60–20–20 mol%) and 4 (44.3–41.9–13.8 mol%) for $ZnCl_2$-KCl-NaCl from previous study[12].

[31]:

$$G_m(T, x_i) = G^{ref} + G^{ideal}_{mix} + G^E \quad (1)$$

$$G^{ref} = \sum_i x_i \, {}^0G_i \quad (2)$$

$$G^{ideal}_{mix} = RT \sum_i x_i \ln x_i \quad (3)$$

where G^{ref} is the contribution from pure components of the phase to the Gibbs energy, G^{ideal}_{mix} is the ideal mixing contribution, x_i is the mole fraction of component i; ${}^0G_i$ is the standard Gibbs free energy of the pure substance i; R is the gas constant, 8.314 $\frac{J}{mol.K}$; T is the temperature. G^E is the contribution due to non-ideal interactions between pure components, also known as the Gibbs excess energy of mixing. G^E is the most important parameter to represent the interaction of components except for the entropy value increase contributed by the ideal mixture. G^E has several kinds of mathematical expressions to represent the interaction between constituents. The Redlich-Kister (RK) model is one of the most common models for binary systems[32] and it has been employed by the expression as follows:

$$G^E = x_{KCl} x_{CuCl} \sum_{v=0}^{n_{ij}} L^{(v)}(T)(x_{KCl} - x_{CuCl})^v \quad (4)$$

$L^{(v)}$ ($v = 0, 1, 2, \ldots$) are the RK interaction parameters between the two end members [28]. It can be written in the general form as a function of temperature as follows:

$$L^{(v)}_{ij} = A + BT + CT \ln T + DT^2 + ET^3 + F/T \quad (5)$$

where A, B, C, D, E and F are constant parameters usually obtained through empirical or semi-empirical methods. A single parameter will always give a symmetrical contribution to the Gibbs energy of excess, thus at least two RK coefficients are needed to describe a subregular solution. Using many coefficients in an RK series should be avoided and normally a linear temperature dependence, *A*+BT, is enough. The composition dependence of the excess enthalpy is described by A and the excess entropy by -B [28]. Therefore, the first two parameters A and B are considered and optimized in this work as the deviation was considered acceptable for this study. The data for pure components of the liquid phase have been taken from the Fact Pure Substances database. To keep consistency, the data for pure solid KCl and CuCl have also been adopted from the same source.

2.6. Intermediate compound

According to the literature, there is a crystallization stage in the binary system KCl-CuCl wherein solids in the form of complex salt 2KCl.CuCl form [33]. The binary system contains an intermediate compound K_2CuCl_3 which has been analysed by X-Ray diffraction (XRD) in a few studies [20,22,34]. Since the thermodynamic data for the intermediate compound is not available in any database from FactSage, it is required to estimate its thermodynamic parameters. The Gibbs energy function of the K_2CuCl_3 can be thermodynamically described as [35]:

$${}^0G_{(K_2CuCl_3)} = 2{}^0G_{KCl} + {}^0G_{CuCL} + A + BT \quad (6)$$

A and B are model parameters describing the enthalpy (A) and entropy (-B) of reaction to form K_2CuCl_3 from the base salts. It is assumed that these are constant in the temperature range of interest. This is equivalent to the simple Neumann-Kopp rule (NKR) [36] to describe the heat capacities of the intermediate compound. The reaction enthalpy of K_2CuCl_3 has been computed using the ab initio calculated formation energies from materialsproject.org[37] and has not been used for further optimization. The reaction entropy with respect to the base chlorides has been obtained from the aiMP database. There, a machine learning model is used to estimate the S^{298K} values based on composition, enthalpy of formation and unit cell volume[38]. The S^{298K} value was taken as starting point and further optimized.

2.7. Optimizing

FactSage was applied in this study to set up the database and calculate the phase diagrams using the same. The in-house tool DataOptimizer [30] has been employed to optimize the parameters based on the experimental data. The experimental results including liquidus temperature, eutectic temperature and composition, peritectic temperature and melting enthalpy were adopted to assess the calculation results in the binary phase diagrams. The procedure involves a weighted least-square optimization of model parameters to minimize the difference between calculated and measured values. Each type of selected data was given a certain weight factor according to the accuracy of data and data importance. Then the try and error method was used to alter the weight factor during the assessment until all of the selected data was reproduced within the acceptable uncertainty limits in DataOptimizer.

3. Results and discussion

3.1. Experimental results

The experimental results including thermal stability, hydrolysis, transition temperatures and melting enthalpy are reported in the section below.

3.1.1. Thermal stability

Fig. 5 shows the mass loss as a function of temperature up to 500 °C for two selected compositions of KCl-CuCl. Both compositions are

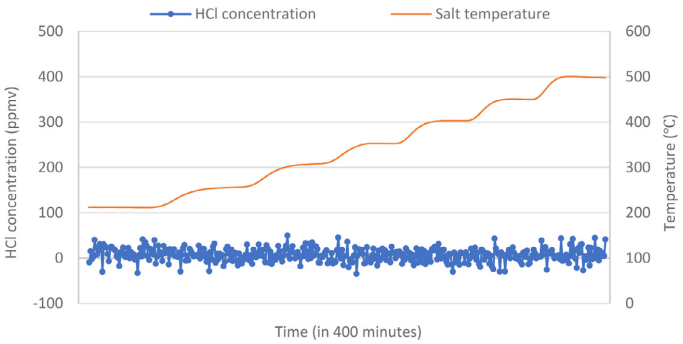

Fig. 6. The content of HCl in the exit gas as a function of temperature from 200 °C to 500 °C when 10 vol% water in N_2 is added to KCl-CuCl compositions.

Table 1
Transition temperatures of the KCl-CuCl system by the DSC and cooling curve methods.

Composition [mol%] KCl	Transition temperature [°C] CuCl	Eutectic	Peritectic	Liquidus	Experimental method
20	80	144.10	–	291.05	Cooling curve
30	70	145.9	–	208.5	DSC
32	68	146.55	–	–	Cooling curve
33	67	145.8	–	183.7	DSC
34	66	145.18	–	–	Cooling curve
35	65	145.9	–	156.7	DSC
36	64	146.82	–	–	Cooling curve
37	63	146.1	–	211.2	DSC
40	60	146.3	–	237.2	DSC
43	57	146.1	–	254	DSC
45	55	145.7	–	250.4	DSC
48	52	145.8	–	383.4	DSC
60	40	–	236.49	513.48	Cooling curve

very stable even at high temperatures up to 500 °C. It follows that binary KCl-CuCl is not only stable at high temperatures, but also appears to exhibit a low vapour pressure since no mass loss was observed in the experiments. The experimental results have been compared to two compositions of $ZnCl_2$-KCl-NaCl with the lowest and highest mass loss from the previous study[12]. The mass loss of the compositions at high temperatures is negligible for KCl-CuCl and even lower than that of for the ternary $ZnCl_2$-KCl-NaCl in the previous work. This can be understood when comparing the partial pressures of $ZnCl_2$ and $(CuCl)_3$ in Fig. 2: The latter is nearly one order of magnitude lower than the first; according to the Hertz-Knudsen equation, the evaporation rate is directly proportional to the partial pressure and therefore much higher for $ZnCl_2$. The high thermal stability of KCl-CuCl makes it possible to use it for liquefaction and subsequent hydro-pyrolysis of biomass at higher temperatures.

3.1.2. Hydrolysis

Fig. 6 shows the HCl level from FTIR-gas analysis of the two KCl-CuCl compositions during step-wise heating from 200 °C to 500 °C with temperature intervals of 50 °C. As the figure shows, for all molten salt compositions the HCl formation is below the detection level indicating that they do not hydrolyse in contact with water up to 500 °C. This is in accordance with the thermodynamic modelling shown in Figure . In comparison with the ternary system $ZnCl_2$-KCl-NaCl in the previous study where HCl release in the range of hundreds to thousands of ppm_v had been observed already at 400 °C[12], binary KCl-CuCl is considered a very promising alternative with minimum hydrolysis rate.

3.1.3. Transition temperatures

Table 1 represents the results from measurements of transition temperatures of selected compositions of binary KCl-CuCl. Thirteen compositions have been studied through different setups and techniques including cooling curve and DSC.

The results from the cooling curves for 80 mol% CuCl showed two cases of undercooling regions during the cooling down which represent the liquidus and eutectic temperatures. However, for compositions between 64 and 68 mol% of CuCl only one undercooling region was detected for each of them. The three compositions investigated are very close to the eutectic point reported by Etter and Wiedenheft [20]. The liquidus and eutectic temperatures have very close values which the cooling curve method cannot differentiate precisely. The sample with 40 mol% of CuCl shows two cases of undercooling which correspond to the liquidus temperature and peritectic temperature respectively.

Temperature calibration is necessary in order to minimize systematic errors due to the thermocouple. The thermocouple was calibrated using deionized ice and water, deionized boiling water, pure tin and pure zinc. The measured melting points based on cooling curves were calibrated using linear regression which is described in the previous study [12]. Table 1 presents the average value of the measured temperatures for all five compositions. These values are generally in good agreement with the few available reports on transition temperatures [20,21].

The eutectic melting temperatures extracted from cooling-curve techniques were very similar to those obtained by DSC measurements (see Table 1). The respective data is that of the 5th heating curve and discussed hereafter. From both data sets (cooling-curve technique and DSC) one can extract an average eutectic temperature of 145.85 °C ± 0.66 °C. DSC measurements also allowed a closer investigation of the liquidus temperatures, which are represented by the offset of the melting peak. It has to be noted that the liquidus temperature reported in Table 1 for DSC measurements is the peak end-temperature. It changes as a function of the heating rate, sample mass and other parameters since it depends on melting / dissolution kinetics and heat transfer. Still, it can be used as indication for the trend in liquidus temperature for a given set of samples if they were measured using the same experimental procedures, such as in this case.

The DSC curves of the measured compositions are shown in Fig. 7. The composition with the sharpest melting peak and lowest liquidus temperature is that at 65 mol% CuCl and 35 mol% KCl. Samples with a lower (63 mol%) or higher (67 mol%) CuCl content already exhibit a pronounced shoulder after the main melting peak which indicates that the 65 mol% CuCl-mixture, which features no shoulder close to the melting peak, is close to the eutectic composition. At concentrations below 65 mol% CuCl, the liquidus temperatures first increase and an additional endothermic peak at ~T_onset = 246 °C is present. The peak is very pronounced at higher KCl-concentrations (52 and 55 mol% CuCl) and represents the peritectic transition of $K_2CuCl_3 \rightleftarrows KCl + \text{liquid}$. A very small but reproducible endothermal reaction at the same temperature is also present for higher CuCl contents up to the eutectic composition. We assume that the presence of the peak arises from partial decomposition, e.g. side reactions with the crucible, local de-mixing, or similar phenomena, given that the cycle evaluated is already the 5th cycle. It is worth

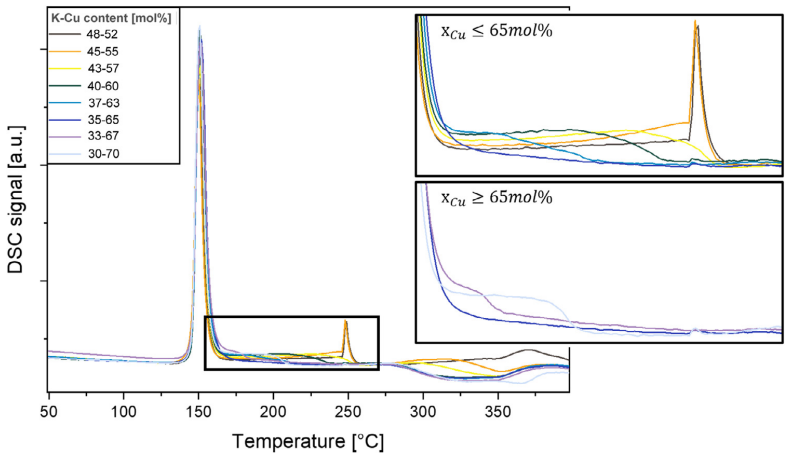

Fig. 7. DSC curves of the different KCl-CuCl samples during heating, with concentrations indicated in the legend of the main figure. Zooms represent data above and below the expected eutectic composition as indicated by the respective labels and serve as guid to the eye. Some DSC plots have been offset along the y-axis for better comparability.

Table 2
Melting enthalpies and heat capacity of KCl-CuCl mixtures from DSC measurements.

KCl-CuCl content [mol%]	Melting enthalpy [J/g]	Heat capacity [kJ/(kg.K)]
30–70	88.6	Not measured
33–67	84.3	0.913 ± 10%
35–65	81.6	0.995 ± 10%
37–63	76.8	Not measured
40–60	89.4	Not measured
43–57	90.3	Not measured
45–55	83.7	Not measured
48–52	72.2	Not measured

mentioning that over the course of the DSC cycles, this peak already was present during the second cycle (of the 35–65 mol%-sample), but its fraction did not increase over the number of DSC cycles, indicating that no further side reactions occurred and that the measurements are reproducible.

3.1.4. Melting enthalpy and heat capacity

The melting enthalpies of different compositions were evaluated using the Proteus Analysis software and are presented in Table 2. While the melting enthalpy of the eutectic mixture and compositions in close proximity was reliable due to a low number of peaks, the presence of the peritectic transition peak at 246 °C made evaluation of the melting enthalpy increasingly difficult. Nonetheless, the data shown presents the melting enthalpies including background fitting with a value of 81.6 J/g for the 35-65 mixture. The same mixture exhibits a heat capacity slightly below 1 kJ/(kg•K). The heat capacity remained constant over temperature within the error of measurement, therefore no temperature correlation is presented.

3.1.5. Observed corrosion

The corrosiveness of the KCl-CuCl mixtures was not measured in the current study but the observation shows that this molten salt is highly corrosive in contact with nickel and stainless-steel materials, especially at high temperature >300 °C. Fig. 8 shows the cooling curve method experimental setup (that was schematically depicted in Fig. 4) after one series of melting point experiments. In this experiment the salt mixture was heated up to 350 °C and after a few hours it was cooled down slowly by the rate of 0.5 °C/min. The process was carried out under inert atmosphere (Ar flow) and repeated three times. The figure shows the corrosion effect on the nickel radiation shields, the nickel crucible containing the molten salt and the nickel-stainless steel setup. The rod on the centre of the setup made of stainless steel is broken due to high corrosion. Etter et al. and Fontana et al. had the same concern. They used fused silica and borosilicate crucibles for their experiments to avoid the corrosion issue [20,21]. Using FactPS database in FactSage, the corrosive nature of KCl-CuCl can be better understood: At 100 °C, a 1:1:1 mixture of KCl:CuCl:Fe forms in equilibrium 0.5 mol of K_2FeCl_4, 1 mol of Cu and 0.5 mol of Fe while a 1:1:1 mixture of KCl:CuCl:Ni forms 0.5 mol of $KNiCl_3$, 0.5 mol of KCl, 0.5 mol of Ni and 1 mol of Cu, indicating that in both cases Cu has a tendency to transfer chlorine to the crucible and steel setup. Similar equilibria are estimated at higher temperature but are less reliable due to the importance of liquid solutions. These thermochemical considerations indicate that copper might be an interesting crucible and construction material in presence of KCl-CuCl mixtures.

Fig. 8. The corrosion of the nickel radiation shields, nickel crucible containing molten salt and nickel stainless steel setup containing KCl-CuCl molten salt after an experiment in temperature range of 50–350 °C under inert atmosphere.

3.2. Modelling results

Based on the experimental results described in Table 1 and the melting enthalpy of the solution, the binary system was thermodynamically assessed. Eutectic temperatures, liquidus line, peritectic temperature and melting enthalpy were first introduced for reproduction of the experimental data. When the Redlich-Kister expression was employed to optimize the binary systems, the related interaction parameters were determined. These are listed in Table 3. The well-established liquidus line and eutectic in the wide temperature and composition ranges as well as the accurately measured melting enthalpy makes it possible to optimize the $L_i (i = 0, 1)$ parameters in Eq. (5). For the intermediate compound K_2CuCl_3 in the KCl-CuCl system, the standard entropy was optimized as well while the enthalpy of formation was fixed as described above.

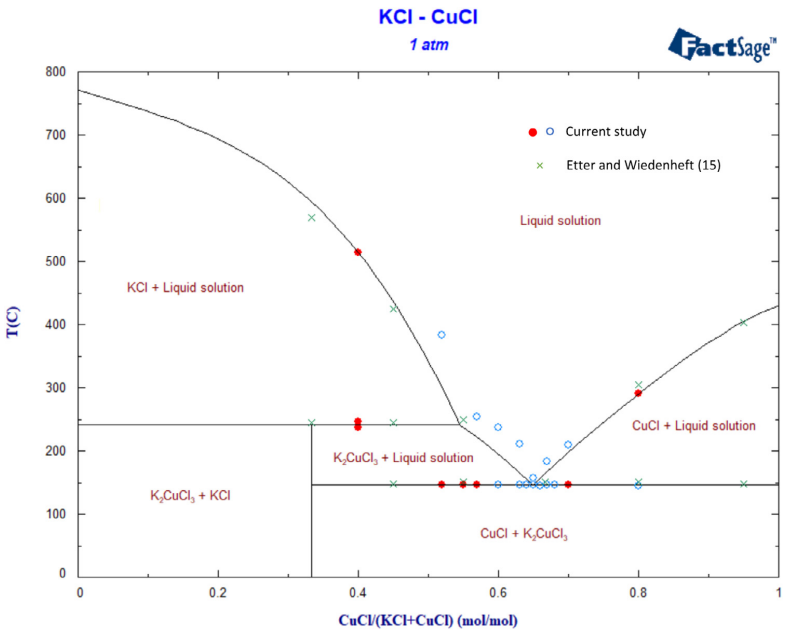

Fig. 9. Calculated phase diagram of KCl-CuCl in comparison with experimental data generated in the present work (red points have been used in optimization) as well as from Etter and Wiedenheft[20] (green crosses).

Table 3
Summary of the interaction thermodynamic parameters in the KCl-CuCl binary system according to the present optimization.

Constituents	Phase type	Phase state	Thermodynamic parameters
KCl, CuCl	Solution	Liquid	$L^0 = -27,373\frac{J}{mol} + 3.94\frac{J}{mol\ K}T$ $L^1 = -15,416\frac{J}{mol} + 25.57\frac{J}{mol\ K}T$
K_2CuCl_3	compound	Solid	$\Delta H^{298}_{K_2CuCl_3} = -1,018,294\frac{J}{mol}$ $S^{298}_{K_2CuCl_3} = 247.92\frac{J}{mol\ K}$

As shown in Fig. 9, the phase diagram of the KCl-CuCl binary systems was evaluated and calculated based on experimental data. No solid solubility was taken into account in this thermodynamic calculation. The calculated eutectic point of the system was located at 145.9 °C and 64.9 mol% CuCl and the peritectic temperature is obtained at 241.2 °C. The calculated enthalpy of melting between 65 and 70 mol% CuCl was within 5% of the values shown in Table 2. The experimental data from the literature[20] are included in the figure to compare the experimental and modelled results from this work and experimental results from the literature. Etter et al. reported slightly higher temperatures for the eutectic temperature (150 °C) and peritectic temperature (245 °C), however Sandonini identified a lower eutectic temperature (136 °C)[20].

It should be noted that the value of S^{298K} thus determined for K_2CuCl_3 is only 2 J/(K mol) or 0.8% higher than the value estimated based on the machine learning model used in the aiMP database development [38]. During the optimization, no experimental evidence indicated a necessity to modify the enthalpy of formation of K_2CuCl_3 that had been fixed based on ab initio calculations.

4. Conclusion

The properties of molten inorganic salt KCl-CuCl have been considered in this study to be a candidate as biomass liquefier. Thermal stability and hydrolysis have been studied experimentally for two compositions including 32-68 mol% and 36-64 mol% of KCl-CuCl which are around the eutectic composition. All three compositions showed very high thermal stability at temperatures up to 500 °C with no mass loss measured by TGA experiments. Hydrolysis experiments were carried out to assess the molten salt resistance in contact with water from biomass. The hydrolysis reaction is considered important since it could form highly corrosive and undesired HCl. The results showed that molten KCl-CuCl were very stable in contact with water in hydrolysis experiments and no HCl was detected by FTIR up to 500 °C. Although these properties make it a promising alternative for liquifying biomass, further work is needed to mitigate the corrosion of Ni and stainless steel in contact with the KCl-CuCl melt as observed here.

Cooling curve and DSC were employed to study thirteen compositions of binary KCl-CuCl. Transition temperatures including eutectic, liquidus and peritectic temperatures were obtained and reported in Table 1. The eutectic composition was measured to be at 65 mol% CuCl and enthalpies of melting have been determined.

Together with ab initio calculated phase stability of the intermediary compound K_2CuCl_3 these results have enabled the first thermodynamic assessment of the binary system KCl-CuCl. It aimed at reproducing the phase diagram based on experimental results and thermodynamic data. Temperature dependant Gibbs energy expressions for the liquid solution and the intermediate K_2CuCl_3 solid compound were derived. The calculated phase diagram of the binary system as well as the melting enthalpy are in good agreement with experimental data. The calculated eutectic point of the system is located at 145.9 °C and 64.9 mol% CuCl and the peritectic temperature occurred at 241.2 °C. This optimisation is a necessary first step for further studies to enable thermodynamic calculations of practical interest for biomass liquefaction, copper electrodeposition from salts or solvent metallurgy.

Acknowledgments

This project has received funding from the European union's Horizon 2020 Research and Innovation programme under grant agreement number 764089.

Supplementary materials

Supplementary material associated with this article can be found, in the online version, at doi:10.1016/j.mtla.2021.101296.

References

[1] X. ZHAO, Z. YAO, J LI, Study on the properties and applications of molten salts, in: Proceedings of the 5th International Conference on Solid Waste Management and Technology, 5, 2010, pp. 125–128.

[2] R. Serrano-ópez, J. Fradera, Cuesta-López S. Molten salts database for energy applications, Chem. Eng. Process. Process. Intensif. 73 (2013) 87–102.

[3] J. Barnes, R. Coutts, T. Horne, J. Thai, Characterisation of molten salts for application in molten salt reactors, PAM Rev. Energy Sci. Technol. 6 (2019) Article ID 1546.

[4] Z. Yang, S.V Garimella, Thermal analysis of solar thermal energy storage in a molten-salt thermocline, Sol Energy (2010).

[5] L.F. Cabeza, Advances in Thermal Energy Storage Systems: Methods and Applications, Elsevier Science, 2014.

[6] Lantelme F., Groult H. Molten salts chemistry: from lab to applications. 2013.

[7] G. Alva, Y. Lin, G Fang, An overview of thermal energy storage systems, Energy [Internet] 144 (2018) 341–378 Available from https://www.sciencedirect.com/science/article/pii/S036054421732056X .

[8] S. Nygård H, E Olsen, Review of thermal processing of biomass and waste in molten salts for production of renewable fuels and chemicals, Int. J. Low-Carbon Technol. 7 (4) (2012) 318–324.

[9] E. Sada, H. Kumazawa, M Kudsy, Pyrolysis of Lignins in molten salt media, Ind. Eng. Chem. Res. 31 (2) (1992) 612–616.

[10] M. Kudsy, H. Kumazawa, Pyrolysis of Kraft lignin in the presence of molten ZnCl2-KCl mixture, Can. J. Chem. Eng. 77 (6) (1999) 1176–1184.

[11] P. O'Connor, J.A. Moulijn, M. Makkee, S. Daamen, R.M. de Almeida, Process For the Conversion of Cellulose in Hydrated Molten Salts, United States; US8846902B2, 2014.

[12] S. Niazi, E. Olsen, S. Nygård H, Hydrolysis of eutectic compositions in the ZnCl2:KCl:NaCl ternary system and effect of adding ZnO, J. Mol. Liq. 317 (2020) 114069 [Internet]Available from http://www.sciencedirect.com/science/article/pii/S0167732220336114 .

[13] W. Ding, A. Bonk, T. Bauer, Molten chloride salts for next generation CSP plants: selection of promising chloride salts & study on corrosion of alloys in molten chloride salts, in: Proceedings of the SOLARPACES International Conference on Concentrating Solar Power and Chemical Energy Systems, 2019.

[14] S. Kuravi, J. Trahan, D.Y. Goswami, M.M. Rahman, Stefanakos EK. Thermal energy storage technologies and systems for concentrating solar power plants, Prog. Energy Combust. Sci. 39 (4) (2013) 258–319.

[15] J.K. Maund, D.M. Earp, Fuels from biomass by conversion in molten salts, in: Research in Thermochemical Biomass Conversion, Springer, Dordrecht, 1988, pp. 542–556.

[16] B. D'Aguanno, M. Karthik, A.N. Grace, A. Floris, Thermostatic properties of nitrate molten salts and their solar and eutectic mixtures, Sci. Reports 8 (2018) 10485.

[17] A. Roine, P. Lamberg, J. Mansikka-aho, P. Björklund, J.P. Kentala, T. Talonen, HSC Chemistry, Outotec Reseaqrch Oy, 2006.

[18] K. Vignarooban, X. Xu, K. Wang, E.E. Molina, P. Li, D. Gervasio, et al., Vapor pressure and corrosivity of ternary metal-chloride molten-salt based heat transfer fluids for use in concentrating solar power systems, Appl. Energy 159 (2015) 206–213.

[19] A. Hoshi, D.R. Mills, A. Bittar, T.S. Saitoh, Screening of high melting point phase change materials (PCM) in solar thermal concentrating technology based on CLFR, Sol. Energy 79 (3) (2005) 332–339.

[20] D.E. Etter, C.J. Wiedenheft, The study of KCl-CuCl eutectic fused salt as a potential intermediate temperature heat transfer and storage medium, Sol. Energy Mater 2 (4) (1980) 423–431.

[21] C.M. Fontana, E. Gorin, G.A. Kidder, C.S. Meredith, Chlorination of methane with copper chloride melts. Ternary system, CuCl–CuCl 2 –KCl, and its equilibrium chlorine pressures, Ind. Eng. Chem. 44 (2) (1952) 369–373.

[22] F.O. Lucas, J.P. McNally, A. Cowley, S. Daniels, L. Bradley, D. Danieluk, et al., Structural, optical and electrical properties of Co-evaporated CuCl/KCl films, Phys. Status Solidi 6 (S1) (2009) S114–S118.

[23] L. Yungang, L. Jie, K. ZHANG1, L LIU, Electrochemical behavior of Cu in the (NaCl-KCl-CuCl) molten salt, Acta Metall. Sin. (English Lett.) 24 (6) (2011) 466–472.

[24] K. Binnemans, P.T. Jones, Solvometallurgy: an emerging branch of extractive metallurgy, J. Sustain Metall. 3 (2017) 570–600.

[25] X. Xu, G. Dehghani, J. Ning, P. Li, Basic properties of eutectic chloride salts NaCl-KCl-ZnCl2 and NaCl-KCl-MgCl2 as HTFs and thermal storage media measured using simultaneous DSC-TGA, Sol Energy 162 (2018) 431–441.

[26] E. Olsen, M. Hansen, S. Nygård H, Hydrolysis of molten CaCl2-CaF2 with additions of CaO, AIMS Energy 5 (2017) 873–886.

[27] M.S. Rahman, N. Guizani, M. Al-Khaseibi, S. Ali Al-Hinai, S.S. Al-Maskri, K Al-Hamhami, Analysis of cooling curve to determine the end point of freezing, Food Hydrocoll. 16 (6) (2002) 653–659.

[28] H.L. Lukas, G. Fries S, B Sundman, Computational Thermodynamics, The Calphad Method, New York: United States of America by Cambridge University Press, New York, 2007.

[29] C.W. Bale, P. Chartrand, S.A. Degterov, G. Eriksson, K. Hack, R. Ben Mahfoud, et al., FactSage thermochemical software and databases, Calphad [Internet] 26 (2) (2002) 189–228 Available from https://www.sciencedirect.com/science/article/pii/S0364591602000354 .

[30] B.H. Reis, Development of a Novel Thermodynamic Database For Salt Systems With Potential As Phase Change materials' [Manuscript Submitted For Publication], Brandenburgische Technische Universität Cottbus-Senftenberg, Cottbus, 2021.

[31] H. Xu, A. Romagnoli, J. Yin Sze, X Py, Application of material assessment methodology in latent heat thermal energy storage for waste heat recovery, Appl. Energy 187 (2017) 281–290.

[32] X. Li, S. Wu, Y. Wang, L Xie, Experimental investigation and thermodynamic modeling of an innovative molten salt for thermal energy storage (TES), Appl. Energy [Internet] 212 (2018) 516–526 Available from https://www.sciencedirect.com/science/article/pii/S0306261917317841 .

[33] J.B. Sardisco, in: Decomposition of 2KCl. CuCl to Produce Cuprous Chloride and Potassium Chloride, 343, Patent nomber 4, U.S, 1982, p. 781.

[34] W.U. Malik, S.M.F. Rahman, S.A. Ali, Studies on the behaviour of cuprous chloride in hydrochloric acid and potassium chloride solutions. I. Chemical analysis in the aqueous phase, J. Inorg. Gen. Chem. 299 (5–6) (1959) 322–327.

[35] I. Barin, Thermochemical Data of Pure Substances, VCH, 1989.

[36] X.X Kopp H, Investigations of the specific heat of solid bodies, J. Chem. Soc. 19 (1866) 154–234.

[37] A. Jain, S.P. Ong, G. Hautier, W. Chen, W.D. Richards, S. Dacek, et al., Commentary: the materials project: a materials genome approach to accelerating materials innovation, APL Mater. 1 (1) (2013).

[38] GTT-Technologies. The ab initio materials project (AIMP) v4.0 database [Internet]. 2021. Available from: https://gtt-technologies.de/wp-content/uploads/2021/04/AiMP-v4.0-documentation.p

Paper III

Niazi, Sepideh; Olsen, Espen; Nygård, Heidi S. “Electrochemical removal of Cu, Fe and Mn from molten $ZnCl_2$:KCl:NaCl”. Submitted to Journal of Separation and Purification Technology.

Electrochemical removal of Cu, Fe and Mn from molten $ZnCl_2$:KCl:NaCl

Sepideh Niazi, Espen Olsen, Heidi S. Nygård

Faculty of science and technology, Norwegian University of Life Science (NMBU), Ås, Norway

Abstract

This study was carried out to investigate the use of electrodeposition for the removal of impurities from molten $ZnCl_2$:KCl:NaCl in order to purify and reuse the molten salt after electrorefining and electrowinning. The deposition of the inorganic compounds Cu, Fe, and Mn from CuCl, $FeCl_2$, $FeCl_3$, and MnO_2 in molten salt at 260 °C was examined using cyclic voltammetry (CV), employing graphite and platinum (Pt) electrodes. Subsequently, a series of potentiostatic electrolysis experiments were conducted to remove the impurities in the salt using a zinc (Zn) electrode. X-ray diffraction (XRD) was used in one case to analyze and confirm that the reduced element was deposited on the surface of the Zn electrode. The results show that Cu and Fe(III) were removed from the molten salt through 1.5 and 2.5 hours of electrodeposition, respectively. The results for removing Fe(II) and Mn were slightly different after 3 hours of purification, despite being mostly effectively separated, there were still some impurities found in the molten salt.

Keywords: electrodeposition, molten salt, cyclic voltammetry, chronoamperometry

1. Introduction

Molten chloride salt mixtures are promising media for various industrial applications due to their excellent thermodynamic properties (1). They have been employed in metallurgy and metal extraction and have had a significant role in the energy sector and renewable energy industries. Molten chloride salts have been used in nuclear plants for decades (2). In addition, they are excellent heat transfer fluids (HTF) and thermal energy storage (TES) materials that are employed in concentrated solar power plants (CSP) (3,4), batteries (5) and biomass pyrolysis in biofuel production (6,7).

In the majority of the mentioned molten salt applications, the melt is in contact with other materials, which can lead to contamination. Therefore, the molten salt needs to be purified in order to recirculate it to the system. There are various methods of separating and removing contaminant elements from molten salts, such as ion exchange (8), the zone freezing method (9), and precipitation (10,11). Another effective method, electrochemical removal requires fewer devices and equipment than the other techniques (12).

Electrolysis in molten salt baths has been used to recover metals from ores (13,14) in metal production industries for a long time. KCl:NaCl was one of the first electrolytes used for recovery of metal at elevated temperatures (900 °C) (15). After some modifications to the process, the electrolyte was changed to the ternary molten salt LiCl:KCl:NaCl, which allowed for performing the process at a lower temperature (500 °C). Another common molten salt used for many similar processes is KCl:LiCl (16).

Apart from metal extraction studies have reported on the electrochemical removal of elements from chlorides (17–20) using various electrodes. Kim et al. performed potentiostatic electrolysis tests on a LiCl:KCl eutectic melt at 500 °C to remove dysprosium (Dy) and gadolinium (Gd) from the salt using a magnesium (Mg) electrode (12). Khalaghi et al. reported the electrochemical study of iron (Fe) in a KCl:LiCl:NaCl melt at 500 °C using a glassy carbon (C) electrode (16). Chen et al. reduced titanium (Ti) from titanium oxide (TiO) in calcium dichloride ($CaCl_2$) at 950 °C using an oxide-scale-coated Ti foil as a working electrode (21). Many studies have reduced silicon (Si) from silicon dioxide (SiO_2) in a $CaCl_2$ melt at high temperatures around 900 °C using various electrodes (22–26). The most widely studied electrolytes include KCl:LiCl (27,28), NaCl:KCl (29,30), $ZnCl_2$:NaCl (31,32), and $MgCl_2$:NaCl:KCl (33), which all require high temperatures (400–600 °C) to keep the salt liquid.

$ZnCl_2$:KCl:NaCl is an interesting molten salt for many applications due to its high thermal stability, low melting point (around 200 °C), and low hydrolysis, especially at lower temperatures (below 400 °C) (34). In our previous research, due to its promising properties, this salt has been studied and introduced as an alternative for liquifying biomass as a pre-step before hydro-pyrolysis. Through hydro-pyrolysis and subsequent hydrodeoxygenation, the biomass can be converted to biofuel. However, the spent salt after this conversion process may have been contaminated by ash or char from the biomass, which can affect the thermodynamic properties of the molten salt. Therefore, the salt needs to be purified before recycling into the system.

Electrochemical removal of impurities from $ZnCl_2$:KCl:NaCl molten salt was investigated in the current study. The low melting point of this molten salt makes electrolysis possible at relatively low temperatures (below 300 °C), but there have been very few studies about its electrochemical behavior. Nitta et al. examined the cyclic voltammetry (CV) for ternary

$ZnCl_2$:KCl:NaCl (60:20:20 mol%) at 250 °C and reported 1.7 V of electrochemical window, which is quite a wide window for removing the various ions (35). The present study used another composition of $ZnCl_2$:KCl:NaCl (44.3:41.9:13.8 mol%) to not only determine the electrochemical window but also to purify the molten salt using an electrochemical method.

CV is commonly used to investigate the reduction and oxidation process of molecular species (36). The objective of the present study was to examine the removal of elements from $ZnCl_2$:KCl:NaCl by electrodeposition using zinc (Zn) and graphite (C) electrodes. Theoretically, it is possible to remove ions that have electrode potential in the range of the molten salt electrochemical window. Although various impurities, such as Ca, K, Al, Na, Fe, Mn, and others, coming from different biomasses may contaminate the molten salt, the ions that theoretically can be removed from $ZnCl_2$:KCl:NaCl were selected for this investigation. The quantity of metal impurities remaining in the molten salt due to the biomass conversion process can vary for each impurity and for different biomass feeds, but it is normally less than 1–2 wt%. In the current work it was assumed that this amount was 0.8 wt% in all cases. The metal ions chosen as representatives included copper (Cu^+), iron (Fe^{2+}, Fe^{3+}), and manganese (Mn^{4+}). They were introduced into the melt through the addition of CuCl, $FeCl_2$, $FeCl_3$, and MnO_2. CV measurements were obtained to observe the redox peak of the molten salt and elements at 260 °C. Subsequently, a series of chronoamperometry constant-potential electrolysis tests, were performed to remove Fe, Cu, and Mn ions from the salt. Finally, the crystalline structure of the extracted electrodeposits was analyzed using X-ray diffraction (XRD). The results for Cu were clear, but the other cases were very noisy, and it was not possible to interpret the results.

2. Cyclic voltammetry

CV is an electrochemical technique for measuring the current that develops in an electrochemical cell under conditions where voltage is in excess of that predicted by the Nernst equation, as given in Eq. (1) (36). This equation relates the potential of an electrochemical cell (E) to the standard potential of a species (E^0) and the relative activities of the oxidation (Ox) and reduction (Red) analyte in the system at equilibrium, as in Eq. (2) and (3).

$$E = E^0 + \frac{RT}{nF} ln \frac{(Ox)}{(Red)} \tag{1}$$

$$(Ox): X \rightarrow X^+ + e^- \tag{2}$$

$$(Red): X^+ + e^- \rightarrow X \tag{3}$$

In the equation, F is Faraday's constant, R is the universal gas constant, n is the number of electrons, and T is the temperature (K). In applying the Nernst equation, the activities are replaced with the concentrations, which are more experimentally accessible. The standard potential is replaced with the formal potential $E^{0\prime}$, and n is set equal to 1 for one electron transfer:

$$E = E^{0\prime} + \frac{RT}{F} ln \frac{[X^+]}{[X]} \tag{4}$$

The formal potential is specific to the employed experimental conditions. The Nernst equation provides a powerful prediction for the system in response to a change of concentration of species or a change in the electrode potential. In practice, when the potential is scanned during CV

experiments, the concentrations of species in the solution near the electrode changes over time (36).
The scan rate of the CV experiments presents the scan speed of the applied potential. Faster scan rates lead to reduction in the size of the diffusion layer and consequently, higher currents are observed. The Randles–Sevcik equation given in Eq. (5) shows how the peak current (i_P) increases linearly with the square root of the scan rate (υ):

$$i_P = 0.446nFAC^0\left(\frac{nF\upsilon D_0}{RT}\right)^{1/2} \quad (5)$$

where n is the number of electrons transferred in the redox event, A (cm^2) is the electrode surface area (usually treated as the geometric surface area), D_0 ($cm^2\ s^{-1}$) is the diffusion coefficient of the oxidized analyte, and C^0 (mol cm^{-3}) is the bulk concentration of the analyte.
Electrolytic solutions have an intrinsic resistance (R_{sol}) in the electrochemical cell. R_{sol} consists of two parts: R_C, which is resistance between the counter electrode and the reference electrode and some potentiostats can compensate for, and R_u, which is the resistance between the working electrode, which some reference electrode, and it is compensated resistance. This resistance may cause ohmic drops in the system that need to be minimized. Ohmic drops can be reduced by three methods (37,38):

- Decrease the current by reducing the size of the working electrode or running in slow scan rates
- Diminish R_{sol} and consequently R_u by increasing the conductivity of the solution with a higher concentration of the electrolyte
- Decrease R_u (and increase R_C) by reducing the distance between the working and reference electrodes

3. Experimental

3.1 Materials

$ZnCl_2$ (VWR, 98.3%), KCl (Sigma, ≥ 99.5%) and NaCl (Sigma, ≥ 99.8%) were dried in a muffle furnace at 200 °C for at least 24 h in separate and closed beakers. The elements to be studied were added as CuCl (VWR, ≥ 95%), $FeCl_2$ (Thermo Fisher, ≥ 99.99%), $FeCl_3$ (Sigma, ≥ 99.9%) and MnO_2 (Thermo Fisher, ≥ 99.9%) by adding each of them to the molten salt in the separate experiments.

3.2 Experimental setup

First, 235 g of the $ZnCl_2$:KCl:NaCl mixture (44.3–41.9–13.8 mol%) was prepared in a graphite crucible just before loading into the furnace, where the salt mixture was heated to around 260 °C. To avoid interference from dissolved oxygen, argon was bubbled through the molten salt for at least 12 h to deoxygenate and remove the residual water, according to the procedure given in (36). Then, 2 g of the impurity was added to the molten salt, and argon was bubbled at the bottom of the mixture to stir the mixture for one hour. The flow of argon was kept over the cell during the experiments to provide an inert atmosphere.

CV and chronoamperometry were performed with an electrochemical measurement system (Autolab PGSTAT302N) and controlled by NOVA software version 2.1 for Windows. The

working electrode was a 6 mm diameter graphite rod in CV or a 3 mm diameter Zn rod in potentiostatic electrolysis, and a 0.5 mm diameter platinum (Pt) wire was used as a reference electrode. A graphite crucible measuring 12.5 cm high, 9.5 cm outer diameter, and 6.5 cm inner diameter was employed as the container for the molten salt. The crucible also functioned as a counter electrode. The temperature was measured during the experiments using a S–type thermocouple located just above the molten salt surface (see Figure 1).

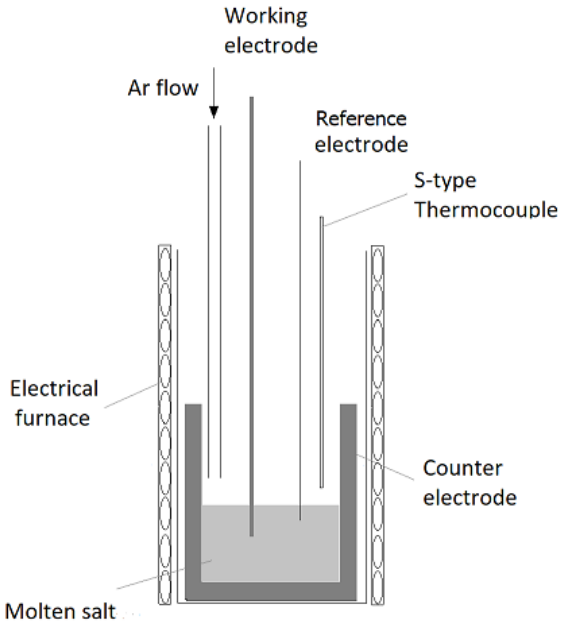

Figure 1. Schematic of the experimental setup for electrochemical salt purification using a graphite crucible as counter electrode, Pt wire as reference electrode and graphite rod or Zn rod as working electrode

3.3 Experimental method

A CV of the molten salt was carried out before adding the impurities for each experiment. The geometric area of the graphite working electrode in contact with the molten salt was 3.8 cm^2, and the counter electrode (the crucible) was 94.4 cm^2. The CV was conducted at a scan rate of 20 mV/s starting at 0 V versus the Pt reference electrode. After adding the impurity, the CV was repeated under the same conditions to detect the new peak related to the impurity. After the peak identification, potentiostatic electrolysis was conducted using chronoamperometry to extract the impurity from the molten salt. The working electrode was changed to the Zn electrode and constant potential was applied. After a time between 30 min and a few hours, the electrolysis was terminated, and the working electrode was removed from the melt. Then the

impurities attached to the working electrode were extracted from the molten salt, and the CV was repeated to compare the voltammogram before and after electrodeposition. The applied potential value for each electrodeposition run was adjusted according to the cathodic peak in the cyclic voltammogram before a new run, as suggested by Kim et al. (12). This phenomenon is caused by shifts in the reference electrode potential, which in the present study was Pt.

For every experiment with a new impurity, a newly prepared salt mixture was used, and the temperature was kept at 260 °C for all experiments. To minimize the ohmic drop in the CV, a slow scan rate was selected (20 mV/s) and large amount of electrolyte was employed to increase the conductivity of the solution, as discussed in Section 2. Moreover, a short distance (1 cm) between the working and reference electrodes was kept during the experiments, as suggested by (37,38).

The deposited compound from purification of the first case (CuCl and molten salt) was analyzed using XRD to characterize the elements. While XRD analyses were carried out for the other cases as well, there was a lot of noise, which made it difficult to interpret the results.

4. Results and discussion

A series of CV tests were carried out to identify the reduction potential of various elements in $ZnCl_2$:KCl:NaCl and a series of potentiostatic electrolysis experiments were subsequently conducted to remove the added impurities.

Figure 2 shows the cyclic voltammogram for molten $ZnCl_2$:KCl:NaCl at 260 °C before adding any impurity. At a lower potential (–0.5 V), the sharp increase of cathodic current defines the nucleation process of the electroreduction of metal. This phenomenon is typically the same as that resulting from the decomposition of a solvent defining the potential window. Therefore, this can confidently be attributed to the deposition of Zn, Na, or K metal (21). Because Zn(II) is more easily reduced than Na or K, the cathodic peak was assumed to represent the electroreduction of Zn(II) from $ZnCl_2$. When the sweep direction was reversed, the corresponding anodic current was observed. It can be seen that the discharge of metal ions started from –0.5 V. On the other side of the electrochemical window, the anodic current observed over 1.4 V is considered to be chlorine gas evolution. Nitta et. al. and Li et al. reported similar voltammograms for $ZnCl_2$:KCl:NaCl and $ZnCl_2$ (35,39), respectively. Based on these results, the electrochemical window of the molten salt was concluded to be –0.5 to 1.4 V for further experiments.

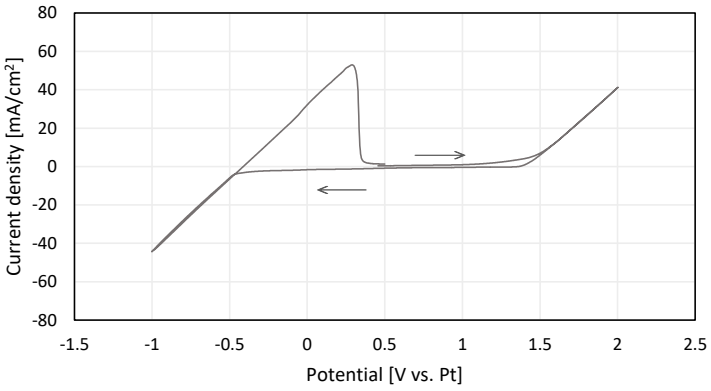

Figure 2. Cyclic voltammogram of $ZnCl_2$:KCl:NaCl recorded on a Zn electrode at 260 °C

4.1 Deposition of Cu from CuCl

Figure 3 shows the results of CV measurements after adding 2 g of CuCl to the melt with a scan rate of 20 mV. A cathodic process was observed at a potential of -0.04 V, corresponding to the bulk deposition of Cu in the molten salt as well as the anodic stripping of Cu. However, other peaks appeared at –1.2 and –0.8 V likely because of either sodium ions or Zn alloy. On the one hand, it is well-known that alkali metals (especially Na) react with graphite, and this leads to the underpotential deposition of these metals (40,41). Because the underpotential deposition had not been observed in the CV of the melt (Figure 2), it can be interpreted that the reversible intercalation of Na in graphite was affected by adding CuCl. On the other hand, the formation of Zn alloy could be another possibility which is thermodynamically favored. Zn easily forms an alloy with other metals such as Na or Cu in the current system, which can appear as redox peaks in the voltammogram.

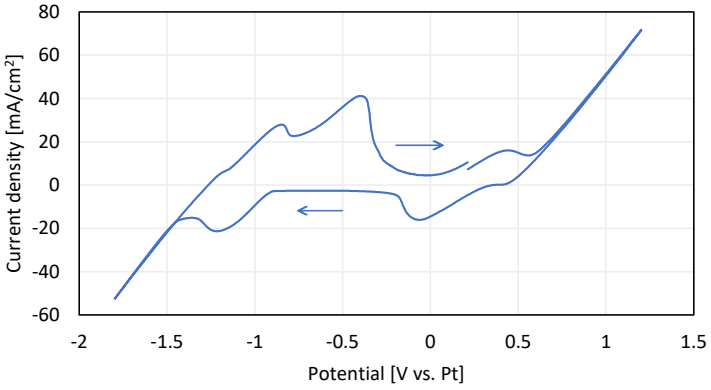

Figure 3. Cyclic voltammogram of $ZnCl_2$:KCl:NaCl containing CuCl (0.8 wt%) at 260 °C.

Because many studies chose slightly higher scan rates than 20 mV for CV experiments (12,35,42,43), CV tests were carried out for 10 mV to 150 mV to illustrate the variation of the cathodic peak potential as a function of scan rate (Figure 4). It can be seen in Figure **4** that the anodic and cathodic peak potentials shifted as the scan rate was increased. Increasing the scan rate led to a decrease in the size of the diffusion layer, and higher currents were observed as a consequence, in accordance with the theory (37). Because the scan rate of 20 mV/s nicely presented the redox peaks and CV details, the same scan rate was chosen for further experiments. Moreover, such a low scan rate can minimize the ohmic drop in CV, thus providing more reliable results (37,38).

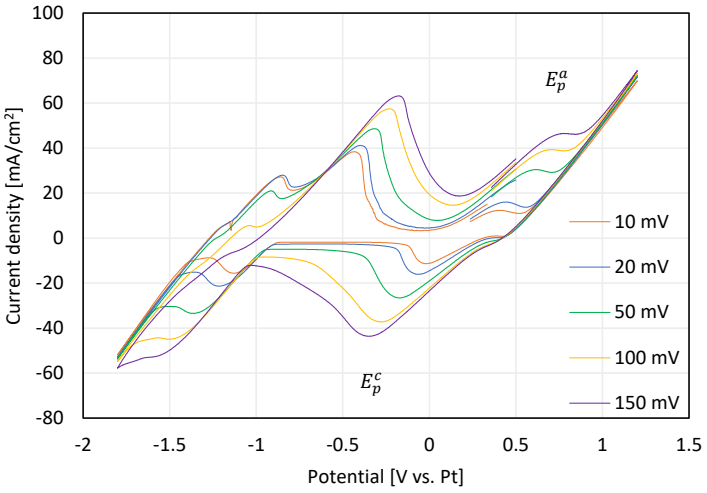

Figure 4. Cyclic voltammograms using a graphite electrode in $ZnCl_2$:KCl:NaCl containing CuCl (0.8 wt%) at 260 °C under the different scan rates of 10, 20, 50, 100, 150 mV/s.

Additionally, the peak potential E_p versus the logarithm of the scan rate $logv$ plot ($\Delta E/\Delta logv$) in Figure 5 showed an almost linear relationship (r = 0.977). Moreover, the peak potential was shifted to a negative direction when the scan rate was increased, which confirms the irreversibility of the process in the experimental condition (44). The hypothesis was strengthened considering the anodic and cathodic peak separation $\Delta E = E_P^c - E_P^a$.

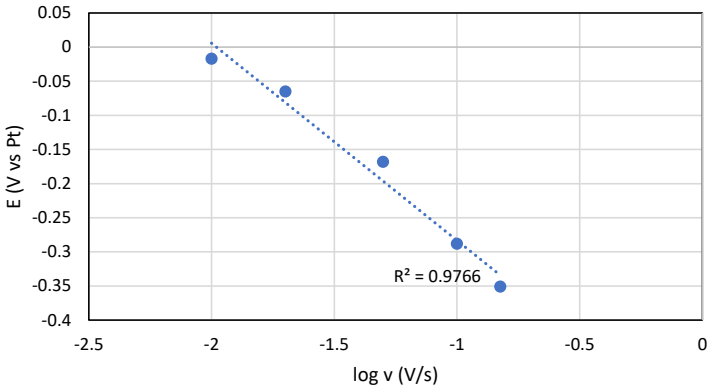

Figure 5. Variation of the cathodic peak potential versus the scan rates

The molten salt purification was carried out in two steps using the chronoamperometry method. In the first step of the purification, a Zn electrode was used as a working electrode to recover Cu from the solution by applying 0.1 V for 30 min. Figure 6 presents the current variation as a function of time, while the constant potential was applied for half an hour. By applying constant potential, the amount of current that passed through the electrode surface was almost constant during the early stage of the electrodeposition process for 600 seconds. Then, it started to decrease slightly due to more deposition on the electrode surface and the reducing concentration of contaminant in the molten salt.

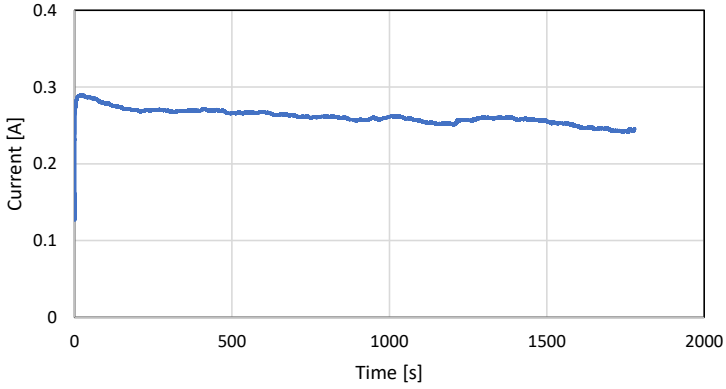

Figure 6. The current variation as a function of time through a chrono amperometry experiment applying constant potential equal to 0.1 V for recovering Cu from the molten salt in the first step of purification.

Figure 7 shows the results of CV measurements after two levels of potentiostatic electrolysis (purification 1 and 2). The redox peak height of Cu^{+} clearly decreased after the first run (purification 1). In the second step (purification 2), the applied potential was positively

increased because the CV was shifted after the first run. Therefore, a constant potential of 0.9 V was applied for another hour. Cu(I) were reduced and deposited onto the surface of the working electrode (see Figure 8). Purification 2 showed that the redox peak of impurity in the salt was clearly diminished, which can be interpreted that all of the Cu(I) from CuCl is reduced by potentiostatic electrolysis. The redox peaks related to the Zn alloys formation also disappeared in the result from purification 2, which can explain the relationship of the alloy formation and the existence of Cu ions.

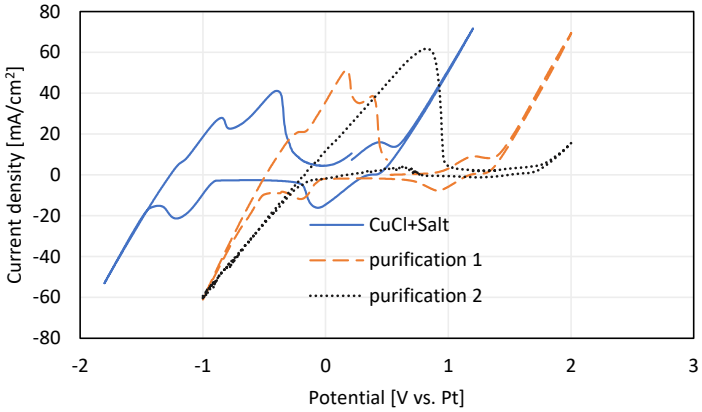

Figure 7. Cyclic voltammogram of $ZnCl_2$:KCl:NaCl containing CuCl (0.8 wt%) before and after each potentiostatic electrolysis run.

Figure 8. The copper deposited from CuCl in the molten salt after 1.5 h of electrodeposition

To confirm that the deposited material was Cu, XRD was performed on the sample. The XRD spectra in Figure 9 shows the strongest diffraction peaks of Cu, indicating that the main chemical composition of the obtained electrodeposits wass Cu. The other peaks were mostly noises due to the presence of some molten salt in the extracted metal.

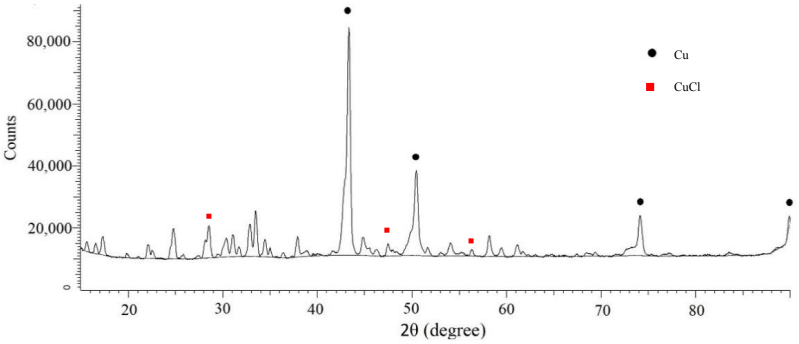

Figure 9. XRD pattern of copper electrodeposits obtained from $ZnCl_2$:KCl:NaCl containing CuCl (0.8 wt%) at 260 °C

4.2 Deposition of Fe from $FeCl_2$ and $FeCl_3$

In separate experiments, 2 g of $FeCl_2$ and $FeCl_3$ were added to the molten salt. Figure 10 shows the voltammogram for Fe(II) and Fe(III) in the molten salt solution. There is one pair of cathodic and anodic current peaks between 0.2 and 1 for $FeCl_2$ and between 0 and 1.2 for $FeCl_3$ presenting the redox peak for Fe ion existence. At a lower potential, the deposition of $ZnCl_2$ starts from almost −0.5 V in both cases while the evolution of chlorine at the other end of the electrochemical window started at less positive values than the pure salt (Figure 2), especially in the case of $FeCl_2$.

a.

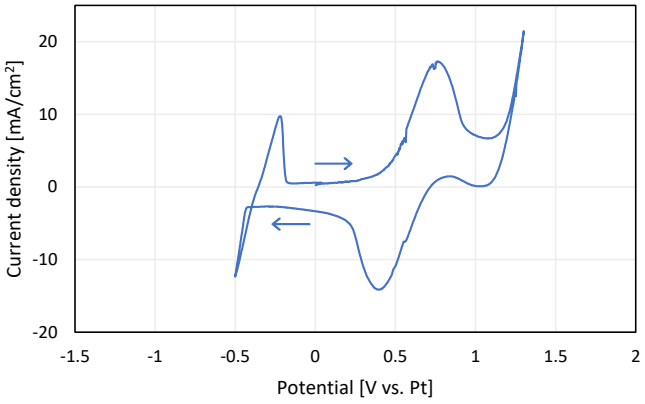

b.

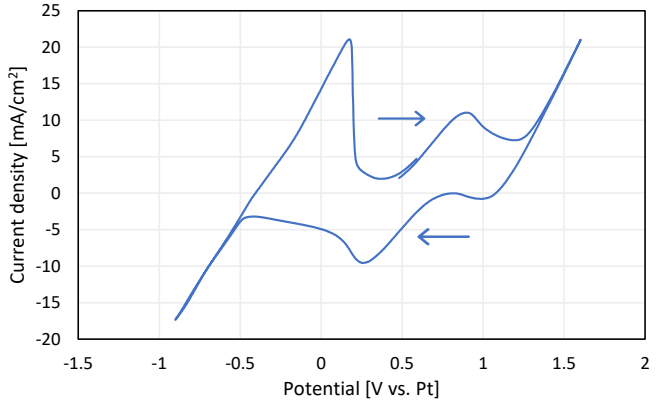

Figure 10. Cyclic voltammogram of $ZnCl_2$:KCl:NaCl containing (a) $FeCl_2$ and (b) $FeCl_3$ (0.8 wt%) at 260 °C

After detecting the impurity, chronoamperometry was applied in both cases to purify the molten salt. Figure 11 shows the voltammogram before and after potentiostatic electrolysis to remove Fe from the melt. In Figure 11(a), the amperometry method was carried out at the potential of 0.7 V for 1.5 hours. Purification 1 shows that the redox peak significantly decreased after just one run, indicating that a considerable amount of impurity (Fe ion) had been separated from the melt. In the second run, a potential of 1.1 V was applied for 1.5 h. As shown in purification 2, the redox peaks were still visible as very small peaks, indicating the presence of small amounts of Fe ions in the solution. The deposition electrolysis continued for another hour, but no significant peak difference was observed, meaning that no more removal was achieved with the current setup and procedure.

Figure 11(b), shows the two steps of electrolysis that were carried out. In the first run, a potential of 0.2 V was applied for 1 h, which highly affected the redox peak, as can be seen in the graph of current purification 1. For the second run, a potential of 1 V was applied due to shifting the voltammogram to a more positive potential. The amperometry method was run for 1.5 h. Purification 2 shows the voltammogram after 2.5 h electrolysis in total, which obviously did not detect any redox peak related to the impurity, meaning almost complete salt purification.

a.

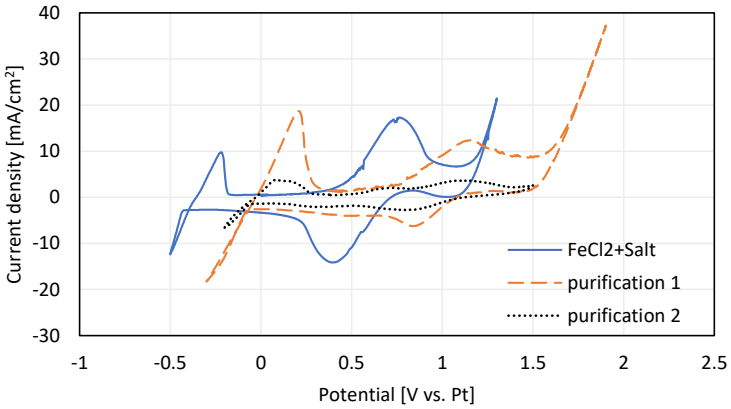

b.

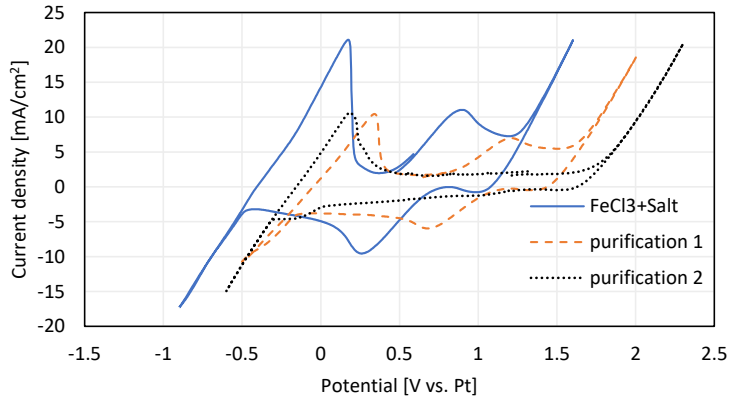

Figure 11. Cyclic voltammogram of $ZnCl_2$:KCl:NaCl containing (a) $FeCl_2$ and (b) $FeCl_3$ (0.8 wt%) before and after each potentiostatic electrolysis run.

Although the voltammogram showed successful impurity ($FeCl_3$) removal, no metal was observed at the surface of the electrode after electrolysis. Therefore, the idea of precipitation of the impurities was assessed by breaking the crucible. As can be clearly seen in Figure 12, a

layer of precipitate with dark color indicates that the impurity was separated and had settled at the bottom of the crucible after electrolysis. However, the brownish color of the molten salt at the top layer can be due to the presence of Fe ions in the salt.

Figure 12.Cross-section of the crucible after 2.5 h electrodeposition of Fe from $FeCl_3$ in $ZnCl_2$:KCl:NaCl showing two separate layers, molten salt on top and Fe compound at the bottom.

Fe(III) is not very stable in chloride melts, and its oxidation potential is very close to chlorine revolution, which makes it difficult to study (27,28). In some studies, Fe(III) was not detected at all (30,32,33,45). However, $FeCl_2$ has higher stability, and it has the favor of $FeCl_2$ and chlorine gas formation (16):

$$FeCl_{3\,(melt)} \rightarrow FeCl_{2\,(melt)} + \frac{1}{2}Cl_2 \qquad (6)$$

According to previous studies, it seems that experimental conditions have a tremendous effect on the stability of $FeCl_3$. At high temperatures, $FeCl_3$ may decompose to $FeCl_2$ and Cl_2, and if the pressure of Cl_2 is kept very low, $FeCl_3$ can decompose completely (16). The electrode may catalyze this reaction or participate in electrochemical reactions through oxidation and reduction of Fe (III) ions (16,30). The composition of the melt can also have a great influence on the stability of Fe (III) (46). $FeCl_3$ can react with alkali chlorides and form the stable complex $MFeCl_4$, where M is the alkali metal (47). In some studies, Fe (III) reduction has occurred in one single reversible step, while other studies reported two steps for reduction (29,31,48).
In the present study, the partial pressure of chlorine gas was almost zero because the solubility of chlorine was very low in this melt. Moreover, the electrochemical cell was open to release the Cl_2, which can move the equilibrium given by Eq. (6) to more $FeCl_3$ decomposition. Conversely, $ZnCl_2$:KCl:NaCl may react with $FeCl_3$ before letting it decompose. This can be the reason for the brownish color of the salt in the top layer in Figure 12.
The XRD results showed a lot of noise, which can be interpreted as different oxide or hydroxide forms of Fe(II) and (III). The existence of these various components made XRD analysis difficult for the current system.

4.3 Deposition of Mn from MnO_2

Figure 13 presents the voltammogram of the molten salt before adding the impurity (gray), after adding 2 g of MnO_2 (blue), after holding for 30 min and after running the potentiostatic electrolysis (orange). It is clear that the plot for molten salt shifted to a more negative potential (−1 V) compared to Figure 2 (pure salt), which can be due to instability of the reference electrode. Although the redox peaks shifted, the electrochemical window was still 1.9 V. After adding the impurity, a couple of peaks, including a reduction peak at −0.6 V and an oxidation peak at −0.25 V, represented the presence of Mn^{4+} in the melt. The oxidation peak at −0.6 V is related to Zn oxidation in the molten salt to generate Zn^{+}. In the purification step, the constant voltage of −0.55 V was applied for 1.5 h using a Zn electrode. The purification curve presents the CV after purification. The peaks clearly show lower current, meaning that lower amounts of the impurity were present. In the next step, electrodeposition electrolysis was performed for another 1.5 h but no significant removal was observed in the CV (not shown here).

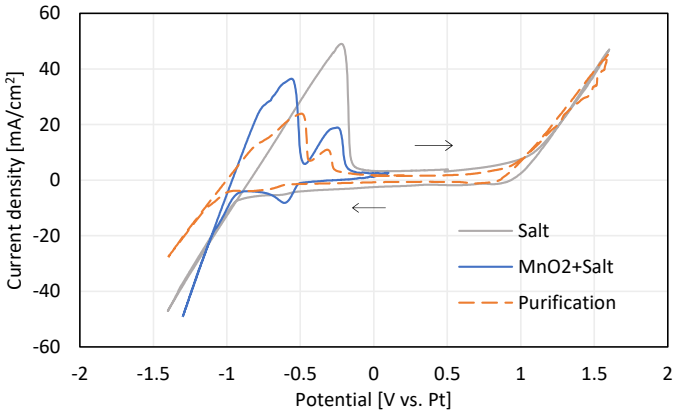

Figure 13. Cyclic voltammogram of $ZnCl_2$:KCl:NaCl containing MnO_2 (0.8 wt%) before and after each potentiostatic electrolysis run.

The process of reducing Mn (IV) to manganese was divided into three steps (42):

$$Mn\ (IV) \rightarrow Mn(III) \rightarrow Mn(II) \rightarrow Mn \qquad (7)$$

Liang et al. reported a couple of redox peaks for every reduction step (42). However, there was only one pair of redox peaks in the current study. This could mean either that the reducing steps happened rapidly or that Mn(IV) was reduced to Mn directly in this solution.

Figure 14 shows the impurity extracted in the impurity removal step (potentiostatic) attached to the working electrode. XRD analysis was carried out for the extracted element. However, the results included noise, making them difficult to interpret. This may have been caused by the presence of different oxides in the sample, which provided various peaks.

Figure 14. The deposited Mn from MnO_2 in the molten salt after 1.5 h of electrodeposition.

To investigate the possibility of purification improvement, the effect of temperature on the removal efficiency was examined. The melt was heated up to 350 ℃, and the chronoamperometry method was employed. After a few minutes, the current had zero values, and examination of the setup showed that the Zn electrode had dissolved in the solution. Given that the Zn melting point is higher than 400 ℃, the reason may be the contribution of the Zn electrode in the deposition process due to the presence of Zn^+ in the salt (12). Increasing the temperature made the electrode potential more positive. In one study, De Bethune et al. expressed an approximately linear correlation between electrode potential and temperature in the range of 0 to 100 ℃ with respect to the standard reduction potential at 25 ℃ (49).

$$E_T = E^0_{298} + (T - 298.15)(\frac{dE^0}{dT})_{298} \quad (8)$$

Thus, the same correlation is assumed for the higher temperature in the current study for Zn, which caused the Zn electrode oxidation at the lower potential. Figure 15 shows the Zn electrode after applying amperometry for a few minutes at 350 ℃.

Figure 15. The Zn electrode after a few minutes potentiostatic experiment in $ZnCl_2$:KCl:NaCl containing MnO_2 at 360 ℃

5. Conclusion

The purification of molten $ZnCl_2$:KCl:NaCl (44.3–41.9–13.8 mol%) and deposition of Cu, Fe and Mn in the molten salt at the relatively low temperature of 260 °C was electrochemically studied using CV and electrodeposition techniques. Graphite and Zn electrodes were used as working electrodes in the CV and deposition experiments, respectively. The CV results exhibited a shift in reduction potentials, mostly due to instability of the Pt reference electrode and underpotential deposition of sodium in some cases. In addition, potentiostatic electrolysis tests were performed to remove the added impurities from the melt. All four cases indicated a high level of impurity removal from the molten salt, according to the CV results. However, the deposition of Cu on the Zn electrode in the molten salt was the most effective purification process. The CV after electrolysis experiments and the XRD results indicate that Cu is removed from the molten salt after 1.5 h of electrodeposition. The impurity from adding $FeCl_3$ was removed after 2.5 h electrodeposition in two steps, while the removal of $FeCl_2$ and MnO_2 after 3 h deposition electrolysis showed partial removal of impurities, according to the CV redox peaks.

Acknowledgment

The authors would like to thank Christian Solheim for assistance with the XRD analysis. This project has received funding from the European Union's Horizon 2020 Research and Innovation program under grant agreement number 764089.

References

1. Ding W, Gomez-Vidal J, Bonk A, Bauer T. Molten chloride salts for next generation CSP plants: Electrolytical salt purification for reducing corrosive impurity level. Sol Energy Mater Sol Cells. 2019;199:8–15.
2. Ladkany S, Culbreth W, Loyd N. Molten salts and applications I: molten salt history, types, thermodynamic and physical properties, and cost. J Energy Power Eng. 2018;12:507–16.
3. Palacios A, Barreneche C, Navarro ME, Ding Y. Thermal energy storage technologies for concentrated solar power A review from a materials perspective. Renew Energy. 2020;156:1244–65.
4. Reilly HE, Kolb GJ. An evaluation of molten-salt power towers including results of the Solar Two project. Sandia National Laboratories, Albuquerque, NM. 2001.
5. Giordani V, Tozier D, Tan H, Burke CM, Gallant BM, Uddin J, et al. A molten salt lithium-oxygen battery. J Am Chem Soc. 2016;138(8):2656–63.
6. Nygård HS, Olsen E. Effect of salt composition and temperature on the thermal behavior of beech wood in molten salt pyrolysis. Energy Procedia. 2014;58:221–8.
7. Kudsy M, Kumazawa H. Pyrolysis of kraft lignin in the presence of molten ZnCl2-KCl mixture. Can J Chem Eng. 1999;77(6):1176–84.
8. Harrison MT, Simms HE, Jackson A, Lewin RG. Salt waste treatment from a LiCl-KCl based pyrochemical spent fuel treatment process. Radiochim Acta. 2008;96(4–5):295–301. Available from: https://doi.org/10.1524/ract.2008.1490
9. Cho Y, Lee T, Choi J, Eun H, Park H, Park G. Eutectic (LiCl-KCl) waste salt treatment by sequencial separation process. Nucl Eng Technol. 2013;45(5):675–82.
10. Eun H-C, Kim J-H, Cho Y-Z, Choi J-H, Lee T-K, Park H-S, et al. An optimal method for phosphorylation of rare earth chlorides in LiCl–KCl eutectic based waste salt. J Nucl Mater. 2013;442(1):175–8. Available from: https://doi.org/10.1016/j.jnucmat.2013.08.021
11. Cho Y-Z, Lee T-K, Eun H-C, Choi J-H, Kim I-T, Park G-I. Purification of used eutectic (LiCl–KCl) salt electrolyte from pyroprocessing. J Nucl Mater. 2013;437(1):47–54. Available from: doi.org/10.1016/j.jnucmat.2013.01.344
12. Kim G-Y, Jang J, Paek S, Lee S-J. Electrochemical removal of rare earth element in LiCl-KCl molten salt. Sci Technol Nucl Install. 2020;2020.
13. Simka W, Puszczyk D, Nawrat G. Electrodeposition of metals from non-aqueous solutions. Electrochim Acta. 2009;54(23):5307–19. Available from: doi.org/10.1016/j.electacta.2009.04.028
14. Inman D, White S. The production of refractory metals by electrolysis of molten salts design factors and limitations. J Appl Electrochem. 1978;8(5):375–90.
15. Chryssoulakis J, Bouteillon J, Poignet JC. Electrochemical behaviour of pure iron in the aluminium refining electrolyte. J Appl Electrochem. 1978;8(2):103–8.

16. Khalaghi B, Kvalheim E, Tokushige M, Teng L, Seetharaman S, Haarberg GM. Electrochemical behaviour of dissolved iron chloride in KCl+LiCl+NaCl melt at 550ºC. ECS Trans. 2014;64(4):301.

17. Castrillejo Y, Bermejo MR, Barrado E, Martínez AM. Electrochemical behaviour of erbium in the eutectic LiCl–KCl at W and Al electrodes. Electrochim Acta. 2006;51(10):1941–51. Available from: https://doi.org/10.1016/j.electacta.2005.07.004

18. Bermejo MR, de la Rosa F, Barrado E, Castrillejo Y. Cathodic behaviour of europium (III) on glassy carbon, electrochemical formation of Al4Eu, and oxoacidity reactions in the eutectic LiCl–KCl. J Electroanal Chem. 2007;603(1):81–95. Available from: https://doi.org/10.1016/j.jelechem.2007.01.018

19. Bermejo MR, Barrado E, Martínez AM, Castrillejo Y. Electrodeposition of Lu on W and Al electrodes: Electrochemical formation of Lu–Al alloys and oxoacidity reactions of Lu(III) in the eutectic LiCl–KCl. J Electroanal Chem. 2008;617(1):85–100. Available from: https://doi.org/10.1016/j.jelechem.2008.01.017

20. Castrillejo Y, Fernández P, Medina J, Hernández P, Barrado E. Electrochemical extraction of samarium from molten chlorides in pyrochemical processes. Electrochim Acta. 2011;56(24):8638–44. Available from: https://doi.org/10.1016/j.electacta.2011.07.059

21. Chen GZ, Fray DJ, Farthing TW. Direct electrochemical reduction of titanium dioxide to titanium in molten calcium chloride. Nature. 2000;407(6802):361–4.

22. Xiao W, Jin X, Deng Y, Wang D, Chen GZ. Rationalisation and optimisation of solid state electro-reduction of SiO2 to Si in molten CaCl2 in accordance with dynamic three-phase interlines based voltammetry. J Electroanal Chem. 2010;639(1):130–40. Available from: https://doi.org/10.1016/j.jelechem.2009.12.001

23. Yasuda K, Nohira T, Ito Y. Effect of electrolysis potential on reduction of solid silicon dioxide in molten CaCl2. J Phys Chem Solids. 2005;66(2):443–7. Available from: https://doi.org/10.1016/j.jpcs.2004.06.037

24. Yasuda K, Nohira T, Amezawa K, Ogata YH, Ito Y. Mechanism of direct electrolytic reduction of solid SiO2 to Si in molten CaCl2. J Electrochem Soc. 2005;152(4):D69.

25. Jin X, Gao P, Wang D, Hu X, Chen GZ. Electrochemical preparation of silicon and its alloys from solid oxides in molten calcium chloride. Angew Chemie Int Ed. 2004;43(6):733–6.

26. Akpinar B, Erdogan M, Akduman B, Karakaya I. The use of silicon wafer barriers in the electrochemical reduction of solid silica to form silicon in molten salts. ECS Trans. 2017;77(11):2011.

27. Inman D, Legey JC, Spencer R. A chronopotentiometric study of iron in LiCl-KCl. J Appl Electrochem. 1978;8(2):269–72.

28. Picard G, Seon F, Tremillon B. Reactions of formation and stability of iron (II) and (III) oxides in LiCl-KCl eutectic melt at 470ºC. J Electrochem Soc. 1982;129(7):1450.

29. Ge XL, Xiao SJ, Haarberg GM, Seetharaman S. Salt extraction process-novel route for metal extraction Part 3-electrochemical behaviours of metal ions (Cr, Cu, Fe, Mg, Mn) in

molten (CaCl2-NaCl-KCl) salt system. Miner Process Extr Metall. 2010;119(3):163–70.

30. Lugovskoy A, Zinigrad M, Aurbach D, Unger Z. Electrodeposition of iron(II) on platinum in chloride melts at 700–750°C. Electrochim Acta. 2009;54(6):1904–8. Available from: https://doi.org/10.1016/j.electacta.2008.10.016

31. Castrillejo Y, Martínez AM, Vega M, Barrado E, Picard G. Electrochemical study of the properties of iron ions in ZnCl2 + 2NaCl melt at 450°C. J Electroanal Chem. 1995;397(1):139–47. Available from: https://doi.org/10.1016/0022-0728(95)04151-9

32. Castrillejo Y, Martinez AM, Vega M, Sanchez Batanero P. Electrochemical reduction of Fe(II) ions on different solid electrodes in fused ZnCl2-2NaCl mixture. J Appl Electrochem. 1996;26(12):1279–85.

33. Shuzhen D, Dudley P, Inman D. Voltammetric studies of iron in molten MgCl2+NaCl+KCl: Part I. The reduction of Fe(II). J Electroanal Chem Interfacial Electrochem. 1982;142(1):215–28. Available from: https://doi.org/10.1016/S0022-0728(82)80017-X

34. Niazi S, Olsen E, S. Nygård H. Hydrolysis of eutectic compositions in the ZnCl2:KCl:NaCl ternary system and effect of adding ZnO. J Mol Liq. 2020;317:114069. Available from: https://doi.org/10.1016/j.molliq.2020.114069

35. Nitta K, Nohira T, Hagiwara R, Majima M, Inazawa S. Physicochemical properties of ZnCl 2 -NaCl-KCl eutectic melt. Electrochim Acta. 2009;54(21):4898–902.

36. Elgrishi N, Rountree KJ, McCarthy BD, Rountree ES, Eisenhart TT, Dempsey JL. A practical beginner's guide to cyclic voltammetry. J Chem Educ. 2018;95(2):197–206.

37. Savéant J-M. Elements of molecular and biomolecular electrochemistry: an electrochemical approach to electron transfer chemistry. John Wiley & Sons; 2006.

38. Oldham KB, Stevens NP. Uncompensated resistance. 2. The effect of reference electrode nonideality. Anal Chem. 2000;72(17):3981–8.

39. Li M, Li Y. Electrodeposition of zinc from zinc oxide and zinc chloride in 1-methylimidazolium trifluoromethylsulfonate ionic liquid. Prot Met Phys Chem Surfaces. 2020;56(1):180–8.

40. Adhoum N, Bouteillon J, Dumas D, Poignet JC. Electrochemical insertion of sodium into graphite in molten sodium fluoride at 1025°C. Electrochim Acta. 2006;51(25):5402–6. Available from: https://doi.org/10.1016/j.electacta.2006.02.019

41. Xu Q, Schwandt C, Chen GZ, Fray DJ. Electrochemical investigation of lithium intercalation into graphite from molten lithium chloride. J Electroanal Chem. 2002;530(1):16–22. Available from: https://doi.org/10.1016/S0022-0728(02)00998-1

42. Liang J, Zhang R, Li H, Wang L, Cai Z, Yan H, et al. The electrochemical mechanism of preparing Mn from LiMn2O4 in waste batteries in molten salt. Crystals. 2021;11(9):1066.

43. Vignarooban K, Xu X, Wang K, Molina EE, Li P, Gervasio D, et al. Vapor pressure and corrosivity of ternary metal-chloride molten-salt based heat transfer fluids for use in concentrating solar power systems. Appl Energy. 2015;159:206–13.

44. Brett CM, Brett O, Electrochemistry AM. Principles, methods and applications. Oxford university press, Oxford; 1993.

45. Lugovskoy A, Zinigrad M, Aurbach D. Electrochemical determination of diffusion coefficients of iron (II) ions in chloride melts at 700-750° C. Isr J Chem. 2007;47(3–4):409–14.

46. Zhao G, Tian Q, DuAn S. Equilibria between ferrous and ferric chlorides in molten chloride salts. Metall Trans B. 1990;21(1):131–3.

47. Cook J, Charles M, Wendell E, Dunn J. The reaction of ferric chloride with sodium and potassium chlorides. J Phys Chem. 1961;65(9):1505–11.

48. Boxall LG, Jones HL, Osteryoung RA. Electrochemical studies on Ag, Fe, and Cu species in AlCl3-NaCl melts. J Electrochem Soc. 1974;121(212).

49. Debethune A, Licht T, Swendeman N. The temperature coefficients of electrode potentials: the isothermal and thermal coefficients—the standard ionic entropy of electrochemical transport of the hydrogen ion. J Electrochem Soc. 1959;106(7):616.

Paper IV

Niazi, Sepideh; Nygård, Heidi S.; Reis, Bruno; to Baben, Moritz. “Thermodynamic modeling of KCl-H_2O and its binary subsystems including H_2O-HCl, KOH-H_2O and KCl-KOH”. Submitted to CALPHAD Journal.

Thermodynamic modeling of KCl–H_2O and its binary subsystems, including H_2O–HCl, KOH–H_2O, and KCl–KOH

Sepideh Niazi[a], Heidi S. Nygård[a], Bruno Reis[b], Moritz to Baben[b]

[a] Faculty of science and technology, Norwegian University of Life Science (NMBU), Ås, Norway

[b] GTT-Technologies, Kaiserstraße 103, Herzogenrath 52134, Germany

Chlorides are applied intensively in many industries, but their hydrolysis is still a challenge, as they have a high tendency to react with water and form highly corrosive acid HCl and metal oxides. In the present work, the liquid phase has been modeled in FactSage, covering the complete composition space among H_2O, HCl, KOH, and KCl and temperatures between 200K and 1,000K. The thermodynamic modeling of phase equilibria in the KCl–K_2O–HCl–H_2O reciprocal system is carried out using an associate solution model for the liquid phase. Using the Calphad technique, the H_2O–KCl, H_2O–HCl, H_2O–K_2O, and KOH–KCl binary systems are critically assessed. This study is the first to model the liquid solution with chlorides and oxides over the complete composition space. The thermodynamic parameters involved in the excess term of the Gibbs energy phases are optimized based on all experimental data available from the literature. The phase diagrams and model parameters were derived from thermodynamic optimization.

Keywords: KCl, Hydrolysis, Calphad, Liquid solution

1. Introduction

KCl is one of the popular chlorides among other salt groups, even halides. This salt is widely used in mixtures with other salts (especially chlorides) as a Heat Transfer Fluid (HTF) or Thermal Energy Storage (TES) (1–5). KCl is chemically highly stable due to its ionic bonding. Its high melting and boiling points (~770 °C and ~1,420 °C, respectively) make it a good candidate to contribute to a high eutectic boiling point when mixed with other salts (1,2). It is also reported that KCl has a positive effect on decreasing the vapor pressure in the salt mixture system (e.g., with NaCl, $ZnCl_2$, $MgCl_2$, $CaCl_2$) in some studies. With an increase in the molar fraction of KCl, the vapor pressure of the eutectic salt becomes lower (1,6). All mentioned properties, in addition to low cost and large availability as natural resources, make it a prevalent salt in many applications.

Phase equilibria studies of inorganic salt systems in contact with water are needed for many purposes, including to understand hydrolysis reactions, the behavior of aqueous salt, or the solubility of salt in water. Moisture is one of the most common detrimental impurities in salts, especially chlorides, due to their hygroscopic nature (7). Although these salts are usually kept at high temperatures to avoid absorbing moisture, small amounts of water may induce hydrolysis of the salt and form a highly corrosive gas (HCl). For KCl, the hydrolysis reaction is given in Eq. 1.

$$2KCl + H_2O \leftrightarrow 2HCl + K_2O \quad (1)$$

Possible mitigation to avoid hydrolysis involves the addition of a metal oxide to decrease the partial pressure and the hydrolysis rate (6,8,9).

Generally, all components in Eq.1 could be dissolved in the liquid solution and make a KCl–K_2O–HCl–H_2O reciprocal system that must be studied. FactSage databases are the largest set of evaluated and optimized thermodynamic databases for inorganic systems in the world (10) containing descriptions on the solubility of KCl in water at ambient temperatures or of oxygen or hydroxide in KCl at an elevated temperature. However, no consistent description exists that can describe the liquid phase over the complete composition space among KCl, KOH, HCl, and H_2O. In fact, the solution models for the liquid in the aqueous community (11,12), are very different compared to the ones used for oxides and salts (13).

This study aims to model, for the first time, the entire KCl–K_2O–HCl–H_2O reciprocal system between 200 and 1,000 K. Because of the limited stability of K_2O under ambient conditions, no experimental data for K_2O–KCl or K_2O–KOH was found from the literature, and it is assumed that K_2O has an ideal contribution to the liquid solution. Therefore, the complete KCl–KOH–HCl–H_2O system can be described, as shown in Figure **1**, at arbitrary temperatures using the database developed. It is shown that the liquid solution can be described by a simple non-ideal associate solution model over the complete temperature and composition space.

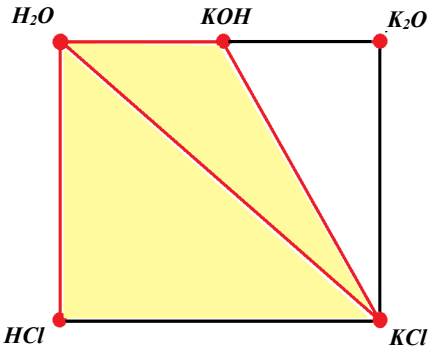

Figure 1. KCl–K_2O–HCl–H_2O reciprocal system using an associate solution model. Red lines: assessed quasi-binary systems, yellow area: composition space covered.

Apart from chloride and oxide, the solubility of the hydroxide in this reciprocal system has been described in this study.

2. Thermodynamic modeling

The software package FactSage (14) is used in the simulations, and the calculation of phase diagrams is carried out using the Phase Diagram module. The Compound module is used to create the individual compounds that serve as a base for the modelling of the entire system, while the Solution module is used to create solutions and their thermodynamic parameters. All calculations in this work are performed for a fixed total system pressure of 1 bar.

Considering the hydrolysis of KCl requires studying some other liquid species, such as oxides and hydroxides, which can be formed due to the reaction between salt and water. Some of the main species that affect this binary system are KOH, K_2O, and HCl. Aqueous ions are other species in this system, but they are omitted from this study, as they do not have a significant concentration in salt-rich systems.

To optimize the phase diagrams and thermodynamic properties of the systems, FactSage 7.2 is used to create the thermodynamic database, while experimental data is collected from many different references in the literature. The optimization itself was carried out with the DataOptimizer program (15). The order of the assessment was to first optimize the H_2O–KCl system with two end members, H_2O and KCl, in the liquid phase. After optimizing all binary systems, H_2O–KCl was reassessed with five end members in the liquid phase, including H_2O, KCl, HCl, K_2O, and KOH. Therefore, the optimized binary systems are H_2O–HCl, H_2O–KOH, KOH–KCl, and H_2O–KCl.

The thermodynamic data for all compounds is taken from Fact Pure Substances (FactPS) database (14), except for HCl, which is calculated in this work. The Non-Ideal Associates Model with Redlich–Kister polynomials for interactions has been used to model the liquid phase, while the solid solution was modeled with compound–energy formalism (CEF) (16), which also uses Redlich–Kister polynomials for its non-ideal interactions.

Calculating the equilibrium between phases in a multi-constituted system requires minimizing the total Gibbs free energy of all the phases at the given conditions. The total absolute Gibbs free energy of a solution phase is expressed by the sum of three parts (17):

$$G_m(T, x_i) = G^{ref} + G^{ideal}_{mix} + G^E \tag{2}$$

G^{ref} is the contribution from pure components of the phase to the Gibbs energy and G^{ideal}_{mix} is the ideal mixing contribution, and they can be written as:

$$G^{ref} = \sum_i x_i \, {}^0G_i \tag{3}$$

$$G^{ideal}_{mix} = RT \sum_i x_i \ln x_i \tag{4}$$

G^E, the excess Gibbs energy is the most important parameter to represent the interaction among components, except for the entropy value increase contributed by the ideal mixture. G^E, also known as the Gibbs excess energy of mixing, is modeled by the Redlich–Kister polynomial formula as follows:

$$G^E = \sum_i \sum_{<j} x_i x_j \sum_{\nu=0}^{n_{ij}} L^{(\nu)}_{ij}(T)(x_i - x_j)^\nu \tag{5}$$

Where x_i is the mole fraction of component i, ${}^0G_i$ is the standard Gibbs free energy of the pure substance i, R is the gas constant, $8.314 \frac{J}{mol.K}$, and T is the temperature (K). For a binary system, $x_2 = 1 - x_1$ and $L^{(\nu)}_{ij}$ $(\nu = 0, 1, 2, \dots)$ is the interaction energy or interaction parameter between two end members (16). It can be written as a temperature expansion as follows:

$$L^{(\nu)}_{ij} = \mathrm{A} + \mathrm{BT} + \mathrm{CT}\ln\mathrm{T} + \mathrm{DT}^2 + \mathrm{ET}^3 + \mathrm{F/T} \tag{6}$$

Where A, B, C, D, E, and F are the constant parameters usually obtained through empirical or semi-empirical methods. A single parameter will always give a symmetrical miscibility gap; thus, at least two Redlich–Kister (RK) coefficients are needed to have an asymmetrical miscibility gap. It should be avoided using many coefficients in an RK series and usually, a linear temperature dependence, $\mathrm{A} + \mathrm{BT}$, is enough. The composition dependence of the excess enthalpy is described by A and the excess entropy by B (16). Therefore, the first two parameters, A and B, are considered and optimized later in this work.

3. Determination of parameters

Estimating the thermodynamic properties is necessary for some substances under conditions in which experimental data is not available. This was the case for liquid HCl in this work. For all other pure substances, the data was taken from the FactPS database and the literature.

Adjustments were made to these data for a better extrapolation of the heat capacity beyond the phase stability of pure liquids.
Then, the model parameters for the H_2O–HCl, H_2O–KOH, KOH–KCl, and H_2O–KCl binary systems were determined using several types of thermodynamic data, i.e., vapor pressure, solubility in water, melting and boiling point, and heat capacity of the solution. The data was collected from the literature (18–22) and the FactPS database.

3.1 Pure substances

The standard properties of the pure liquid and solid KCl, KOH, K_2O, and H_2O, as well as gaseous H_2O and HCl, are taken from the FactPS database. Extrapolation is a well-known and widely used mathematical method to estimate the function of thermodynamic properties for the metastable region, which is limited by available experimental data (23). The heat capacities of liquid K_2O and liquid KOH for metastable regions have been extrapolated assuming the constant values 107 and 78.659 J/mol.K, respectively, for the lower temperatures below the melting points down to 298.15 K. This is important because, through the validity of equation (4), a liquid solution that is formed by such species and that can be stable at lower temperatures will have a more reasonable estimate for its heat capacity at lower temperatures also (24).
Regarding the HCl, there was no data for liquid and solid HCl in the FactSage databases. Giauque and Wiebe report the Cp of liquid HCl in the range of the melting and boiling points (25). The Cp of liquid HCl is assumed to have a constant value equal to the Cp at the boiling point (58.9 J/mol.K) and at temperatures below the boiling point (188.07 K), as well as a linear function with a negative slope in the range from the boiling point (188.07 K) to 298 K to prevent the liquid phase from becoming stable at high temperatures before the gaseous HCl. For higher temperatures, it is assumed equal to the Cp of gaseous HCl.
Giauque and Wiebe have also reported the heat of vaporization of HCl as 16,200 J/mol. This information, together with the other data gathered for liquid and gaseous HCl, allows for the calculation of the heat of formation and absolute entropy of liquid HCl, as shown in equations (7) and (8):

$$\Delta H_{vap}^{188} = \Delta_f H^o_{298_{(gas)}} + \int_{298}^{188} C_{p_{(gas)}} dT - \Delta_f H^o_{298_{(liquid)}} - \int_{298}^{188} C_{p_{(liquid)}} dT \quad (7)$$

$$S^{298}_{(gas)} - S^{298}_{(liquid)} = \Delta H^{188}_{vap}/T + \int_{188}^{298} c_{P_{(gas)}} \cdot dT \,/\mathrm{T} - \int_{188}^{298} c_{P_{(liquid)}} \cdot dT/T \quad (8)$$

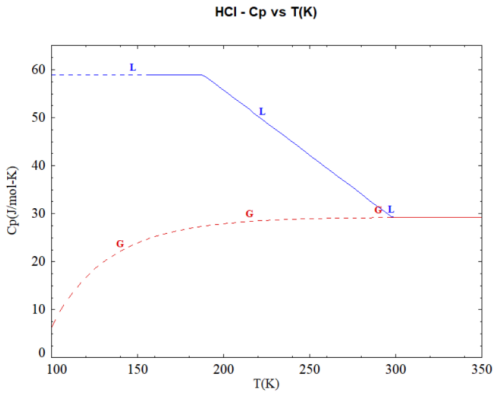

Figure 2. The heat capacity of HCl.

Table 1 provides values for the $c_{P_{liquid}}$, $H_{298(liquid)}$, and $S^{\circ}_{298(liquid)}$ applied in this work.

Table 1. Extrapolating $c_{P_{liquid}}$ and calculating $H^{\circ}_{298(liquid)}$ and $S^{\circ}_{298(liquid)}$ for HCl, KOH, and K_2O

	$c_{P_{liquid}}(J/mol.K)$	$H^{\circ}_{298(liquid)}$ *(J/mol)*	$S^{\circ}_{298(liquid)}$ *(J/mol.K)*	*Temperature range (K)*
HCl	58.9	-106,818.44	108.41	158.91–188.07
	109.78–0.2705 T			188.07–298.15
	13.38+0.0173 T -623137.74/T^2 -3.80 E-6 T^2 +5347.39/T			298.15–1,700
KOH	78.66	-410,349	101.10	298.15–677
	83.11			677–2,000
K_2O	107.00	-349,861.30	100.09	298.15–1,300

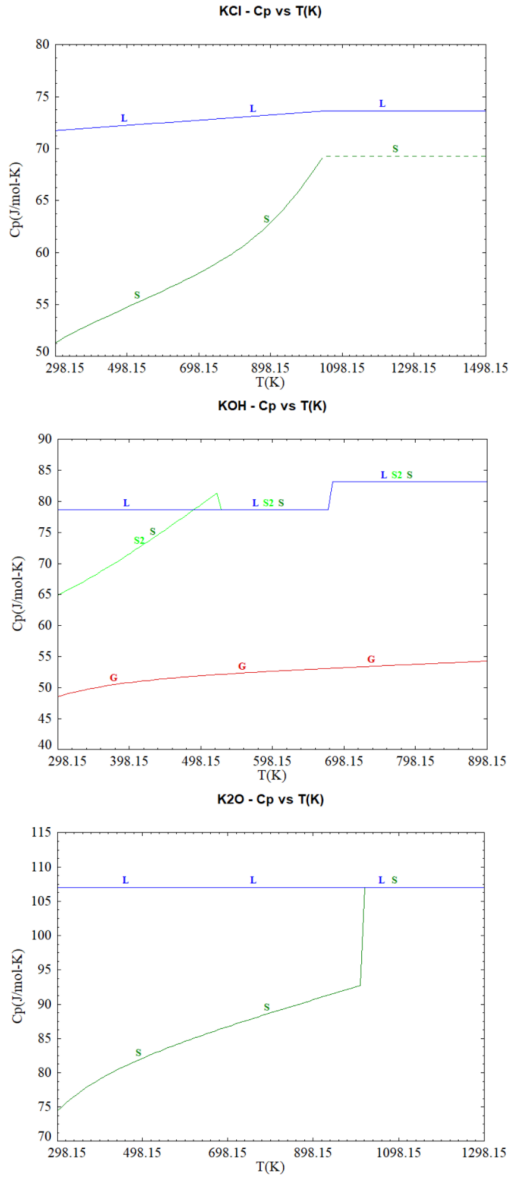

Figure 3. Heat capacity of KCl, KOH, and K_2O.

3.2 H_2O-KCl system

Several researchers have measured the solubility of KCl in water, and their results are in good agreement (18,19,26–29). Sunler and Baumbach measured the solubility of KCl between 290 and 360 K (18), and Li et al. reported the freezing-point depression in a very dilute solution of 0–3.3 mol KCl in 1 kg water (55.51 mol) (19). In total, 30 data points from the literature have been employed in the assessment. Moreover, the saturation pressure of 1 to 4 molal of an aqueous KCl solution at 100 °C (30) is used in the optimization.
The heat capacity of liquid KCl below the melting temperature is optimized as a linear function of temperature in this system. The standard enthalpy and entropy for liquid KCl are also estimated according to the optimized linear heat capacity and its heat of melting. The interaction parameters between KCl and H_2O in the liquid phase, including the first and second term ($A + B \cdot T$) of L^0 and L^1, are optimized (see Table 3).

3.1 H_2O–HCl system

The experimental data employed in modeling the H_2O–HCl system, including the melting point, boiling point, vapor pressure of the solution, and specific heat capacity of the liquid solution for a few different compositions based on the mass fraction, are shown in Table 2 (31–33).

Table 2. The experimental data employed in the modeling of the H2O–HCl system

H_2O–HCl wt%	Melting point (K)	Boiling point (K)	Vapor pressure (bar)	Specific heat capacity (J/g.K)
90–10	256.15	377.15	0.0195	3.47
80–20	215.15	382.15	0.014	2.99
70–30	-	364.15	0.0213	2.6
68–32	-	358.15	0.0373	2.55
66–34	-	345.15	0.0724	2.5
64–36	-	335.15	0.145	2.46
62–38	-	322.15	0.283	2.43

The interaction parameters, including the first and second term ($A + B \cdot T$) of L^0 and L^1 between HCl and H_2O in the liquid phase, are optimized and presented in Table 3.

3.2 H_2O–K_2O system

There is no experimental data available for K_2O's contribution; therefore, it is assumed that it has an ideal contribution to the liquid solution. Furthermore, KOH has been introduced as an associate in the system. However, K_2O's properties (standard enthalpy and entropy) have been included in the model. Potassium hydroxide is soluble in water to extremely high concentrations (34). Kirgincev et al. reported the liquidus temperatures for different compositions of KOH and water, including 30.9:69.1, 93.3:6.7, and 100:0 wt% KOH:H_2O at 210.35, 521.15, and 677.15 K, respectively (35). Balej reported the logarithm of the partial vapor pressure of an aqueous solution of KOH for 0–300 °C and 0–18 molal-KOH, both experimental and theoretical values (21). The experimental data for 2, 4, 10, and 18 molal-KOH (63 data points) have been used in the current study for modeling, as well as to optimize the thermodynamic parameters. The first and second term ($A + B \cdot T$) of L^0 and L^1 between KOH and H_2O in the liquid phase is optimized and reported in Table 3.

3.3 KOH–KCl system

In addition to the liquid solution, the solid solution is also modeled, and it presents the formation of a miscibility gap. Ruby et al. reported the 48 experimental transition temperatures using a heating curve for solid and liquid solutions and made a phase diagram based on the data (36). Dessureault et al. reported a similar phase diagram using experimental data based on cooling and heating curves (37). These data have been used to optimize the parameters and regenerate the phase diagram.

Table 3 presents the optimized interaction parameters, including the first and second ($A + B \cdot T$) terms of L^0 and L^1 between KCl and KOH, for the solid and liquid solutions.

4. Results and discussion

The optimized interaction parameters of the systems and standard enthalpy and entropy are presented in Table 3. OptimizedThese data have been employed in the phase diagram module in FactSage 7.2 to calculate the phase diagrams of the quasi-binary systems. The calculated phase diagrams are shown in Figure 4 and compared to the literature values. As shown in Figure 4, the solid–liquid equilibria data (i.e., the points on the solubility curve and the invariant points) are reproduced well by the current models.

Table 3. Optimized thermodynamic parameters of the H_2O–HCl, H_2O–KOH, KOH–KCl, and H_2O–KCl systems using the Redlich–Kister model

System	Phase type	Phase name	Thermodynamic parameters
H_2O–HCl	Solution	Liquid	$L^0 = -44928+110.82T$ $L^1 = -11618 + 131.32T$
H_2O–KOH	Solution	Liquid	$L^0 = -47375 + 2.33\ T$ $L^1 = -5545 + 16.94\ T$
KCl–KOH	Solution	Liquid	$L^0 = 3296 - 8.78T$ $L^1 = 5714 - 1.26T$
		Solid	$L^0 = 8331 - 0.40\ T$ $L^1 = -12551 + 13.38T$
H_2O–KCl	Solution	Liquid	$L^0 = 10443 - 26.23T$ $L^1 = -10478 - 21.71T$
KCl	Solution	Liquid	$H^{298}_{KCl(liquid)} = -421103$ $S^{298}_{KCl(liquid)} = 88.02$ $Cp^{<1044K}_{KCl(liquid)} = 70.957\ + 0.002528\ T$

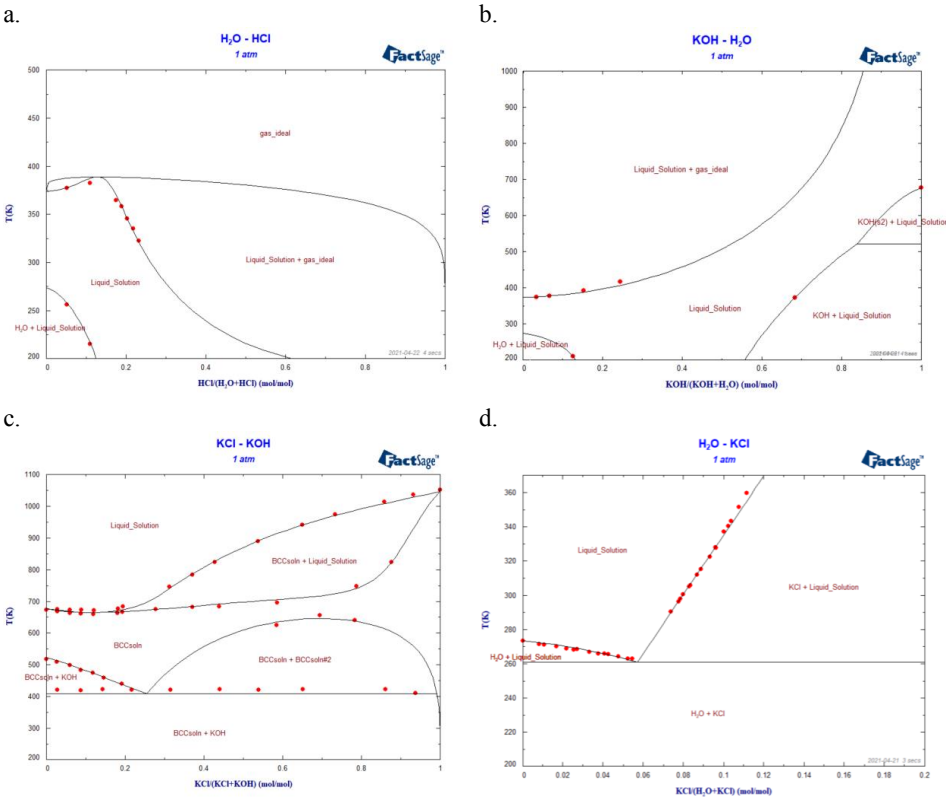

Figure 4. Phase diagram for binary systems. Lines: The present model results. Red points: Experimental data. a. H_2O–KCl, b. H_2O–HCl, c. H_2O–KOH, d. KCl–KOH solution

Smith et al. presented the H_2O–HCl phase diagram from 0 to 110 °C at the pressure of 1.0133 bar (38). The calculated H_2O–HCl phase diagram is shown in Figure 4.a. The experimental points employed from the literature meet the calculated liquidus.

The heat capacity of the H_2O-HCl solution was evaluated in FactSage and compared with the experimental results, as shown in Figure 5.a. The Cp values for seven data points of 10 wt% HCl to 38 wt% HCl are evaluated from 280 to 310 K. Although they are not in excellent agreement with the experimental results, they show the same tendency. The agreement could be improved by introducing higher-order terms to the temperature dependence of the RK expression. Figure 5.b. shows the evaluated vapor pressure for the same compositions within the same temperature range and compares them with the experimental results from the literature. These data show particularly good agreement, especially for the more dilute solution at room temperature, 293.15 K.

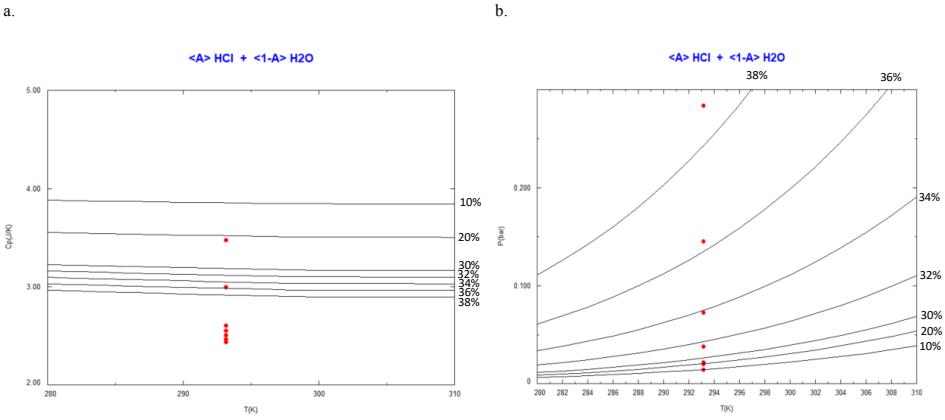

Figure 5. Comparing the experimental (red dots) and theoretical values of the H_2O–HCl solution for 10, 20, 30, 32, 34, 36, and 38 wt% HCl for a. heat capacity and b. vapor pressure

Figure 6 shows the comparison of the vapor pressure of the H_2O–KOH solution between the model results and the data from Balej et al. (21), which cover a temperature range of 273.15–573.15 K and KOH concentrations of 2, 4, 10, and 18 molalities. As shown in the figure, the model results are in excellent agreement with the experimental data.

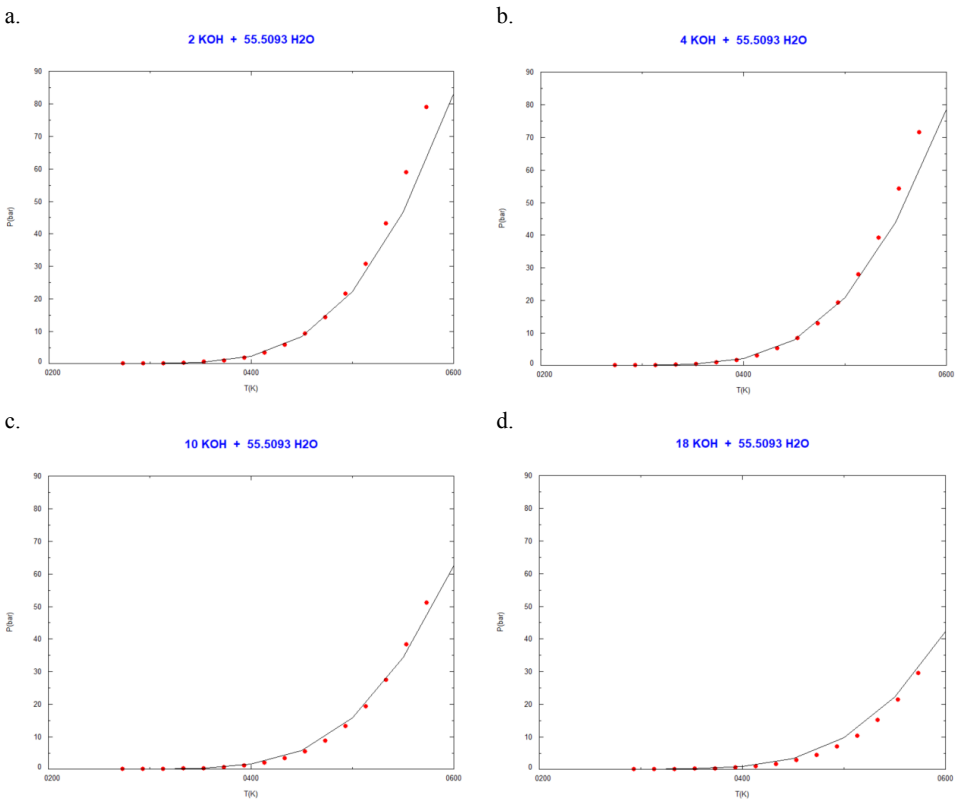

Figure 6. Comparing the experimental data (red dots) and modeling results of vapor pressure of the KOH–H_2O solution a. 2 Molality, b. 4 Molality, c.10 Molality, and d. 18 Molality

After optimizing all three sub-binary systems, including H_2O–HCl, H_2O–KOH, and KOH–KCl, the main H_2O–KCl system's phase diagram is reassessed, including 5 end members H_2O, KCl, KOH, HCl, and K_2O to ensure no significant change in the calculated parameters.

5. Conclusion

This study has modeled the thermodynamic properties of KCl hydrolysis in the liquid phase in FactSage. In addition to KCl, H_2O, and HCl, hydroxide and oxide KOH (here only K_2O) are also included, as hydroxides significantly affect the partial pressure of HCl in the chloride solutions. For the first time, it is shown that a simple associate model can be used to model an aqueous solution, the liquid acid and base, and liquid salt as a single phase.

Various thermodynamic properties (i.e., melting point, boiling point, vapor partial pressure, heat capacity) were collected and employed to fit the model parameters. It is shown that the associate model in the present thermodynamic framework can represent the properties of the liquid phase in all binary sub-systems (H_2O–HCl, H_2O–KOH, H_2O–KCl, KOH–K_2O, KOH–

KCl) in various aspects over wide temperature and concentration ranges. Consequently, the entire KCl–K_2O–H_2O–HCl reciprocal system has been modeled for the first time using a single subregular model in FactSage.

References

1. Li P, Molina E, Wang K, Xu X, Dehghani G, Kohli A, et al. Thermal and transport properties of NaCl–KCl–ZnCl2 eutectic salts for new generation high-temperature heat-transfer fluids. J Sol Energy Eng. 2016;138(5).

2. Li Y, Xu X, Wang X, Li P, Hao Q, Xiao B. Survey and evaluation of equations for thermophysical properties of binary/ternary eutectic salts from NaCl, KCl, MgCl2, CaCl2, ZnCl2 for heat transfer and thermal storage fluids in CSP. Sol Energy. 2017;152:57–79. Available from: https://www.sciencedirect.com/science/article/pii/S0038092X17301792

3. Xu X, Dehghani G, Ning J, Li P. Basic properties of eutectic chloride salts NaCl-KCl-ZnCl2 and NaCl-KCl-MgCl2 as HTFs and thermal storage media measured using simultaneous DSC-TGA. Sol Energy. 2018;162:431–41.

4. Etter DE, Wiedenheft CJ. The study of KCl-CuCl eutectic fused salt as a potential intermediate temperature heat transfer and storage medium. Sol Energy Mater. 1980;2(4):423–31.

5. Mohan G, Venkataraman M, Gomez-Vidal J, Coventry J. Assessment of a novel ternary eutectic chloride salt for next generation high-temperature sensible heat storage. Energy Convers Manag. 2018;167:156–64. Available from: https://www.sciencedirect.com/science/article/pii/S0196890418304485

6. Niazi S, Olsen E, S. Nygård H. Hydrolysis of eutectic compositions in the ZnCl2:KCl:NaCl ternary system and effect of adding ZnO. J Mol Liq. 2020;317:114069. Available from: http://www.sciencedirect.com/science/article/pii/S0167732220336114

7. Guo S, Zhang J, Wu W, Zhou W. Corrosion in the molten fluoride and chloride salts and materials development for nuclear applications. Prog Mater Sci. 2018;97:448–87.

8. Ding W, Bonk A, Bauer T. Molten chloride salts for next generation CSP plants: Selection of promising chloride salts & study on corrosion of alloys in molten chloride salts. In: Solarpaces 2018: International Conference on Concentrating Solar Power and Chemical Energy Systems. 2019.

9. Maksoud L, Bauer T. Experimental investigation of chloride molten salts for thermal energy storage applications. In: 10th International Conference on Molten Salt. 2015. p. 273–80.

10. Jung I-H, Van Ende M-A. Computational Thermodynamic Calculations: FactSage from CALPHAD Thermodynamic Database to Virtual Process Simulation. Metall Mater Trans 50th Anniv Collect. 2020;51:1851–74.

11. Harvie CE, Møller N, Weare JH. The prediction of mineral solubilities in natural waters: The Na-K-Mg-Ca-H-Cl-SO4-OH-HCO3-CO3-CO2-H2O system to high ionic strengths at 25°C. Geochim Cosmochim Acta. 1984;48(4):723–51. Available from: https://www.sciencedirect.com/science/article/pii/001670378490098X

12. Helgeson H, Kirkham DH, Flowers G. Theoretical prediction of the thermodynamic

behavior of aqueous electrolytes at high pressures and temperatures - Parts I through IV. Am J Sci.

13. Pelton AD. Phase diagrams and thermodynamic modeling of solutions. 2018. Academic Press;

14. Bale CW, Chartrand P, Degterov SA, Eriksson G, Hack K, Ben Mahfoud R, et al. FactSage thermochemical software and databases. Calphad. 2002;26(2):189–228. Available from: https://www.sciencedirect.com/science/article/pii/S0364591602000354

15. Reis BH. Development of a novel thermodynamic database for salt systems with potential as phase change materials [PhD thesis]. Brandenburgische Technische Universität Cottbus - Senftenberg; 2021.

16. Lukas HL, G. Fries S, Sundman B. Computational thermodynamics, the Calphad method. New York: United States of America by Cambridge University Press, New York; 2007.

17. Xu H, Romagnoli A, Yin Sze J, Py X. Application of material assessment methodology in latent heat thermal energy storage for waste heat recovery. Appl Energy. 2017;187:281–90.

18. Sunier AA, Baumbach J. The solubility of potassium chloride in ordinary and heavy water. J Chem Eng Data. 1976;21(3):335–6.

19. Li D, Zeng D, Yin X, Han H, Guo L, Yao Y. Phase diagrams and thermochemical modeling of salt lake brine systems. II. NaCl+H2O, KCl+H2O, MgCl2+H2O and CaCl2+H2O systems. Calphad. 2016;53:78–89.

20. Sanahuja A, Cesari E. Heat of solution of KCl in water at 303.15 K. Thermochim Acta [Internet]. 1985;85:163–6. Available from: https://www.sciencedirect.com/science/article/pii/0040603185855556

21. Balej J. Water vapour partial pressures and water activities in potassium and sodium hydroxide solutions over wide concentration and temperature ranges. Int J Hydrogen Energy. 1985;10(4):233–43.

22. Tianwei Z, Hao L, Zhiyue H, Zhiming D, Yong W. Active substances study in fire extinguishing by water mist with potassium salt additives based on thermoanalysis and thermodynamics. Appl Therm Eng. 2017;122:429–38. Available from: https://www.sciencedirect.com/science/article/pii/S1359431116338959

23. Bychinskii VA, Tupitsyn, A. A. Chudnenko, K. V. Mukhetdinova, A. V. Fomichev S V., Krenev VA. Extrapolation of thermodynamic functions in calculation of phase equilibria by the Gibbs energy minimization method. Russ J Inorg Chem. 2013;58:1197–202.

24. Sergeev D, Reis BH, Dreger I, to Baben M, Hack K, Müller M. Thermodynamics of the Ca(NO3)2 – NaNO3 system. Calphad. 2019;67:101688. Available from: https://www.sciencedirect.com/science/article/pii/S0364591619301464

25. Giauque, WF and Wiebe R. The Entropy of Hydrogen Chloride. Heat Capacity from 16 K. to Boiling Point. Heat of Vaporization. Vapor Pressures of Solid and Liquid. J Am Chem Soc. 1928;50(1):101–22.

26. H. Rodebush W. The freezing points of concentrated solutions and the free energy of solution of salts. J Am Chem Soc. 1918;40(8):1204–13.

27. Simão P. P, A. Macedo E. Solubility of NaCl, NaBr, and KCl in Water, Methanol, Ethanol, and Their Mixed Solvents. J Chem Eng Data. 2005;50(1):29–32.

28. Donald L. H, Sterner SM, J. Bodnar R. Freezing point depression of NaCl-KCl-H 2 O solutions. Econ Geol. 1988;83(1):197–202.

29. Shearman RW, W. C. Menzies A. The Solubilities of Potassium Chloride in Deuterium Water and in Ordinary Water from 0 to 180°. J Am Chem Soc. 1973;59(1):185–6.

30. Shibue Y. saturation pressure of H2O+NaCl and H2O+KCl solution. Rock Geophys Sci. 2003;32:185–91.

31. Lide DR. CRC Handbook of Chemistry and Physics on CD-ROM, 2000 Version. CRC Press LLC New York; 2000.

32. PERRY R, GREEN D. Perry's Chemical Engineers' Handbook, volume 6th edition. Mcgrawhill. 1984.

33. Aspen Properties, binary mixtures modeling software (calculations by Akzo Nobel Engineering utgave), Aspen Technology, 2002–2003.

34. LI Z, PITZER KS. Thermodynamics of aqueous KOH over the full range to saturation and to 573 K. J Solution Chem. 1996;25(9):813–23.

35. A. Kirgincev, L. Trushnikova and VL. Rastvorimost neorganicheskih veschestv v vode. In: Handb Leningr. 1972.

36. Ruby C, Sebaoun A.S. VJ-C. No Title. CR Acad Sci Paris. 1968;267(1043).

37. Y Dessureault, J Sangster AP. Evaluation critique des données thermodynamiques et des diagrammes de phases des systèmes AOH-AX, ANO3-AX, ANO3-BNO3, AOH-BOH où A, B = Li, Na, K et X = Cl, F, NO3, OH. J Chim Phys. 1990;87:407–53.

38. Smith WR, Nezbeda I, Francová M, Jirsák J, Škvor J. Molecular-level simulation of electrolyte systems in the copper-chlorine hydrogen production cycle.

ISBN: 978-82-575-2008-3
ISSN: 1894-6402

Norwegian University
of Life Sciences

Postboks 5003
NO-1432 Ås, Norway
+47 67 23 00 00
www.nmbu.no